TIME RESOLVED SURFACE ENHANCED RAMAN SCATTERING STUDIES OF SURFACE PHOTOCHEMISTRY AND ELECTROCHEMISTRY

by

WEI ZHANG

A dissertation submitted to the Graduate Faculty in Chemistry in partial fulfillment of the requirements for the degree of Doctor of Philosophy, The City University of New York.

1995

This manuscript has been read and accepted for the Graduate Faculty in Chemistry in satisfaction of the dissertation requirement for the degree of Doctor of Philosophy.

9-14-95
Date

Chair of Examining Committee

9/14/95
Date

Executive Officer

Supervisory Committee

THE CITY UNIVERSITY OF NEW YORK

ABSTRACT

Time Resolved Surface Enhanced Raman Scattering Studies of Surface Photochemistry and Electrochemistry

by

Wei Zhang

Adviser: Professor Ronald L. Birke and Professor John R. Lombardi

Applications of time resolved surface enhanced Raman scattering (TRSERS) techniques for the study of surface photochemistry and electrochemistry were demonstrated.

As an example of TRSERS applications in surface photochemistry studies, direct photoinduced charge transfer from adsorbed flavin mononucleotide (FMN) to a Ag electrode was observed by TRSERS and complementary experiments. Two short lived photoproduct radical ion intermediates with life time of 775ns and 1.5μs were observed and confirmed as enol-keto forms of a photo-oxidized FMN monocation radical by TRSERS of FMN and deuterated FMN with the help of normal mode calculations. New mechanisms of photo-induced charge transfer between FMN and a Ag electrode and for the photogalvanic effect on a dye modified electrode were proposed as a result of the experiments.

As an example of TRSERS applications in an electrochemical study, p-Nitrobenzoic acid (PNBA) was studied by TRSERS following the application of a double potential step to a Ag electrode. The spectral bands of three stable intermediate products, p-nitrosobenzoate, hydroxylamine, and azoxy compounds were observed. In addition, the transient bands of an unstable intermediate were

seen at 996, 1233, and 1580cm^{-1} with a life time of about 70ms during the oxidation process of the hydroxylamine compound which itself is generated electrochemically by a 200ms potential pulse. We suggest these bands represent the p-nitrosobenzoate free radical anion intermediate formed during the oxidation of the hydroxylamine compound.

In addition, three redox states of FMN and interactions of FMN with a Ag electrode were studied by SERS, UV/Vis absorption spectrophotomerty and normal mode calculations. The adsorption site and orientation of FMN on a Ag electrode were found depending on the Ag electrode surface potential. The SERS spectrum of FMN hydroquinone was reported for the first time.

ACKNOWLEDGMENTS

During the past five years of my graduate study, I continued to learn from my teachers and colleagues at City College of The City University of New York. Without the inspiration and the support of those acknowledged below, this dissertation would not have been possible.

First, I wish to thank my advisors, Professor Ronald L. Birke and Professor John R. Lombardi, whose enthusiasm and guidance have not only spurred the advance of my research projects, but also quickened my interest in many scientific areas. Their deep understanding in science and technology, their fluency and clearness in presenting and conveying science and technical ideals, their eagerness in learning and participating in new scientific frontiers, and their patience in allowing me to make mistakes are the qualities which I shall always remember.

Especially I want to thank Professor John R. Lombardi again. Without his help, I could not have come to study at CUNY. He is not only my mentor, but also my true friend in life.

My fellow coworkers in Birke and Lombardi's group are specially recognized for their assistance in sharpening my laboratory skills and for many helpful discussions. It was George Sukenik who helped me solved many computer problems, Chongtie Shi who taught me how to use potentiostats, Alberto Vivoni who helped me to do normal mode calculations. Special thanks are due to Mingfa Wang for her continuously encouragement and help.

I am deeply grateful to Cathy Abrams and Charles Hosten for their helping me to settle down when I first came here, for providing a supportive social environment that is vital for my interaction with Americans and for their friendship.

Finally, I would like to thank the Department of Chemistry of the City College of CUNY for five years of financial support.

TABLE OF CONTENTS

LISTS OF TABLES

LISTS OF ILLUSTRATIONS

Chapter 1 Overview and Perspective

1.1 Introduction

During the past two decades a large amount of research effort has been continuously devoted to the fundamental study of surface structures and surface dynamics [1-10]. It has been realized from the beginning that such an endeavor will not only enrich our understanding of surfaces at the atomic and molecular level, but also fertilize the development of many important technological areas such as heterogeneous catalysis [11-13], fabrication of thin film microelectronic devices [14], solar energy conversion and storage [15] and corrosion control [16-18]. The purpose of this dissertation is to exam the problems and the possibilities of application of time resolved surface enhanced Raman spectroscopy (TRSERS) in studies of photoinduced surface photochemistry and potential induced electrochemistry at an electrode surface. The first two sections of this chapter intend to review previous research work and bring readers necessary background regarding surface spectroscopy, surface enhanced Raman spectroscopy (SERS) and TRSERS, while the last section gives the goal of my research.

1.2 Surface Spectroscopy and Surface Enhanced Raman Spectroscopy

Today modern surface scientists have been equipped with an array of surface characterization techniques which involve the interaction of a probe beam of photons, electrons, or ions with target surfaces and the subsequent detection of ejected particles. The combined use of these techniques can provide complementary information on different physical-chemical properties of

an interface [19-28], including compositions by Auger electron spectroscopy (AES), X-ray photoelectron spectroscopy (XPS), and secondary ion mass spectroscopy (SIMS); geometric structures by low energy electron diffraction (LEED), transmission and scanning electron microscopies (TEM and SEM), scanning tunneling microscopy (STM), and ion scattering spectroscopy (ISS); electronic structure by ultraviolet photoelectron spectroscopy (UPS) and XPS; finally, adsorbate structures by high resolution electron energy loss spectroscopy (HREELS), infrared spectroscopy (IR, FT-IR), and Raman spectroscopy. However, while some of those techniques were extended to solid-liquid interfaces, which are of practical importance and particular interest to electrochemists, many obstacles have been encountered. For example the use of ultrahigh vacuum (UHV), which is essential to electron and ion scattering spectroscopic techniques is excluded at solid-liquid interface, and the use of IR and normal Raman techniques suffered low sensitivity and difficulties of distinguishing signals from surface and from bulk solution. One strategy to avoid this difficulty has been designed by Hubbard et al. , who have utilized LEED and HREELS to study adsorbate structure on single crystal electrodes which were transferred to a UHV chamber after electrochemical measurements [29-31]. The drawback of this method is that the derived information may not reflect the state of the electrode in-situ.

It is clear that in-situ examination of structures and dynamics at an electrochemical interface depends on the successful application of those techniques which employ non-reactive photons (spectroelectrochemistry) or tunneling electrons as probe particles. A wide variety of techniques employ photons, with energy ranging from X-ray to infrared. In the UV-Vis and infrared region, the available techniques can be categorized into two groups: Surface

electronic spectroscopy [32-38] and surface vibrational spectroscopy [39-40]. The former includes specular reflection spectroscopy, absorption spectroscopy, ellipsometry, and electrochemiluminescence, while the latter includes surface infrared spectroscopy and surface Raman spectroscopy. Research in these areas initially focused on surface electronic spectroscopy and latter shifted to surface vibrational spectroscopy because the latter has higher molecular specificity, which provides directly interpretable information on the structure of surface adsorbates as well as the bonding nature of surface chemisorption.

Two major problems have been recognized during the development of spectroelectrochemical techniques. The first problem is the large penetration depth of photons in bulk solution of an electrochemical cell which manifests itself as the inability of the probe photons to differentiate the molecules on the surface from molecules in the bulk. The second problem, the limited sensitivity, arises not only from the intrinsic adsorption or scattering cross section of molecules which change after they are adsorbed on a surface but also from the number of molecules adsorbed on the surface which is 4 to 6 orders of magnitude smaller than that in the bulk solution. For example, in the application of surface infrared spectroscopy to studies near the electrode region, attenuated total reflectance (ATR) configurations and thin layer electrochemical cells have been utilized to avoid the problem of strong adsorption of IR photons by common electrochemical solvents, especially water [41-44]. However, this arrangement not only enables molecular structural changes both in the solution and interfacial region to be examined [45-46], but also restricts the electrochemical methods that can be used. In comparison, the main problem in using surface Raman spectroscopy to study the electrode/electrolyte interface is its low sensitivity. Interference from electrochemical solvents is negligible since most of them do not absorb UV-Vis

light and the solvent Raman spectra are relatively simple. Although one still has to distinguish the Raman signal of the adsorbed molecules from the Raman signal from the molecules in the diffusion layer, it is more critical to solve the problem of low sensitivity.

The first observation of a large intensity Raman signal from adsorbed molecules on a silver electrode was made by Fleischmann et al.. [47] Later it was realized by Van Duyne et al. and Albrecht and Creighton [48-49] that the effect was a surface enhancement, which opened the door for Raman spectroscopy in surface science. The giant Raman signal enhancement of up to six orders of magnitude compared to molecules in solution, which was called "surface enhanced Raman scattering" (SERS), completely solved the low sensitivity problem [50]. In addition, SERS strongly discriminates against the molecules in the diffuse layer since the enhancement factor falls off rapidly as the substrate-adsorbate separation increases [51]. Consequently, in-situ monitoring of adsorbate structures with SERS can be achieved without the use of a thin layer electrochemical cell or ATR configuration. Another strength of SERS is its complementary nature with respect to surface infrared spectroscopy; IR and Raman are governed by different selection rules, and the vibrational spectra of a molecule obtained by the two techniques exhibit different relative intensity patterns [52-54].

Many advances along with unanswered questions have been made since discovery of SERS in the middle of the 1970s. The bulk of experimental studies during the first seven years had been devoted to the understanding of the SERS mechanism and its experimental characteristics. Despite controversy, there appears to be a general agreement that two mechanisms have to be considered; the electromagnetic (EM) and the chemical enhancement mechanism [55-67].

The basic idea of the EM enhancement is that the SERS intensity is enhanced by a localized dipolar surface plasmon resonance effect and by an antenna effect. For the first effect, incident laser light develops a localized dipolar surface plasmon resonance which enhances the laser electric field near the surface of a metal particle which in turn enhances the emitting molecular dipole. For the second effect, the oscillating molecular dipole near the surface induces a dipole in the metal particle. Thus the metal sphere acts as an antenna for the near field of the oscillating molecular dipole, which contributes enhancement of Raman radiation. The surface roughness or spheroid metal particle shape is essential in order to make the surface plasmon radiate. A great deal of theoretical calculation has been done to find out the functional dependence of the enhancement factor on several critical parameters such as the nature of metal substrates, the size and shape of an isolated spheroid, the excitation energy of the incident photons, and the degree of coupling between metal particles [68-77]. In general, the results of these calculations agree reasonably well with the experimental observations, including the extraordinary large enhancement for coinage metals (Cu, Ag and Au), the long range nature of EM enhancement as shown by spacer experiments and the excitation profile as measured on microlithographically produced silver ellipsoids [78-86]. However, more detailed and thorough verification of EM theories, especially a quantitative comparison on the enhancement factor, is hampered by the experimental difficulties in controlling the size, the shape, and the inter-particle couplings of real SERS active substrates. In some cases, a discrepancy of one to two orders of magnitude was found in the enhancement factors for different types of molecules [87].

This discrepancy, together with some unexplainable observations such as

short range effects, has led some researches to think that there are additional enhancement mechanisms, dubbed as chemical enhancement mechanisms, which involve dynamic charge transfer between metal and adsorbate and consequently depend on the electronic structures of adsorbates and the localized surface [88-97]. One such chemical mechanism, the photon-driven charge transfer mechanism, originated in a verbal description by Burstein et al. [88] of a number of mechanisms for coupling electron-hole pair excitations in the metal to molecular vibrations. A more explicit treatment was given by Gersten, Birke and Lombardi. [89-90] The supporting experimental evidence for chemical models mainly includes; 1) The irreversible loss effect, where the loss of ad-atoms is believed to cause the large drop in SERS intensity as observed on a cold-deposited Ag film when it warms to room temperature and on an electrochemical roughened Ag electrode when the electrode potential is stepped to a value more negative than -0.8V Vs. SCE; and 2) the dependence of the optimum potential, at which SERS intensity maximizes, on the incident excitation energy [98-116]. As with the EM mechanism, because of the difficulties in quantitative theoretical calculations of enhancement factors and in experimental control over the SERS active sites on the atomic scale, direct quantitative confirmation of the chemical enhancement models is still not possible. Furthermore, there is no absolute and clear separation, both in theory and experiment, between the contribution from the EM enhancement and that from chemical enhancement. At present the dominant view is that the main enhancement factor is from the EM effect while the chemical effect contributes a factors of 30-100 [117-119].

After the first several years, the bulk of the SERS research was shifted to focus on the applications of SERS to many interesting systems such as biomolecules, Langmuir-blodgett films, electrochemical adsorption/desorption

and reaction kinetics, catalysts, and molecular sensors [120-138]. Recent development of SERS research has been moved into many practical applications which are beyond the laboratory research level. Such applications included immunoassay [139], medicine [140], thin-layer chromatography [141], and HPLC [142]. One possible application of SERS, which has not been fully explored, is time resolved surface enhanced Raman spectroscopy (TRSERS) for in-situ monitoring of surface dynamic processes such as adsorption/desorption kinetics, surface diffusion, electrochemical kinetics, reorientation of adsorbates and laser induced surface photochemical reactions. Especially those surface dynamic processes faster than ms time scale had not been frequently reported. Research along this line is both promising and challenging for two general reasons. First, many fundamental studies on surface dynamics under UHV environment have been done by using a variety of perturbation techniques, including temperature programmed desorption (TPD), electron stimulated desorption (ESD), pulsed laser-induced desorption, modulated molecular beam scattering, and laser induced thermal phase grating, with detection techniques such as mass spectroscopy, EELS, FTIR, surface second harmonic generation, laser induced fluorescence, laser enhanced multiphoton ionization and field ion microscopy [1-10, 143-160]. Such studies have provided a basic picture of surface dynamics as well as specific information, e.g., rates of surface reaction, and adsorption energy and adsorption site distribution. However, the UHV environment required by these techniques eliminates applications of the techniques to many of the practically important systems, such as electrochemistry and surface photochemistry for solar energy conversion and storage which involve a solid-liquid interface. Second, modern electrochemistry has a genuine need for understanding electrode kinetics at the molecular level as is seen from the research activities

concerning heterogeneous electron transfer processes and response measurements on chemically modified electrodes [161-170]. Traditional electrochemical techniques , which often involve current, charge, and potential measurements, are ineffective in these studies, since , despite good sensitivity, they lack sufficient molecular specificity. Currently, only SERS can provide molecular structure specificity of adsorbates on surfaces and can be applied to study the solid-liquid interface without ATR or a thin-layer configuration. We believe that a key point in the study of in-situ surface dynamics with molecular specific information at variety interfaces is the development of short time TRSERS.

1.3 Overview of Time Resolved Surface Enhanced Raman Spectroscopy

There are only a few TRSERS studies which have been reported during last twenty years. With limited applications, TRSERS has been applied to study slow or the slow part of dynamic processes, such as adsorption / desorption dynamics, growth or aggregation of Ag particles, CV processes and surface photochemical reactions.

The applications of TRSERS in the study of SERS mechanisms and adsorption / desorption dynamics were demonstrated by the following experiments: the first TRSERS study was reported by Jeanmaire and Van Duyne [171] and was employed to monitor the time response of Raman signal to double potential steps. In this experiment, Raman intensity time profile tracks the excitation potential signal with only a small amount of time lag, which was attributed to double layer charging time, in contrast with a bulk solution response.

This experimental result led to a conclusion that the pyridine Raman signal was indeed of surface origin, rather than a diffusion or bulk solution effect. This observation provided a fundamental basis for the understanding that the giant Raman signal of adsorbed pyridine was from a surface enhancement. This phenomena latter called surface enhanced Raman scattering, along with other experiments, led to the understanding of the SERS mechanism. Recently, a similar TRSERS study was carried out by Takahashi et al.[172] to further verify the SERS mechanism of the origin of the SERS intensity enhancement. Their conclusion was that the surface enhancement of the Raman signal of pyridine on a Ag electrode originates from an EM mechanism rather than from chemical enhancement. The monitoring of the time response of SERS intensity to double potential steps also was applied to the study of electrochemical adsorption / desorption kinetics at electrode-electrolyte interfaces by Chen [173], Stacy [174] and Pemberton [175]. Quantitative analysis of SERS intensity-time data in the context of diffusion-controlled adsorption was presented. These preliminary results demonstrated the potential of TRSERS as a method capable of providing quantitative information on rates of adsorption in electrochemical systems.

The application of TRSERS in the study of Ag particle growth and their surface potential change with time in Ag halide solutions and in photographic emulsions was carried out by Kneipp et al. [176-178]. In these experiments, SERS spectra of pseudoisocyanine dye (PIC) in silver bromide sols show a strong time dependence. The enhancement factor, in general, follows the formation (and destruction) of SERS active colloidal silver in the silver halide sols examined by laser illumination during the Raman measurement. Changes in the relative intensities within a characteristic triplet line of the SERS spectrum show that the surface potential which is "seen" by the dye molecules shifts to more positive

values with longer times. In particular, the values of the potential hint at the existence of Ag_1, Ag_4, Ag_5 and Ag_6 clusters as SERS active adsorption sites of the dye molecules in AgBr sols. Recently, further TRSERS studies of kinetics of colloid aggregation and the fractional structure of colloidal aggregations were carried out by Zhang et al. [179-180]. Good relationships between TRSERS intensity and the fractional dimension of colloidal fraction aggregates formed in both the diffusion and reaction limit regimes were established.

Application of TRSERS to monitor the cyclic voltammetry (CV) process of an electrochemical system has been carried out by many groups [181-190], which consists of a large part of TRSERS research in recent years largely due to development of the optical multichannel analyzer coupled with the photodiode array detection technique. The SERS signal obtained during a CV experiment provides real time, in-situ, and molecular specific information of adsorbed molecules, which makes it possible to identify transient chemical structures and, thus, to investigate pathways of electroorganic reductions with the CV experiment. It has been shown that TRSERS is an extremely important tool to elucidate electrochemistry mechanisms.

TRSERS studies of surface photochemistry of adsorbates at a Ag electrode was first observed by Sun et al.[191]. The photolysis rate was determined as a function of photon flux, excitation energy, electrode potential, and the nature of the solvent. A charge transfer mechanism was described for the surface induced photochemical reduction. Photochemical decomposition of flavin mononucleotide (FMN) on a Ag colloidal surface was observed by Lee [192]. The FMN was found decomposed to lumiflavin (LF) under 488nm laser light excitation which may be explained as a result of surface potential and size of SERS active Ag particles changing with time in Ag colloidal solution [193-194]. In

the course of this thesis a 337nm nitrogen laser pulse pump, CW laser probe TRSERS technique was developed in which the photochemical reaction was initiated by pumping with nitrogen laser pulses and the reaction was probed by a cw laser probe beam and a gated detector. By applying this technique, short lived intermediates were observed within the ns time domain after the pump laser pulse [195-196].

There have been two major problems with previous TRSERS studies. (1) One was very limited applications; there has been a great lack of TRSERS experiments compared with the large bulk of steady state SERS studies [197]. Published TRSERS studies during the last twenty years were only one percent of the total SERS publications (See literature search reported in Appendix A). (2) The TRSERS studies reported prior to our work were only applied to study the slow part of surface chemical reactions with a time resolution from a few ms to seconds or even longer. This slow time resolution may have been the result of the single shot detection mode adopted by most researchers which requires long detection time to integrate enough SERS signal. The slower time resolution eliminates TRSERS applications, since many of the important reaction steps take place at time scale shorter than ms, especially the primary reaction steps of a photoinduced surface photochemical reaction [198], such as the molecular excitation state, charge transfer between adsorbate and substrate, and formation of radical ions. The dynamics and molecular structure of intermediates developed during these fundamental steps are essential to elucidate photochemical and electrochemical reaction mechanisms.

Theoretically, the TRSERS is an idea tool for short time resolved surface dynamic studies due to following advantages: (1) The spectrum has molecular specification which originates from molecules adsorbed on surface; (2) The

giant Raman signal enhancement enables detecting submonolayer molecules; (3) The fluorescence is quenched by a SERS active metal surface which reduces the background signal; (4) It is capable of being applied to important practical systems, such as the solid-liquid interface, enabling in-situ, real time monitoring; (5) A fs time scale Raman process could enable SERS experiments to follow the fastest reaction processes.

In this thesis, I will be most concerned with the study of photoinduced radical ion transitions with ns time scale TRSERS. Such studies have not been reported prior our work, and these studies could provide fundamental knowledge of primary photochemical and electrochemical processes which can occur at the surface of SERS active metals like Ag and Au. As indicated by Birke et al.,[117] such events might include photoionization, photoisomerization, photodecomposition, surface and solvent interactions of photoproducts, and chemical kinetics following electron transfer for molecules either adsorbed on the surface or in the electrical double layer at the metal electrode surface. These processes are important for electrocatalysis, photoelectrocatalysis, photoelectrochemical energy conversion, energy storage, photography, electrophotography, and photobiological as well as having fundamental implications. Also, an important aspect in nanoscale chemistry is the ability to activate surface reactions without acting on bulk reactions. It is easy to appreciate that optically and electrochemically induced radical and radical ion reactions on surfaces may have important and novel applications in such nanoscale chemistry.

The high resolution spectra obtainable with the TRSERS technique coupled with pulsed laser methods should certainly provide an experimental tool to probe dynamics of molecular transformations on metal surfaces.

1.4 Objective and Organization of This Dissertation

Having evaluated the pros and the cons of TRSERS with respect to other surface characterization techniques, I envisioned the following goals for the implementation of time resolved surface enhanced Raman spectroscopy (TRSERS):

- Demonstration of ns time scale TRSERS spectroscopy as a useful technique to study surface photochemistry, which includes monitoring surface photochemistry dynamics and determining the chemical structure of surface photochemical intermediates.
- Demonstration of time resolved SERS spectroscopy as a useful technique to study electrochemical kinetics with identification of the chemical structure of intermediates.

Our strategy to reach these goals was to attack a critical problems in surface photochemistry and electrochemistry, vis, the application of TRSERS with ns time resolution to study radical ion intermediates during photoinduced surface photochemistry at an electrode surface which was initiated by a laser pulse and the application of TRSERS with ms time resolution to study dynamics and to identify the intermediate structure of radical ions initiated by electrode potential steps. We believe that the development of a repetitive pump-probe detection mode is necessary to obtain ns time resolution spectrum and the development of single-shot detection mode can be applied to obtain ms time resolution spectrum. To improve the surface stability and to obtain higher SERS intensity is also important in order to carry out such studies.

As a result, in the case of the study of surface photochemistry, I decided to

study molecules which are strongly adsorbed on a Ag electrode surface, having strong absorption bands at the pump laser pulse wavelength and at the probe laser beam wavelength. The adsorbed molecules also undergo reversible photochemical reaction under electrochemical control. We employed a N_2 laser pulse to initiate a photochemical reaction and a CW laser with gated detector to probe the SERS spectrum of chemical intermediates. The repetitive pump-probe mode was employed to study the dynamics and intermediate chemical structures in the photochemistry. In the case of the study of electrochemical reactions, we were mainly concerned with methods to generate intermediates electrochemically. Shift of vibrational bands, formation of new bands and change of band shape in the TRSERS spectrum following primary photochemical or electrochemical events have been used to elucidate the mechanism of fundamental kinetics and to identify the structure of radical ion intermediates.

We demonstrated here two examples of TRSERS applications.

The study of surface photochemistry of FMN on a Ag electrode by TRSERS as illustrated in chapter 3. In order to elucidate the charge transfer mechanism of adsorbed FMN with Ag electrode, complementary experiments are also discussed in this chapter.

In chapter 4, we will discuss more SERS studies of FMN in detail. SERS studies of the interactions between FMN adsorbate and substrate and the SERS studies of hydroquinone are presented.

Applications of TRSERS studies with an electrode potential pulse to initiate electrochemical reactions is demonstrated in chapter 5. The dynamics and short lived intermediates of para-nitrosobenzoic acid (PNBA) during an electrochemical reaction were identified by this technique.

The principles and techniques of TRSERS for these studies are discussed

in chapter 2.

The work presented in this thesis has not completely accomplished the goals described earlier, but it may stimulate new applications of TRSERS for the study of surface reaction dynamics, especially surface photochemistry. In order to study irreversible photochemical reactions and faster reaction process, a flow cell with a SERS active Ag colloid system and a repetitive laser pulse pump and laser pulse probe detection model is suggested in chapter 2. Such studies may provide a way to look at fundamental surface photochemistry processes, e. g. excitation state and quenching dynamics at surfaces.

Chapter 2 Principle and Experimental Techniques

2.1 Principle of TRSERS for Surface Photochemistry

It is clear that information of surface dynamics and intermediate structures is extremely important to elucidate mechanisms of physical and chemical reactions on a surface. Unfortunately, the traditional SERS technique used for most SERS studies during the last twenty years can only provide steady state information of reactants and products on the surface and information on the structure and dynamics of short lived intermediates is not available. A traditional SERS system which consists of a scanning monochromator equipped with photocounting detection requires 30-60 minutes to obtain a spectrum from 100 cm^{-1} to 3000 cm^{-1}. The time for recording one spectrum is much longer than the life time of most intermediates and surface dynamic processes. As an example, consider that an electrochemical reaction during a potential step experiment undergoes an EC process.

$$A + e^- \longrightarrow B \qquad E^0, k^0$$

$$B \longrightarrow C \qquad k_c$$

where E^0 and k^0 are the standard electrode potential and heterogeneous rate constant for the electron transfer reaction respectively, and k_c is the rate constant of the chemical step. The SERS spectrum of the steady state at a potential more positive than E^0 provides information on species A and the steady state SERS spectrum obtained at more negative than E^0 is related to species C. Assuming that the chemical reaction following the electron transfer is not extremely slow, the intermediate species B will be converted to final product C at short times.

The information on intermediate B can not be obtained by the traditional SERS measurements.

In general, suppose we have compound A undergoing the following change:

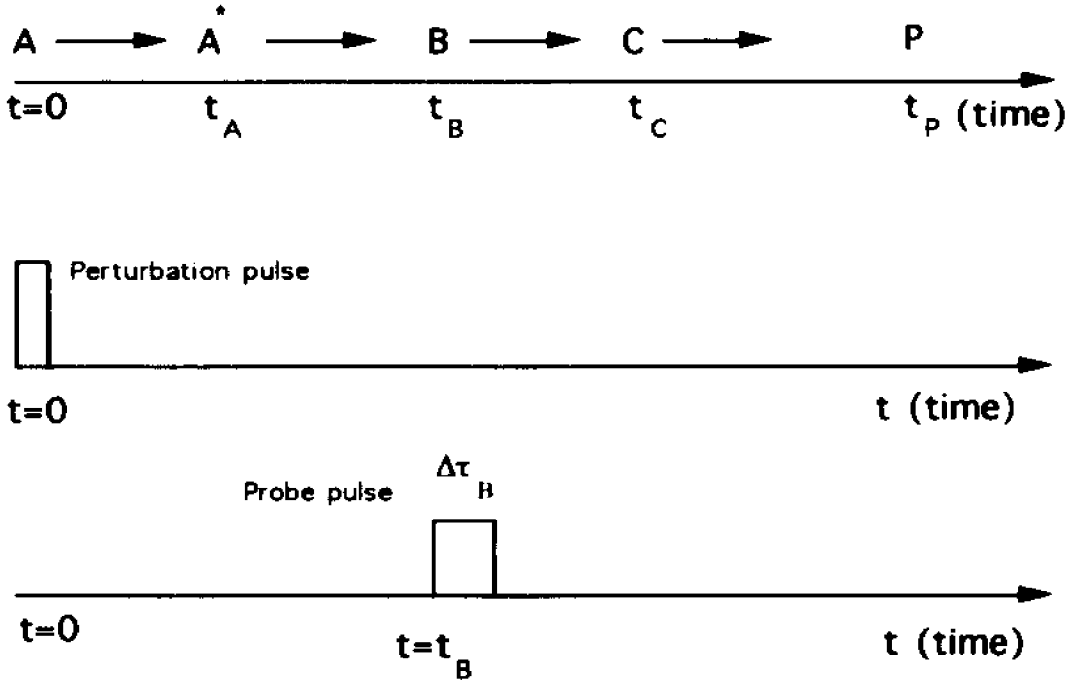

where t_i are characteristic times for the different transformations. The first transformation is induced by a sudden perturbation pulse of duration short compared to the characteristic time t_A. The perturbing pulse could be a pulse of electrons or γ rays (as in pulse radiolysis), a pulse of potential applied on a working electrode (as in electrochemistry), a sudden pH change, mixing of another reagent, or a pulse of light to induce the A to A^* change photochemically. In the latter case transitions can be to an excited state of A or a new chemical species.

During or after the perturbation, the reactant, compound A, can undergo a series of changes which may involve excited state A^*, followed by electron

transfer with its environment to form an anion or cation radical B, which in turn may react with another compound to form intermediate C and so on, finally forming the stable product P.

In order to obtain information from intermediate B, a probe beam (or probe pulse) should be sent to the same sample at time t_B after the pump perturbation to generate a detectable intermediate signal, e.g., the SERS signal from B. The detection system should be able to collect signal only at time t_B and within a time interval not longer than the life time of intermediate B. The detection process for obtaining signal from B should be performed by setting a proper delay time t_B between the initial perturbation pulse and probe pulse and then integrating the SERS signal during a time interval $\Delta\tau_B$ which is shorter than the life time of B.

A time resolved spectroscopy technique requires that the instrument should be able to produce enough intermediate population from the perturbation to generate detectable signal from the intermediate using a probe beam (or pulse) at short times.

In the case of the photoinduced surface photochemistry of adsorbate at an electrode surface, which we shall focus on in this thesis, the population of relatively stable intermediate (which is initiated by a laser pulse) strongly depends on : the number density of reactants N_0 (or surface density of adsorbate), the pump laser pulse intensity I_0 (number of photons), the absorptivity of the adsorbate molecule at given excitation wavelength ρ_λ, the quantum efficiency between ground state and excited state ϕ_1 (if an excitation state of adsorbed molecule is involved), and the charge transfer efficiency between adsorbates and substrates ρ_E. The total efficiency ρ therefore is represented by

$$\rho = \rho_\lambda \ \phi_1 \ \rho_E \qquad (1.1)$$

and the population of intermediates $n_{int.}$ is given by

$$n_{int.} = N_0 I_0 \rho_\lambda \phi_1 \rho_E \qquad (1.2)$$

Generally speaking, only a small amount of adsorbate can be converted to the intermediate, since each coefficients in equation (1.2) is less than one.

The detectable intermediate surface Raman signal, $S_{int.}$, is proportional to intermediate population $n_{int.}$, the probe laser intensity I_p and the Raman transition quantum efficiency ϕ_2 between the ground state and virtual excited state of the intermediate.

$$\begin{aligned} S_{int} &= n_{int} I_p \phi_2 \\ &= N_0 I_0 \rho_\lambda \phi_1 \rho_E I_p \phi_2 \end{aligned} \qquad (1.3)$$

Usually, the SERS signal of the intermediate represented by equation (1.3) is very weak in comparison with that of parent molecule. Examining this equation, we find that the SERS signal $S_{int.}$ is proportional to ρ_λ, ϕ_1 and ρ_E which are characteristics of the adsorbed parent molecule. In order to obtain detectable signal at very short time, it is necessary to select the parent molecules and wavelength of the pump laser pulse to give the highest absorption coefficient ρ_λ. Molecules best suited for this experiment either have a strong absorption band at the pump laser wavelength or it is possible to change the pump laser pulse wavelength to match the absorption wavelength of the parent molecule. It should be also possible to select parent molecules which have high quantum efficiency ϕ_1, e. g. molecules having a high transition dipole momentum between ground and excitation states. It is also necessary in order to observe radical ion formation to have a proper molecule-electrode system which facilitates charge transfer, i.e., to have a high ρ_E, which can be facilitated by applying a proper electrode potential to adjust the Fermi level of the electrode to facilitate electron transfer between electrode and adsorbed molecules. The intermediate

population also depends on the intensity of the pump laser pulse I_0, and the surface density of the adsorbed molecules N_0. Therefore, a higher pump laser intensity is preferred , and proper pretreatment of the electrode is not only necessary to generate SERS activated substrate but also to adsorb enough molecules. Since the SERS signal, S_{int} is also proportional to ϕ_2 and I_p, it is also very important to select the proper wavelength of the probe laser beam for the intermediate to obtain higher Raman transition quantum efficiency ϕ_2 , e. g. to obtain surface enhanced resonance Raman signal from the intermediate. A pulse laser probe source is preferred which can provide a high light intensity I_p at a very short detection time interval. However, the excitation pump pulse I_0 and the probe pulse I_p must be controlled in order not to destroy the surface morphology.

The intermediate TRSERS signal is always very weak compared with the parent molecule SERS signal. This is not only due to the fact that only a small amount of parent molecules can be converted to intermediate but also, more importantly, to the short detection time which is limited by the intermediate life time. Normally, if the detected SERS frequency band from intermediates is different from the parent molecule, there is no problem to identify the intermediate's structure and kinetics with this new frequency band. However, if a SERS band from the intermediate is the same as that of the parent molecule, therefore will be difficulties in determining the mechanism. In most of the cases, the frequencies from intermediates are only shifted a very small amount from that of the parent molecule because the structure of intermediates may only change slightly from that of parent molecule. At very short times after the perturbation of the pump pulse, the intermediate may only undergo charge redistribution (e.g. the excitation state of a molecule) or a charge transfer or a proton transfer with environment or from one part of molecule to another part of the same molecule.

The basic molecular structural frame may still remain unchanged at these initial reaction steps. Therefore, the vibrational frequencies from these intermediates may show only a small change from its parent molecules. In order to obtain clear information on the formation of an intermediate , a differential spectrum between the intermediate and parent molecules is usually necessary.

Another important aspect is that a repetitive pump-probe detection mode may be necessary for most TRSERS experiments in order to generate a reasonable signal to noise ratio, especially for the time domain shorter than few ms. From our experience, we can achieve good signal to noise ratio (S/N), within a few ms by a single detection with laser power of 30mw for the probe beam at an electrode. The energy delivered to an electrode during a 10ms detection time will be $3x10^{-4}$ J. On the other hand, using the same laser power for the probe beam for time resolved SERS detection with a detection time of 100ns, requires a repetitive detection of 100,000 samples to deliver the same energy, $3x10^{-4}$ J, to the electrode in order to generate a reasonable S/N ratio for the spectrum. In that case, the repetitive pump-probe TRSERS can only be applied to study reversible reactions in order to ensure that each pump-probe detection is started from the initial reactant and that the spectrum generated by this method represents real information about the intermediate.

However, if a pulse laser is used as a probe beam, only a few pulses which have typical probe pulse energy of 0.1mJ /pulse within the pulse duration of 10ns are required to deliver $3x10^{-4}$ J to generate a reasonable S/N ratio for the spectrum.

Theoretically, the TRSERS techniques can be applied to study a variety of surface phenomena to provide kinetic and structure information on intermediates. The arrangement of TRSERS instrumentation and methods for processing data

may be quite different and strongly depend on the nature of the problems to be studied. For example, the study of photochemistry require a laser pulse to initiated the formation of intermediates, and a ns time domain TRSERS pump-probe detection mode is required. On the other hand, the study of an electrochemical adsorption / desorption process following an applied potential step may not need the generation of intermediate species or structural information for the intermediate . It is only necessary to apply a positive or negative enough potential at which the molecules are adsorbed or desorbed. In order to apply TRSERS to determine a short lived intermediate structure during a EC reaction, the perturbation potential should be negative or positive enough to produce reduced or oxidized species which in turn undergoes a chemical reaction. Since the relatively slow reaction process of the electrochemistry and a large current can be provided by a potentiostat, the population of intermediate may increase to a large percentage compared with the reactant in a relatively short time interval. The intermediate life time may be long enough for TRSERS to provide an intermediate signal in a single-shot detection. These experimental details will be discussed in detail in the following sections.

2.2 Instrumentation

The following is a list of instruments used in my thesis:

Lasers: A nitrogen pulse laser model NRG-0.5-150/B (National Research Group, Inc.) and a cw Ar^+ laser model 164 (Spectra Physics) were used as pump and probe light sources for TRSERS experiments; a cw Ar^+ laser model 2020 (Spectra Physics), a cw Kr^+ laser model 2000 (Spectra Physics) and a dye laser

model 375 (Spectra Physics) were used for electrode potential-excitation laser photon energy relationship studies; a pulse nitrogen laser model UV14 coupled with a tunable dye laser model DL-II (Molectron Corp.) and a cw He-Cd laser model 3074-20M (Omnichrome) were used as complementary light sources for photogalvanic studies.

The nitrogen laser model NRG-0.5-150/B (National Research Group, Inc.) currently operates at 337nm wavelength with 5 ns pulse duration. Single pulse energy is about 2mJ running at 15 Hz rate. About 1mJ/pulse was delivered to the electrode as a pump pulse which was focused to 0.1cm^2 at the electrode surface giving a peak power of about 10^6 w/cm^2. The cw Ar^+ laser, model 164 (Spectra Physics) outputs the 488nm or 514.5nm wavelength. A laser power of about 30mw at electrode was focused to about 50μm diameter at the electrode for the probe light source. The Kr^+ laser, mode 2000 (Spectra Physics) output at 647.1nm wavelength was used with power of about 30 mw at the electrode surface as a probe pulse. The dye laser, model 375 (Spectra Physics) pumped by the Ar^+ laser, outputs wavelength from 560nm to 640nm, and its power is higher than 100mw as a probe source. The He-Cd laser model 3074-20M (Omnichrome) outputs a maximum power of 30mw, at wavelength 320nm. The pulse nitrogen laser model UV14 (Molectron Corp.) pumps a tunable dye laser model DL-II (Molectron Corp.) to output a few mw of average power with wavelength from 370nm to 600nm, depending on dyes used. Power at the electrode surface was calibrated by experiment.

Spectrometers: A double monochromator model 1401 (SPEX Industries, Inc.) coupled with photomultiplier tube (PMT) and a photocounting detection system was used as a SERS scanning detection system. Properly selecting entrance and exit slit widths, scan rate, and data acquisition time, we

successfully resolved two peaks with a difference of 1.6cm^{-1} at around 19,436 cm^{-1}. The advantage of this system is its high spectral resolution and sensitivity. A triplemate monochromator model 1877 (SPEX industries, Inc.) coupled with an intensified photodiode array (IPDA) which was controlled by optical multichannel analyzer (OMA) was used in time resolved detection systems. A grating of 1800 groves per mm gave a spectral coverage of about 900 cm^{-1} for a Tracor Northern IPDA and 860 cm^{-1} for the EG&G PARC IPDA. The former IPDA has 512 channels which gave a resolution about 1.8 cm^{-1} /channel, and the latter IPDA has 700 channels which gave resolution about 1.2 cm^{-1} /channel, at 19,436cm^{-1} respectively.

Detection systems: (1) Scanning detection system; the PMT signal was amplified and processed by a conventional photon counting electronic unit. A digital output from this unit was fed to a PDP8 computer and processed by a home made program. Spectra can be saved on a floppy disk and plotted by X-Y plotter. (2) An Optical Multichannel Analyzer (OMA) model TN-1710A (Tracor Northern Inc.) was used for single-shot TRSERS detection. This unit which includes main control unit, memory subgroup model 1710-28, sequential scan module model 1710-37, optical spectrometer model 1710-21, and IPDA detector model TN-1223-2I enables one to record a single spectrum following each trigger-in signal while operating in the trigger-in data acquisition mode. Up to 16 spectra can be recorded in sequence during one experiment. The shortest data acquisition time of this system is 1.32ms which includes exposure time and data transfer to extended memories. Typical single-shot time resolved SERS with a data acquisition time of 10ms which generated very good signal to noise ratio spectra was found with this system. (3) An Optical Multichannel Analyzer (OMA) (EG&G PARC) system was used for the repetitive pump-probe detection mode.

This OMA system includes model a 1461 main controller, model 1303 gate pulse interface, model 1304 gate pulse amplifier, model 1302 high voltage fast pulser, and model 1455 gate IPDA detector. The entire system was controlled by a Macintosh computer through the model 1461 main controller. The program MacOMA version 1.02 was used to take spectrum and to process data. The model 1455 gate IPDA detector can operate either in a gated detection mode or normal detection mode. When operating in the gated detection mode, the detector only integrates signal while it is supplied by a -200V high voltage gate pulse from the model 1304. When operating in the normal detection mode, the detector is activated by the "scan" command of the program with the shortest data acquisition time, 30ms. The model 1304 only amplifies TTL gate pulse signals from the model 1303, and outputs -200V high voltage gate pulses to activate the detector with the same gate pulse profile as that received from the model 1303. The model 1303, which was controlled by the model 1461, outputs a TTL gate pulse to the model 1304 after receiving an input trigger signal which can be either an optical pulse or an electrical pulse (in our experiment, the trigger signal is a very small portion of pump laser pulse). The delay time between input trigger signal and output TTL gate pulse was determined by the program, MacOMA version 1.02 with a 1ns time interval increment. The TTL gate pulse width also can be programmed from 100ns to 13ms. With system model 1303 and 1304, the instrument has an intrinsic delay time of 75ns which includes trigger pulse input at the model 1303 and high voltage gate pulse output (-200v) at the model 1304 detector. Therefore, the minimum delay time of this system is 75ns and the minimum gate width is 100ns. In order to perform TRSERS at shorter than 75ns time resolution , it is necessary to replace models 1303 and 1304 by model 1302 which gives a delay time from 5ns to 140ns and a gate

pulse width of 25ns.

Electrochemical instruments: A potentiostat model 173 (EG&G PARC) with a wave form generator model 175 (EG&G PARC) was used for cyclic voltammetry, potential perturbation of TRSERS, and steady state SERS studies. A three electrodes cell was used. The Ag electrode was used as a working electrode which has a 1mm diameter, cut at 45° to give a 0.0111cm^2 electrode surface area. A Pt wire was used as counter electrode and a saturated calomel electrode (SCE) was used as reference. The electrochemical cell is made of quartz since UV light was used as pump light. The cell window was at 45° to the probe and pump light beam but it was parallel to the electrode surface. The cell's configuration enables the reduction of absorbed incident light and Raman scattered light by electrolyte solution in the cell. A digital ionalyzer model 720 (Orion Research Corp.) was used to measure the pH value of solutions.

Instrument for photogalvanic studies: A lock-in amplifier model 840 (Keithley Instruments), electrometer model 614 (Keithley Instruments), and a multimeter model 169 (Keithley Instruments) were used. An illuminator model 9741-50 (Cole Parmer Industries Inc.) also was used as light source.

2. 3 Optical Pump-Probe TRSERS Method

Due to instrumental limitations, we applied a nitrogen pulse laser as a pump source and a cw Ar^+ laser as a probe source. The system shown in Figure 2.1 proved successful for time resolved SERS from 200ns to the ms time domain. The pump pulse of 337nm from the nitrogen laser and the probe beam of 488nm from the Ar^+ laser were focused on Ag electrode on which the test molecules

were adsorbed. A dichroic mirror which totally reflects the 337nm laser light was placed at 45^0 to the normal of the incident nitrogen laser beam and transmits the 488nm probe beam, allowing the two laser beams to overlap at the electrode. In order to ensure the overlap of the pump pulse with the probe beam and to avoid surface damage, we defocused the 337nm laser pulse at the electrode to about a $0.1cm^2$ size, and focused the 488nm beam to about a 60 μm diameter size.

A very small portion of the pump pulse ("leaked" from the dichroic mirror) was collected by an optical adapter and transmitted through a fiber optics to trigger the model 1303 gate detection system, OMA (EG&G PARC). After receiving the optical pulse trigger signal, the model 1303 outputs a TTL gate pulse which has a delay time t_1 which is related to the trigger-in optical pulse signal, and has a pulse duration t_2 (so called gate pulse width) to trigger model 1304. The t_1 and t_2 of the TTL gate pulse can be preset by program through the Macintosh computer and are determined by the intensity of SERS signal from intermediate and the life time of the intermediate. The model 1304 amplifies the TTL gate pulse which is from the model 1303 and outputs a high voltage gate pulse, -200V potential to activate the gate detector. The gate detector, model 1455 operating in the gate mode, only records SERS signal while it is gated by the gate pulse, the -200V potential. Therefore, the SERS signal detected by the gate detector is that delayed by time t_1 from the nitrogen laser pump pulse and the signal integrated within the gate pulse time t_2. If an intermediate is formed on the electrode by the pump pulse with a life time longer than t_1+t_2 , the SERS spectrum obtained will represent the intermediate information. The timing sequence for pump-probe instrumental set up is shown in Figure 2.2.

The potentiostat model 173(EG&G PARC) with wave form generator

model 175(EG&G PARC) was used to apply a potential to the Ag working electrode during the experiment and for the electrode pretreatment before the experiment. A three electrodes quartz cell was employed. The potentials quoted in this thesis are all vs. the SCE except as otherwise indicated.

A small f number (f/d=1.2) lens, which was placed near the electrode cell, to collect as much Raman signal as possible. A second lens should match the f number of the triplemate monochromator. The triplemate model 1877 (SPEX Industries Inc.) was coupled with the gated IPDA detector model 1455 to give a spectral range of 850cm^{-1} with a resolution of about 1.2cm^{-1} / channel.

The OMA was controlled by a Macintosh computer. MacOMA program version 1.02 from EG&G PARC was used for data acquisition and processing. Data acquisition mode 5 was used for TRSERS experiments. Since the delay time t_1 was limited by the instrumental intrinsic delay time (75ns) and the gate width t_2 was limited by SERS signal intensity from intermediate, the shortest time resolution of the TRSERS spectra which we obtained is 75ns time delay after pump pulse with a 200ns gate width.

2. 4 Single-Shot TRSERS Method

The single-shot TRSERS instrumentation which has proven to be a powerful tool for studying electrochemical reactions is shown in Figure 2.3. An Ar^+ laser was used as SERS probe source with output laser power of 140mw and about 30mw at electrode. An excitation wavelength of 488nm or 514.5nm was used in most of our experiments. An electronic shutter was used to eliminate possible photoinduced chemical reactions by the probe beam. The full

open time of the electronic shutter is shorter than 7ms. A potentiostat and a wave form generator was used to initiate an electrochemical reaction by applying a potential on the working electrode. The delay time from the trigger-in signal at the wave form generator to the potential applied on the electrode is a few μs which is fast enough to carry out the single-shot TRSERS which is normally in the ms time scale. A Tracor Northern OMA system was used for detection of the TRSERS spectrum. The triplemate monochromator coupled with OMA IPDA which has 512 channel gave about 900 cm^{-1} spectral coverage with a resolution of 1.8cm^{-1} / channel. The trigger generator is used to synchronize the electronic shutter, the pump potential (the potential for initiating an electrochemical reaction), and the OMA detection system. In our laboratory, we can obtain very reasonable signal to noise ratio for SERS spectra with exposure times of about 5 to 10 ms for most of organic compounds with this OMA system. This OMA system can only be applied to ms or longer time domain TRSERS. Since some electrochemical reactions , many chemical reactions following electrochemical reactions, as well as adsorption/desorption processes takes place in the ms time domain, this system proved very successful for the study of electrochemical dynamics. The advantage of this system is that it can be applied for studying both reversible and irreversible reaction since no repetitive pump-probe detection is required. Figure 2.4 shows the time sequence of single-shot detection which was applied to monitor a cyclic voltammetry process.

2. 5 Other Possible Optical Pump-Probe TRSERS Methods

Due to the limitation of our presently developed TRSERS techniques, we

only studied reversible surface photochemistry processes with a ns time scale. It is my intention to point out that the TRSERS techniques should have a wider application for the study of both a *faster time scale and irreversible* surface photochemistry and electrochemistry processes. With some modifications of our presently developed instrumentation, the TRSERS techniques theoretically can be applied to study surface dynamic processes in the ps time domain. Before ending this chapter, I want to briefly propose a general TRSERS method which is not only suitable for studying the ns time domain and a reversible reaction process but is also applicable for studying ps or even faster time domain and irreversible reaction processes. The following discussion is based on the experience gained from our previous research work, and this proposed technique should have wide application for further research work.

The instrumentation for TRSERS can be based on that used for most of time resolved resonance (TR^3) Raman studies. An ideal TRSERS instrument for studying surface photochemistry should employ two pulse lasers which pump two dye lasers respectively. The dye lasers in turn output two different wavelength of laser pulses, one for pumping and the other for probing. Normally, the pump laser pulse has higher photon energy (short wavelength) and higher light intensity, while the probe laser pulse has lower photon energy (longer wavelength) and lower light intensity. The proposed TRSERS system setup is illustrated in Figure 2.5. The delay time between pump and probe pulses is controlled by a trigger pulse generator. The time between probe pulse and detection is also synchronized by the same generator. The detection time interval within which the detector records the SERS signal is controlled by an OMA gate system or the pulse duration of the probe laser (when the wavelengths of pump and probe laser pulse are different). The SERS spectrum,

obtained after a pump laser pulse at delay time t and within gate detection time τ, will represent structural information for an intermediate which was formed at time t after the pump laser pulse, while the spectrum intensity (or band shape, band width etc.) which changes with delay time t should give dynamic process information. Due to response time limitation of the pulse generator, the delay time between pump pulse and probe pulse may be limited to only few ns. Therefore, the setup as shown in Figure 2.5 is only good for time resolution from ms to few ns domain.

For the purpose of shorter time resolved studies, such as from ns to ps, a ps or fs pulse laser should be employed. One such pulse laser is used to pump two dye lasers by a beam splitter device and an optical time delay system is used to generate the delay time between the pump laser pulse and the probe laser pulse. With this system, time resolution up to fs can be obtained. Such a system is shown in Figure 2.6.

Usually, a gated detection system is not necessary to carry out TRSERS experiment, if two pulsed lasers are used for the pump-probe detection mode and if the wavelength of the pump pulse is different from that of probe pulse. Because the delay time t_1 between the pump pulse and the probe pulse is controlled either by an electric trigger generator or an optical delay system, the duration of the detection time is directly determined by the duration of the probe pulse; and furthermore, the noise generated by the pump laser pulse can be completely filtered by the triplemate monochromator. Therefore, the Raman signal recorded is that only generated from the probe laser pulse which represents the intermediate's SERS signal at delay time t_1 and detection time t_2.

Since a repetitive pump-probe mode is necessary to generate reasonable signal to noise ratio for short time resolution, the study of photochemistry on a

SERS active electrode surface must be limited to reversible processes. In order to study irreversible surface photochemistry process, a windowless flow jet sample cell, combined with a SERS active Ag colloid-molecule system could be proposed, which is depicted in Figure 2.7. This setup can ensure fresh sample for each pump-probe detection; therefore, it can be applied to study irreversible surface photochemistry. The advantages of above proposed TRSERS systems are clear:

(1) TRSERS signal will be greatly enhanced since the probe laser pulse can deliver a large amount of photo-energy at very short times (within probe pulse duration). Comparing with using a cw laser probe mode; the 30mw power of a cw laser only delivers $3x10^{-10}$ J energy to the sample within a 10 ns detection time interval which is comparable to one laser pulse duration, but a laser pulse for the probe with duration of 10 ns typically can deliver 0.1 to 1 mJ energy to a sample which is 5 to 6 orders higher energy than with the CW detection. The SERS signal therefore is expected to have several orders higher intensity than a CW laser detection. This is extremely important for short time detection since detector dark current also increases with detection time.

(2) Faster time resolution is achievable, even up to fs domain. The time resolution of this method is only limited by the pump and probe laser pulse duration.

(3) This proposed technique can be applied to both irreversible and reversible surface photochemical reactions, since sample can be refreshed by the flow cell at any time.

The disadvantage of the above proposed TRSERS system is the higher cost.

TRSERS originated from molecules adsorbed on SERS active surfaces

provides in-situ detection with molecular specificity. The giant Raman enhancement combined with fluorescence quenching can be used at the solid-liquid interface to make possible very short time surface dynamics studies. It can be expected that this TRSERS method will have many applications for the determination of surface dynamics.

Figure 2.1. Optical pump-probe TRSERS instrument for ns or longer time scale photoinduced surface photochemistry studies. A nitrogen pulse laser model NRG-0.5-150/B (National Research Group, Inc.) which outputs wavelength 337nm, energy 2mJ/pulse with 5ns pulse duration was used as pump source to initiate surface photochemistry. A cw Ar^+ laser model 164 (spectra Physics) which outputs wavelength 488nm with power 30mw at the electrode surface was used as probe source to generate the SERS signal of the intermediate. The pump and probe laser light was overlapped on a Ag electrode surface by applying a dichroic mirror. An Optical Multichannel Analyzer (OMA) system, which consists of model 1461, 1303, 1304 and gate diode array detector model 1455 (EG&G PARC), combined with triplemate monochromator model 1401 (SPEX Industries, Inc.) were used for detecting SERS spectrum of the surface photochemical intermediate at given time after the pump laser pulse. Quartz electrochemical cell was used in this experiment.

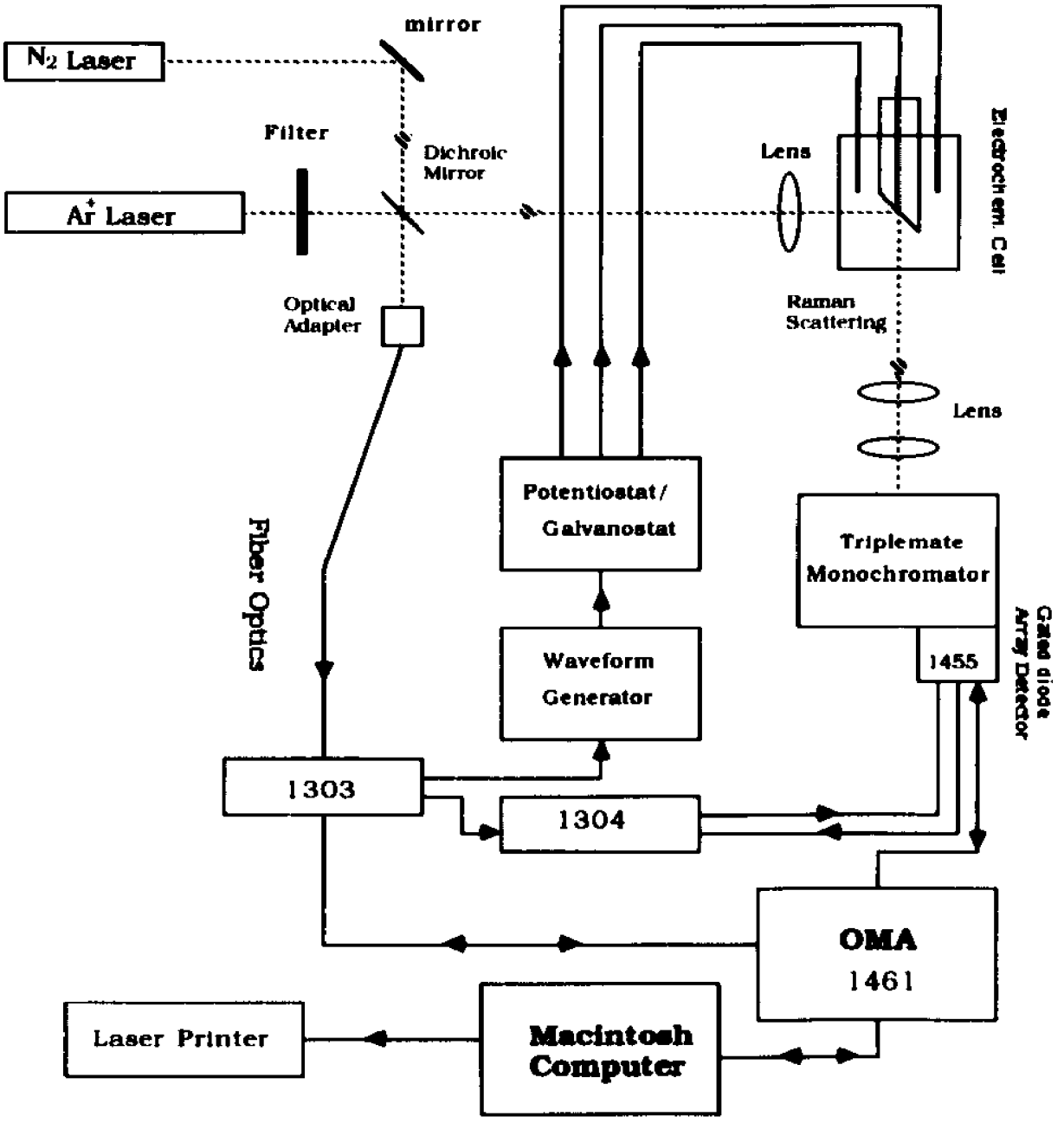

Figure 2.1 Optical pump-probe TRSERS instrument for ns time scale photoinduced surface photochemistry studies

Figure 2.2 Timing sequence for the pump-probe instrumental set-up of Figure 2.1. (a) The major part of the pump pulse which is reflected off the dichroic mirror and directed towards the working electrode. (b) The very small part of the pump pulse which passes through the optical adaptor and triggers the PARC model 1303 pulse gating generator. (c) Output of the model 1303 which provides a TTL gating pulse of width t_2 and delay time t_1. This output triggers the PARC model 1304. The voltage waveform generator can also be triggered by the model 1303 or steady state voltage can be applied to the electrode. The CW probe laser output in this experiment is always applied to the working electrode. (d) Output of the PARC model 1304 pulse amplifier showing that the gating pulse has been amplified to -200V for control of the PARC gate diode array detector model 1455. The PARC OMA model 1461 controls the delay time t_1 and the gate width t_2 through the model 1303. (e) Delay time and dwell time of the detector. The OMA model 1461 allows many repetitions of this timing sequence at fixed delay time t_1, for ensemble averaging. Variation of t_1 then allows a series of TRSERS spectra to be recorded as a function of time. True time resolution occurs when t_2 is much shorter than t_1.

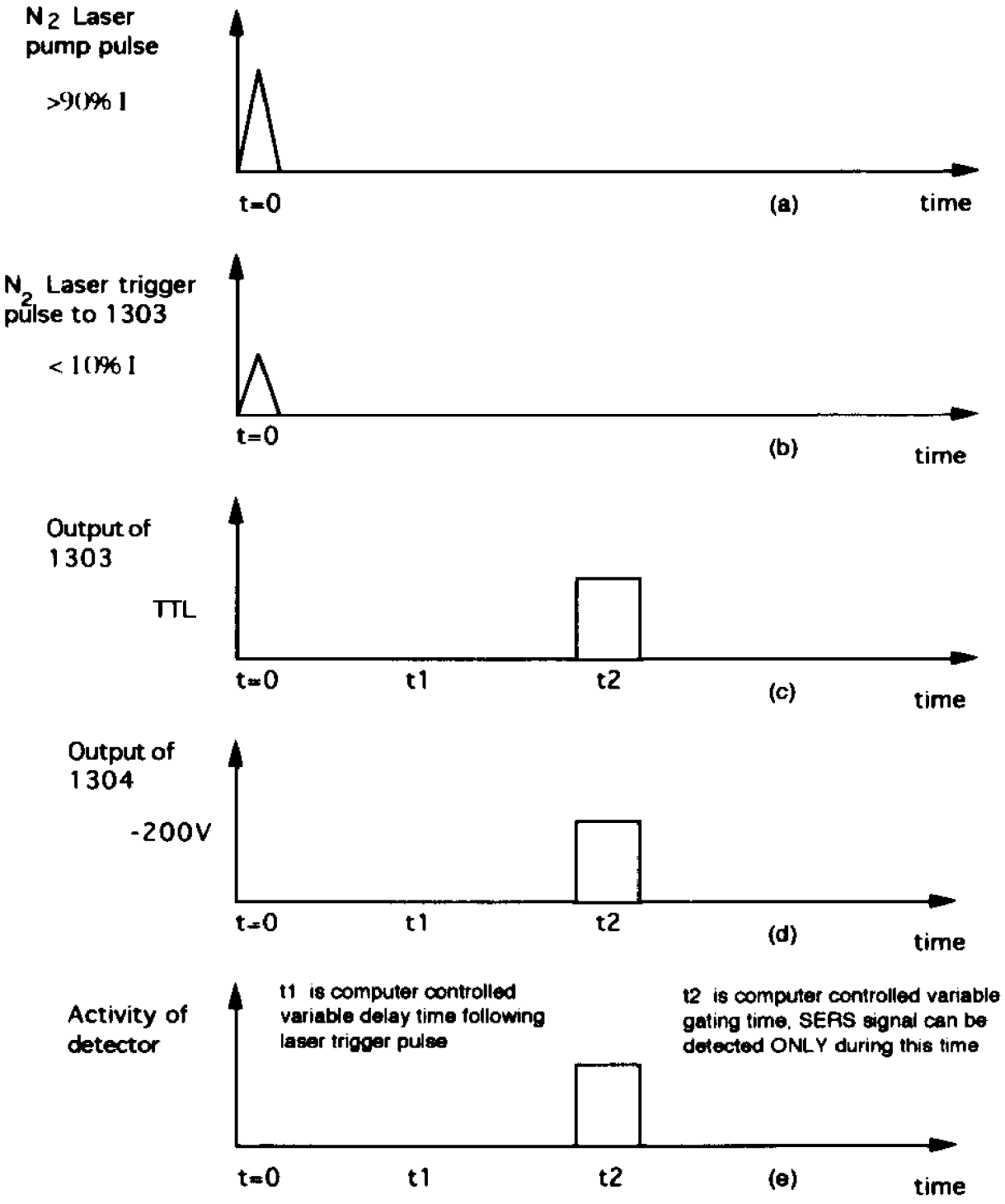
N2 Laser
pump pulse
>90% I
t=0
(a)
time
N2 Laser trigger
pulse to 1303
< 10% I
t=0
(b)
time
Output of
1303
TTL
t=0
t1
t2
(c)
time
Output of
1304
-200V
t=0
t1
t2
(d)
time
Activity of
detector
t1 is computer controlled
variable delay time following
laser trigger pulse
t2 is computer controlled variable
gating time. SERS signal can be
detected ONLY during this time
t=0
t1
t2
(e)
time

Figure 2.2

Figure 2.3 Single-shot TRSERS instrument for ms to second in-situ real time probing of potential induced electrochemical reactions. A Tracor Northern OMA and diode array detector were employed. An Ar^+ laser beam is applied to the working electrode of the electrochemical cell with simultaneous application of voltage waveform. An entire SERS spectrum is obtained within the dwell time of the detector and this spectral acquisition is repeated under OMA control several times during the duration of one or more cycles of the potential waveform.

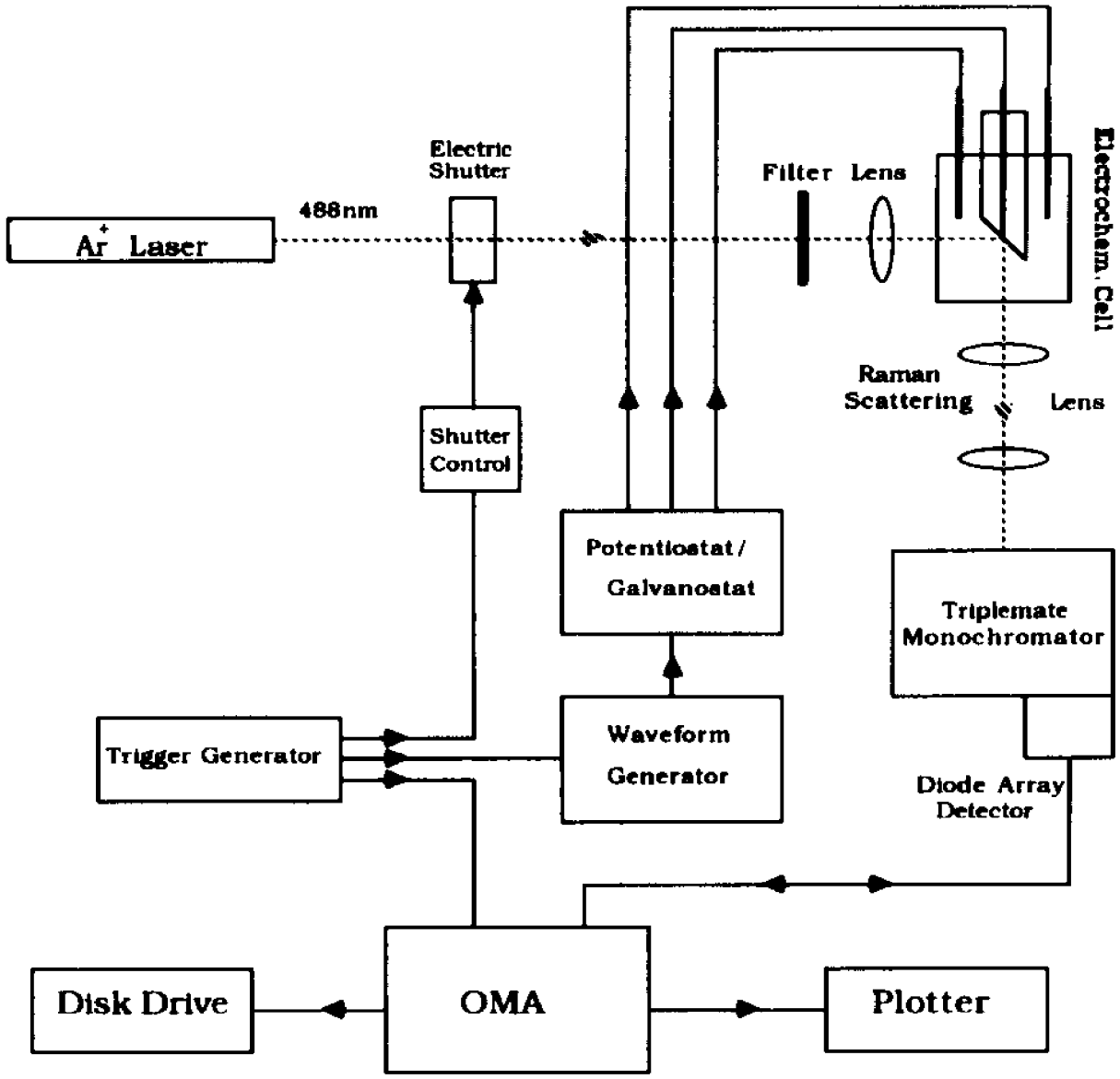

Figure 2.3 Single-shot TRSERS instrument for ms to second in-situ real-time detection of potential induced reaction.

Figure 2.4 Timing sequence for TRSERS measurements with a voltage ramp waveform in the instrumental set-up of Figure 2.3. (a) Sequence of TTL pulses from the trigger generator. (b) Triangular voltage ramp applied to the working electrode. Depending on the OMA used up to around 40 spectra can be obtained on one or more cycles of the waveform. (c) Schematic of the rise time of the electronic shutter which controls the rise time of the light on the working electrode. (d) Control of the diode array detector activity by the OMA. The delay time between acquisition of each spectrum is t_1 and the time of the detector dwell time is t_2.

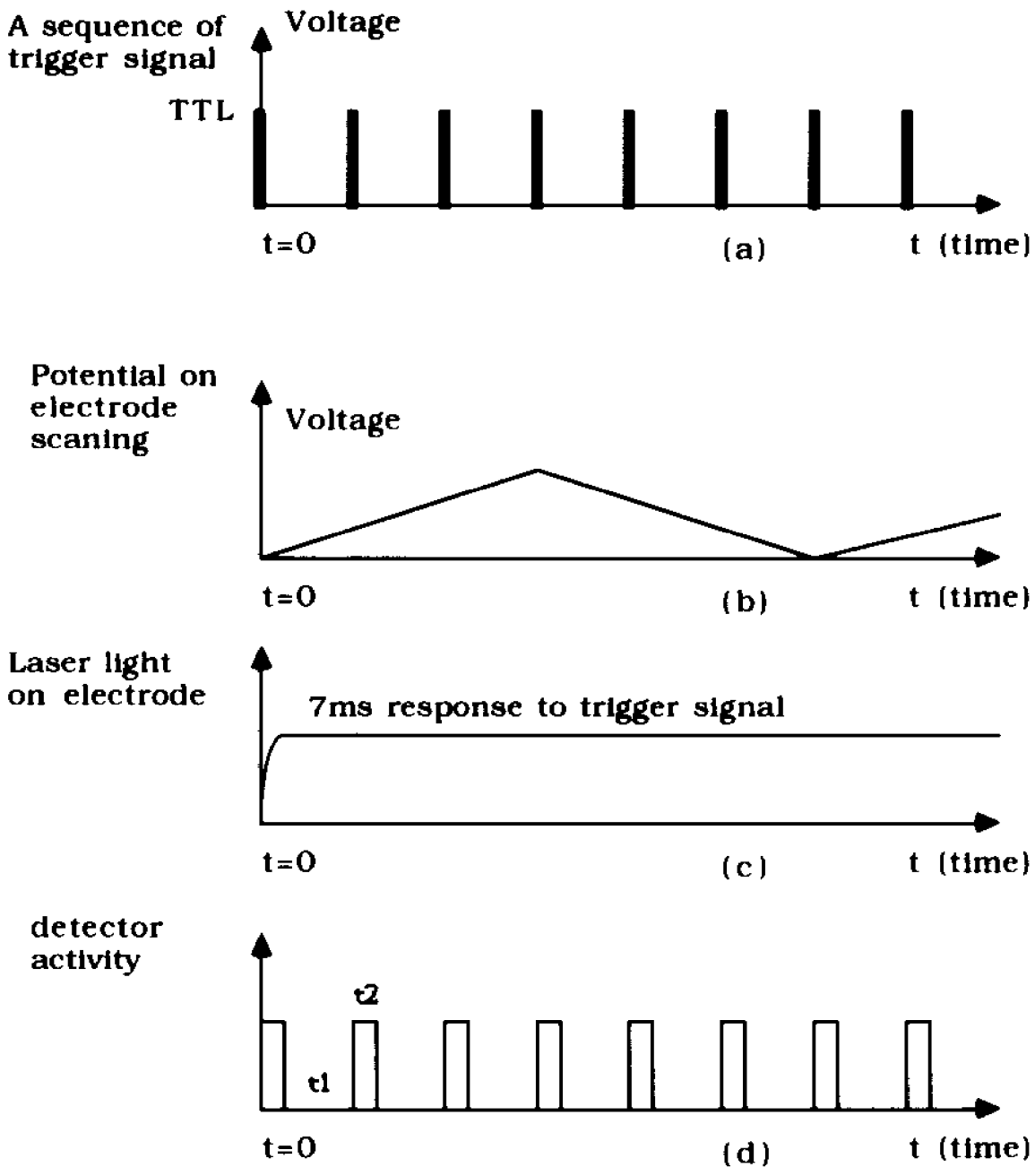
A sequence of trigger signal
Voltage
TTL
t=0
(a)
t (time)
Potential on electrode scaning
Voltage
t=0
(b)
t (time)
Laser light on electrode
7ms response to trigger signal
t=0
(c)
t (time)
detector activity
t2
t1
t=0
(d)
t (time)

Figure 2.4

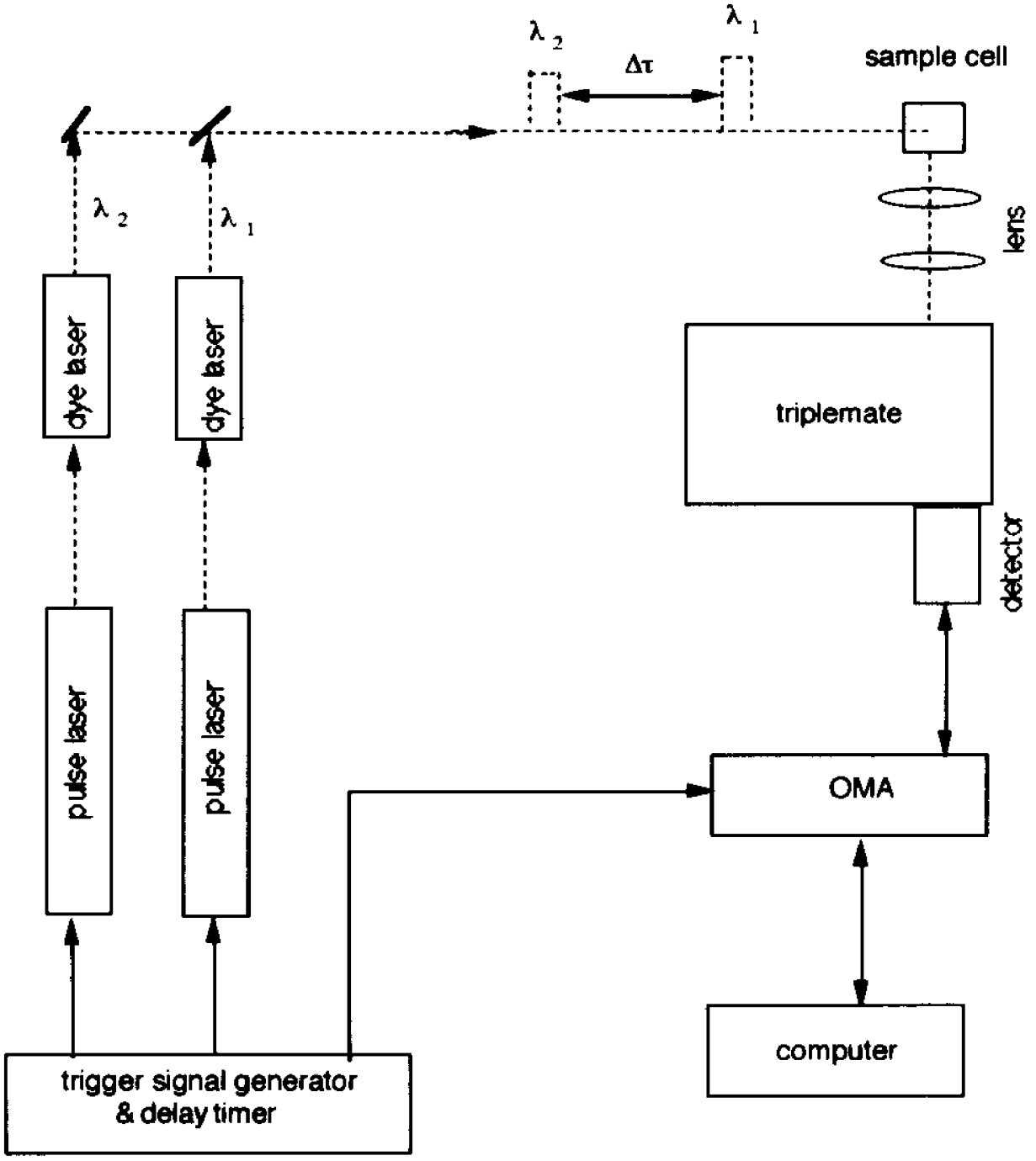

Figure 2.5 Proposed optical pump-probe TRSERS instrument for ns to ms time scale studies. Two pulse lasers and electronic timing device are employed.

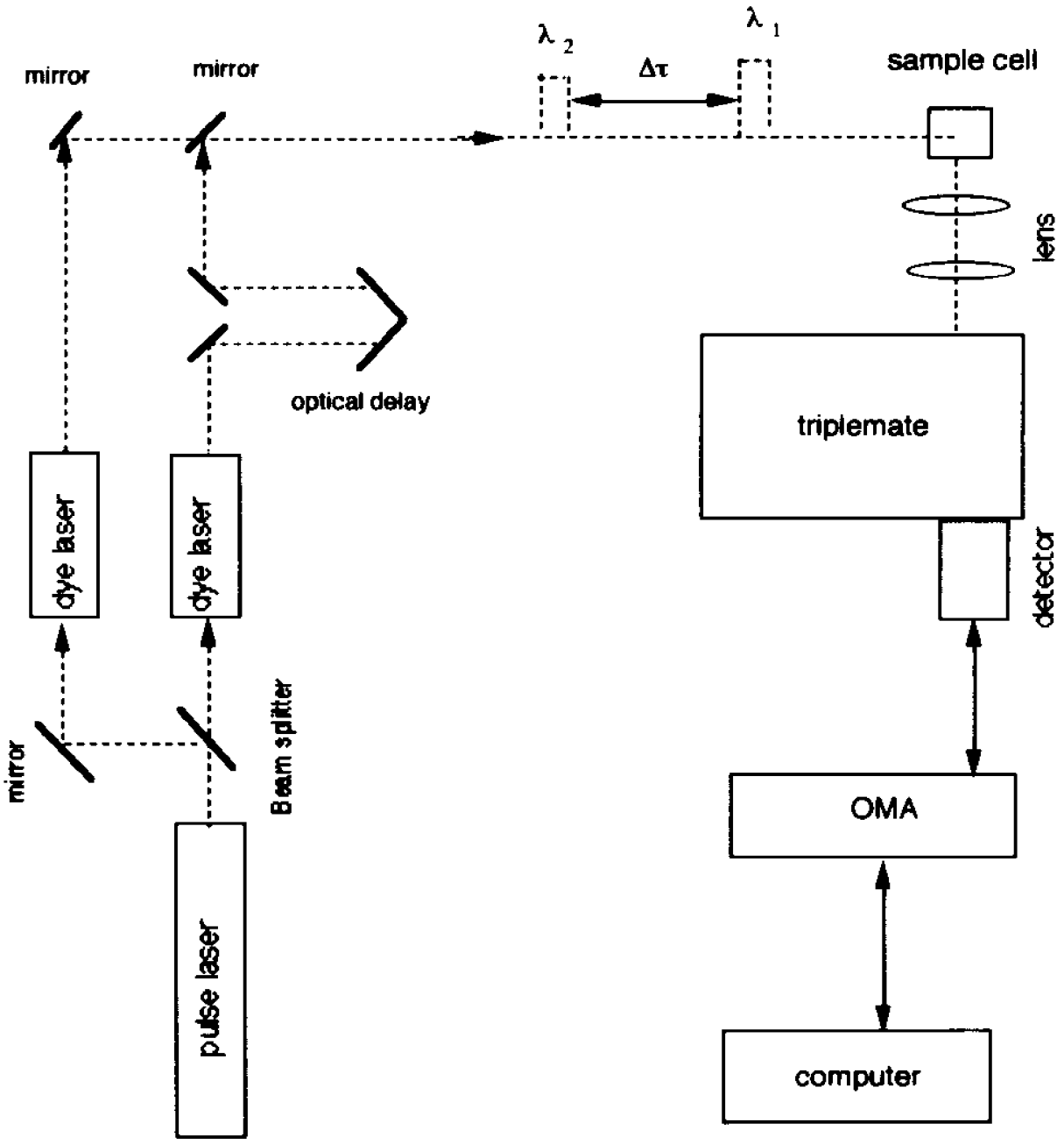

Figure 2.6 Proposed optical pump-probe TRSERS instrument for fs to ns time scale studies. Two pulse lasers and optical time delay system are employed.

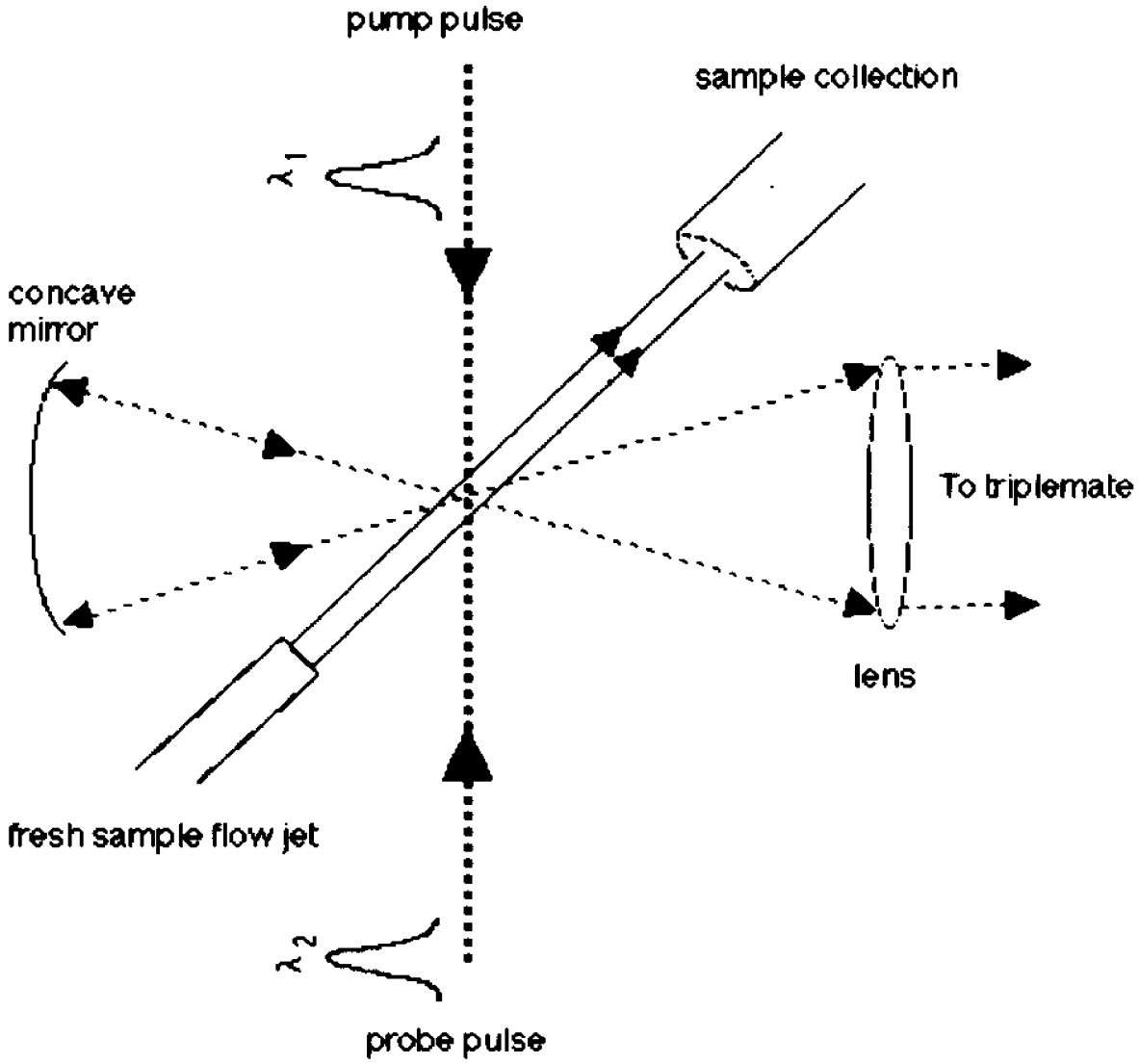

Figure 2.7 Windowless flow jet sample cell for TRSERS experiment by using a flowing colloid sample.

Chapter 3 Time Resolved SERS Study of Direct Photochemical Charge Transfer Between FMN and a Ag Electrode

3.1 Introduction

In almost all flavoproteins the flavin is found in the forms of flavin mononucleotide(FMN) or flavin adenine dinucleotide(FAD). FMN and FAD are coenzymes which contain an isoalloxazine ring, and in the process of flavoprotein catalysis, the isoalloxazine ring plays an essential role. For this reason, the structure of flavin derivatives and their various reaction mechanisms have been extensively studied by various techniques such as UV-Vis absorption [1,2], circular dichroism [3], nuclear magnetic resonance [4], fluorescence [1,2], electrochemistry [5,6], IR [7], resonance Raman ,RR, [8,9] and surface enhanced Raman scattering , SERS [10-12]. Among spectroscopic methods, SERS has the advantage of higher sensitivity and that fluorescence is quenched, thereby facilitating the acquisition of vibrational spectra at very low concentration. SERS applied to research on free flavin derivatives and chromophore organic compounds has been well established [13,14]. In the present study, we amplify our previous Time-Resolved SERS (TRSERS) investigation [10] of free flavins adsorbed on a silver electrode surface.

TRSERS has been applied to study electrochemical dynamic processes, such as adsorption and desorption processes of organic molecules on electrodes [15,16] and to spectroelectrochemical cyclic voltammetry experiments. [17-20] We have also emphasized the use of this technique to investigate photo-induced charge transfer processes. [10,20] For example, in our study of the time evolution of the SERS spectrum of p-nitrobenzoate adsorbed on Ag island films and roughened Ag electrodes, [21] we found that a red-shifted photo-induced charge transfer process occurs at the Ag-adsorbate surface as a result of

illumination with 488 nm Raman excitation light (Ar^+ laser). [21] This process involved electrochemical and chemical reactions coupled to the photoprocess causing spectral changes to takes place in the millisecond to second time range. [19-21] The photolytic process for adsorbed flavins on Ag electrodes [10] induced by 337 nm light is a much faster process, and in order to study this process, we developed a TRSERS ns pump-probe technique. [10]

Our previous report was in the form of a letter [10] and in the present study, we have more fully considered the TRSERS spectral results. This earlier work[10] demonstrated that a nanosecond 337 nm nitrogen laser pulse induced two distinct short-lived photo products of FMN. The first photoproduct was produced within the first 75 ns (laser pulse plus initial detector delay), while the second product decayed to the initial reactant within 1500 ns. Both products remained adsorbed on electrode during the reaction and were shown to be cation forms of FMN. However, in our previous work there was insufficient experimental evidence to unequivocally identify these species. In this study, we provide further proof of the identity of these two photoproducts. Photoproduct I is shown to be an enolized form of the radical cation, while we show that the longer lived photoproduct II is the keto (i.e. unenolized) form of the radical cation. These identifications are made on the basis of additional evidence provided in part by deuterium substitution. The resulting spectral shifts are analyzed by normal coordinate calculations which enable localization of vibrational motions to well-defined parts of the molecule. Since all the vibrations involved are on the three isoalloxazine rings, we supplement our studies with lumiflavin(LF) which is composed entirely of the isoalloxazine ring system. This is especially useful in confirming the normal coordinate analysis.

We also have examined an interesting application, FMN as a dye utilized

in a surface modified photogalvanic cell to convert solar energy to electric energy or hydrogen gas. Our TRSERS and photogalvanic results, along with photo-induced potential as a function of incident photon energy , and photo-current measurements lead to the conclusion of a direct charge transfer mechanism at the surface for the FMN-Ag electrode system. Thus a photogalvanic effect for dye modified metal electrodes is found which is localized to the interface and quite different from the traditionally proposed photogalvanic mechanisms which involve excited dye molecules in solution.

3.2 Experimental Section

Flavin mononucleotide (FMN), lumiflavin (LF) and D_2O were purchased from Sigma Chemical Co. and used as received. Reagent grade K_2SO_4, EDTA (as the disodium salt) and $NaHSO_4$ were purchased from Fisher Scientific Co. and used as received. All aqueous solutions were prepared with deionized distilled water and deaerated by nitrogen bubbling for 20 min. before starting each experiment. The pH of solution was adjusted by adding reagent grade H_2SO_4 and NaOH and measured with an Orion Research digital ionalyzer (Model 720). The deuterated solutions were prepared in a nitrogen gas bag just before starting each experiment and purged with nitrogen gas at the top of solution during the experiment.

The sample cell consisted of a silver working electrode with 1.11 mm^2 geometric surface area, a Pt counter electrode, and a saturated calomel electrode (SCE) as the reference. All potentials reported in this study are quoted vs. SCE. For the SERS and TRSERS experiments of FMN, the Ag electrode

was roughened by an oxidation-reduction cycle, ORC, pretreatment which was accomplished in the presence of FMN ($1x10^{-4}$ M) in 0.1M K_2SO_4 aqueous solution by applying a potential step from -0.4V to 0.5V for one second. For the SERS and TRSERS experiments of deuterated FMN, the Ag electrode was roughened by the same process as for FMN, i.e., in the presence of the deuterated FMN ($1x10^{-4}$ M) in 0.1M K_2SO_4 deuterated aqueous solution. For these pretreatment conditions, about a monolayer of FMN or deuterated FMN was adsorbed on the Ag electrode (see the voltammetry section below). After the ex-situ ORC pretreatment, the Ag electrode was placed in solution and SERS and TRSERS experiments ,as well as other experiments mentioned above, carried out in 0.1M K_2SO_4 aqueous or deuterated supporting electrolytes in the absence of FMN in solution. Hereafter, the FMN in aqueous solution is referred as (3N-H)FMN or FMN, and the FMN in deuterated solution is referred as (3N-D)FMN, in which the N_3-H is deuterated. Figure 3.1 shows the structure and atom numbering of isoalloxazine ring of flavins.

The SERS experimental setup was similar to that described elsewhere [22]. A Spectra Physics Model 164 argon ion laser at 488 nm was used as a Raman excitation source. The laser power at the electrode was approximately 30 mW. Spectra were recorded with a Spex Model 1401 double monochromator with a wave number resolution of 2 cm^{-1}. Photon counting detection was used. SERS spectra were used to monitor the potential threshold vs incident photon energy by varying the applied potential and the incident photon energy until a photo-product spectrum was observed. Yellow or red light was obtained with a Spectra Physics Model 375 tunable dye laser, while a high power Spectra Physics Model 2020 argon ion laser was used to obtain a 350 nm CW line .

The pump-probe TRSERS instrumental set up was described in detail in

our earlier report [10]. In the TRSERS experiments, adsorbed FMN or (3N-D)FMN were excited by a nitrogen laser pulse of 1mJ/pulse and 10ns pulse width. Excited FMN, (3N-D)FMN or their photo-product intermediates generated by 337 nm laser pulse were probed by the 488nm line of the Ar^+ ion laser. The excitation was followed by a delayed probe in which the detector was gated. The exciting nitrogen laser pulse energy density on the electrode surface was adjusted by changing the focus of the impinging light or the nitrogen gas pressure of the nitrogen laser. In order to ensure overlap of the two laser beams, the 337 nm laser pulse was focused to about 0.1 cm^2 on the Ag electrode. The energy density on the electrode surface of the exciting nitrogen laser pulse was about $1x10^6$ W cm^{-2}. For steady-state photoproduct studies, a 350 nm CW laser line was used as a pump beam with the 488 nm CW probe beam in the same overlapping configurations as in the pulsed studies.

Linear sweep voltammetry (LSV) experiments were carried out using a EG&G PARC Model 175 universal programmer and EG&G PARC Model 173 potentiostat. The Ag electrode was roughened by applying an electrode potential step from -0.4V to +0.5V for one second. In our experiments, three types of Ag electrodes were used; (1) a smooth electrode, (2) an electrode roughened in K_2SO_4 electrolyte solution and (3) an electrode roughened in FMN+0.1M K_2SO_4 electrolyte solution.

Photogalvanic effect studies were carried by observing photo-current vs time curves, photo-current as a function of FMN surface concentration, photo-current vs incident light intensity, and photo-current or photo-potential vs incident photon energy (the photo-current action spectrum). The photogalvanic device consisted of two compartments connected by a salt bridge. A two electrode system was used with a Ag working electrode in one compartment on which

FMN was adsorbed by pretreatment as in SERS experiments. A Pt counter electrode was used in the other compartment. The working electrode was immersed in a solution containing only EDTA in $NaHSO_4$ or K_2SO_4 electrolyte, and the Pt electrode was immersed in a solution containing only $NaHSO_4$ aqueous electrolyte. A Keithley picoammeter (model 614) electrometer and X-Y recorder was used for these experiments.

The photo-current vs. potential experimental arrangement is shown in Figure 3.2. A CW Ar^+ laser line 488 nm used as an excitation light source. A light chopper was used to modulate the light. A lock-in amplifier, Keithley model 840 Autoloc amplifier with an auxiliary 103A nanovolt amplifier, EG&G PARC Model 175 universal programmer and EG&G PARC Model 173 potentiostat as well as three electrode system were used in this experiment. Current was measured as function of scan potential as shown in Figure 3.3.

3.3 Results and Discussion

3.3.1 Steady State SERS Measurements

Figure 3.1 shows the structure and atom numbering of isoalloxazine ring of flavins. The FMN and LF only differ by the R group which is bonded to N_{10} on ring II. Figure 3.4(a) shows the SERS spectrum of oxidized (3N-H)FMN adsorbed on a roughened silver electrode at an applied potential of -0.4V vs. SCE with only K_2SO_4 aqueous solution in the bulk when excited with 488 nm laser light. The solution contained 0.1M K_2SO_4 at a pH about 7. As found by cyclic voltammetry, at this pH the electrochemical reduction of FMN occurs at electrode potentials more negative than -0.5V vs. SCE. The SERS spectrum of

oxidized LF, which was obtained under the same experimental condition as FMN, reveals the identical SERS spectra as FMN. This indicates that the side chain is not involved in SERS enhancement or that in any case the side chain does not affect the vibrational modes of the isoalloxazine ring very much in these experiments.

Figure 3.4(b) shows the SERS spectrum of oxidized (3N-D)FMN adsorbed on a roughened silver electrode at an applied potential of -0.4V vs SCE in D_2O with 0.1M K_2SO_4 solution when excited with 488nm laser light. The (3N-D)LF SERS spectra is identical to (3N-D)FMN. Comparing the SERS spectra of (3N-D)FMN and (3N-D)LF with the SERS spectra of (3N-H)FMN and (3N-H)LF, the SERS bands of (3N-D)FMN and (3N-D)LF show the same shift and relative intensity changes. This implies that the replacement of H by D influences only the isoalloxazine vibrations.

3.3.2 TRSERS Results for (3N-H)FMN and (3N-D)FMN

The (3N-H)FMN and (3N-D)FMN nanosecond time resolved SERS experiments were carried out at an applied potential -0.4V vs. SCE. Two kinds of photo-product intermediates, which were induced by nitrogen pulse laser at 337 nm, were observed by TRSERS. A cation form of the FMN photo-product intermediate caused by one-electron photooxidation was implied by potential threshold vs excited laser light energy and photo-potential measurements.[10] Further evidence for this process is seen in the photo-current vs. electrode potential measurements in Figure 3.3 for the FMN coated Ag electrode. In the absence of 488 nm laser light on the Ag electrode, Figure 3.3(a), there is no photo-current. However, in the presence of the laser light an anodic current

results as the potential is moved in the positive direction clearly showing that a cationic flavin species is produced from the film at the electrode surface. It is shown below that this mechanism of photo induced charge transfer from FMN to the Ag electrode under electrochemical control is supported by the TRSERS results and our normal mode calculations.

For the purpose of analysis and discussion, we reproduce our previous TRSERS results [10] , Figure 3.5 and 3.6. Figure 3.5(a) shows the stationary SERS spectrum of FMN at applied potential -0.4V, and Figure 3.5(b) shows the TRSERS spectrum of FMN delayed by 75ns from the initiating laser pulse. The wave numbers on these spectra have been recalibrated with a resolution of 2 cm^{-1} and show a 3-4 cm^{-1} increase for all bands over the previously reported values. [10] Figure 3.5(c) shows the difference spectrum for Figure 3.5(b) and 3.5(a) which high-lights the photo-product TRSERS spectrum. Figure 3.6 shows the time evolution of the photo-product spectra from 75 ns to 775 ns. Comparing the stationary SERS spectra with the TRSERS results, the following changes are found:

a) The TRSERS spectra change both in wave number and intensity with time. The intensity of the difference spectra decrease with time finally decaying to zero at 1500 ns. Thus the final product is converted back to FMN itself under an applied potential of -0.4V vs SCE. This is also confirmed by the fact that stationary SERS spectra which were taken before and after TRSERS experiments are exactly overlapped.

b) Bands at 1398 cm^{-1}, 1424 cm^{-1} and 1540 cm^{-1} in the stationary spectrum, Figure 3.5(a), disappear at 75 ns TRSERS. New bands at 1196cm^{-1}, 1534cm^{-1} and 1554cm^{-1} appear at 75ns, Figure 3.5(c).

c) The band at 1196cm^{-1} , which is a new band in the 75 ns TRSERS,

Figure 3.5(c), disappears at 775ns and a new band at 1326cm^{-1} appears at 775ns, Figure 3.6(c).

d) Band shifts from 1092 cm^{-1} to 1096 cm^{-1}, 1260 cm^{-1} to 1272 cm^{-1}, 1348 cm^{-1}, to 1362 cm^{-1}, and 1576 cm^{-1} to 1580 cm^{-1}, occur at 75 ns, Figure 3.5. The band 1096 cm^{-1} shifts to a higher wave number at 1099 cm^{-1}, but the band at 1272 cm^{-1} shifts to a lower wave number at 1255 cm^{-1}, at 775 ns, Figure 3.6.

From the above observations, which are quite reproducible, the TRSERS spectral results show two types of spectra with time. One is observed in the 75 ns to 775 ns time range and the other in the 775 ns to 1500 ns time range. Thus at least two kinds of photo-product intermediates exist after the 337 nm initiating laser pulse. We denote photo-product I (PP-1) as the species produced at times shorter than 75 ns, and photo-product II (PP-2) as the species produced at 775 ns which then decays at the longer time scale.

The time resolved SERS experimental results along with the potential threshold vs excitation light photon energy, photo-induced (with 488nm laser light) transient current vs. applied potential as well as photo-voltage vs. incident light photon energy measurement results [10] (see also discussion below) indicate that the photo-products are a cation form of FMN and undergo a photo-enolization process.

Thus we propose that the over all photo-induced kinetic process or the mechanism can be described as follows:

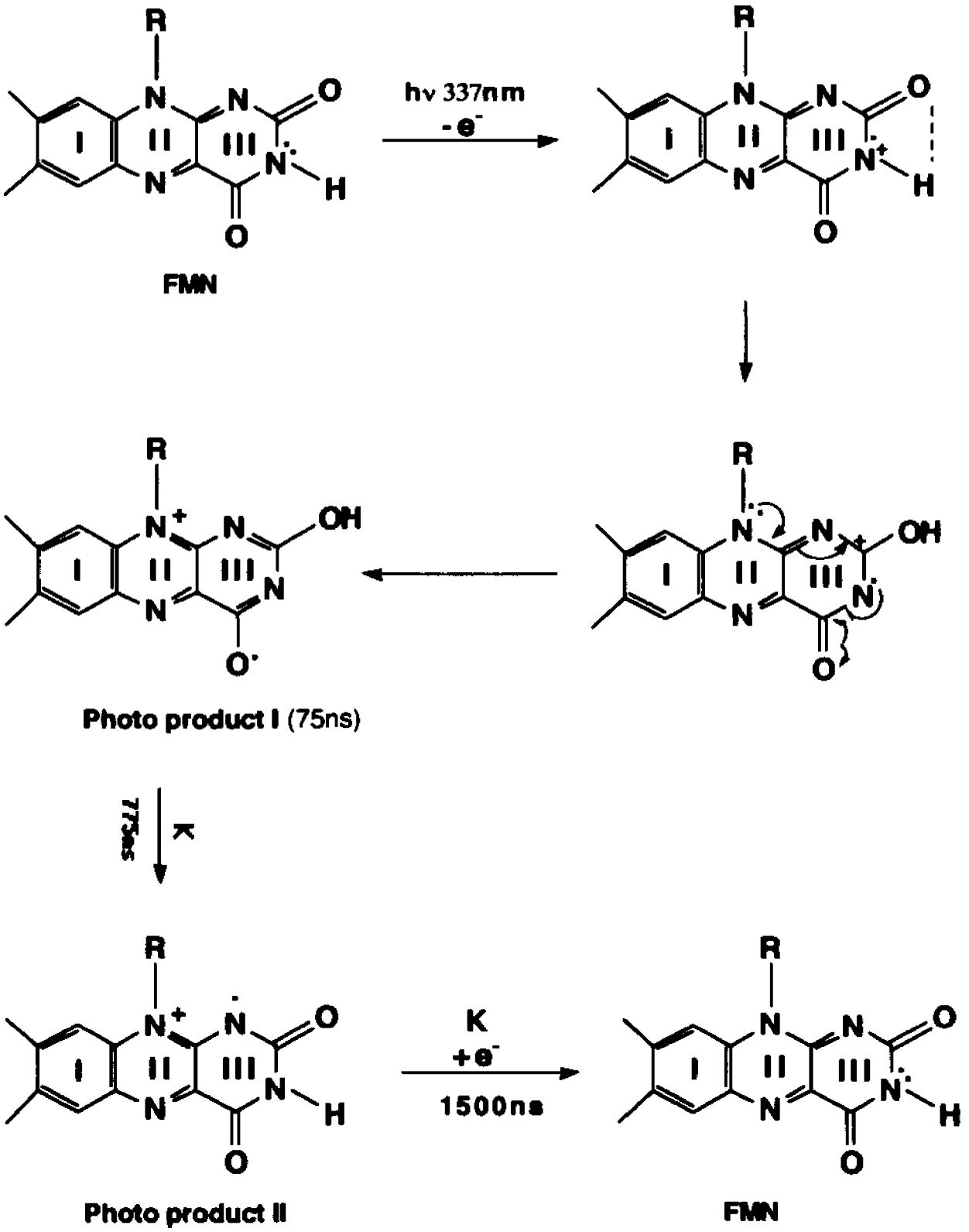
hν 337nm
-e⁻
FMN
Photo product I (75ns)
K
Photo product II
K
+e⁻
1500ns
FMN

In addition to a TRSERS pump-probe experiments, the same photoproducts can be observed with steady-state pump-probe experiments, as we previously described for FMN in making a plot of threshold potential vs. photon excitation energy. [10] In this experiment, a CW 350 nm laser line is focused on the electrode for excitation and a CW 488 nm laser line is used to detect the SERS spectrum of FMN at -0.4V, Figure 3.7. It is seen that a better S/N ratio is found compared with the TRSERS spectra of FMN obtained using the pulsed nitrogen laser for excitation. The resulting difference spectrum, Figure 3.7c , is a mixture of the two photoproducts , PP-1 and PP-2 identified by TRSERS. It is clear from Figure 3.7, which has less noise than the TRSERS of the same system at 75 ns, that the bands at 1398 and 1424 cm^{-1} (clearly seen in either Figures 3.4a or 3.7a) disappear in the spectrum of the product bands (Figure 3.7c) and that a new band is observed at 1194 cm^{-1} in the photoproducts. Also, the same band shifts and band splitting which occur on going from parent FMN to photoproduct-1, noted in the discussion above, part b) and d), for the 75 ns TRSERS result can be observed between Figure 3.7c and 3.7a for the steady state spectra excited by 350 nm light .

TRSERS experiments were also made with deuterated FMN in deuterated aqueous electrolyte solution. In Figure 3.8, curve (a) shows the stationary SERS spectrum of (3N-D)FMN at applied potential -0.4V, curve (b) shows the TRESRS spectrum of (3N-D)FMN delayed by 75 ns from the initiating laser pulse, and curve (c) shows the normalized difference between (a) and (b). Many of the spectral band shifts in the 75 ns TRSERS spectrum of (3N-D)FMN are similar to those band shifts found on exciting (3N-H)FMN. However, a significant new feature with the deuterated species is that a band at 1172 cm^{-1} in the parent

spectrum, Figure 3.4b or 3.8a, disappears at 75 ns on pumping with 337 nm light. Also new bands, were observed to be present at 848, 900, 926, 1070, 1228, 1397, 1522, 1540, and 1592 cm^{-1} at the same delayed time, 75 ns. The bands clearly seen at 926 cm^{-1} and 1070 cm^{-1} in the 75 ns are indicative of a new intermediate species and these bands are still evident at 2 μs finally decaying after ms illustrating that the deuterated species involves much slower kinetics than the protonated species. The increased noise observed in the TRSERS spectrum of (3N-D)FMN may be due to decreased production of the deuterated radical species.

3.3.3 Normal Mode Assignments for SERS of Oxidized FMN , LF, and Photoproduct I in Aqueous and D_2O Solution

In Table 3.1 are listed the assignments of the SERS bands for (3N-H)FMN and (3N-D)FMN. The calculated normal mode wave number and potential energy distribution (PED) of each normal mode are also listed in this table. These assignments were obtained by; (1) Comparing our steady state (3N-H)FMN, (3N-H)LF SERS results with (3N-D)FMN and (3N-D)LF steady state SERS results, (2) by examining the TRSERS experimental results, (3) by comparing steady state SERS and TRSERS experimental results with our own normal mode calculations, and (4) also by comparing our results with the experimental results from resonance Raman, isotopic substitution resonance Raman, and normal coordinate calculations cited in chapters by Abe [8] and Morris and Biestock. [9] The bands are listed in order of decreasing wave number.

The molecular parameters and the force constants used in our normal mode calculation were adopted from Abe's work [8]. The first step in our normal

mode calculation was to reproduce these results [8]. Then we employed a SIMPLEX optimization program to fit our SERS experimental results by automatically optimizing the force constants. The difference between resonance Raman [8,9] and SERS, therefore, shows up in the calculated differences for the PED of the two calculations, i.e. , the former using solution force constants to fit resonance Raman data and the latter using SIMPLEX optimization to fit the SERS data. The differences should represent effects on the internal modes of the molecule caused by interactions between molecule and Ag surface and changes in solvation at the surface. A detailed discussion of these interactions and band assignments for SERS spectra of the redox series : FMN cation, FMN, semiquinone FMN and hydroquinone FMN will be published in another paper [23]. On the other hand , in the present paper we present the details of spectral assignments for the nondeuterated and deuterated photoproduct species which also requires a discussion of the assignments for (3N-H)FMN and (3N-D)FMN as well.

Comparing our SERS spectra with RR spectra [8,9], we can find that they have a parallel pattern in frequency and intensity. Most of the bands of SERS are the same as that of RR. However, some changes can be observed. These changes are attributed to the different interactions between FMN molecules with different substrates, such as with Ag electrode in SERS and with protein in some resonance Raman results. [8,9] The similarity and difference in spectra will also be shown in the two calculations. As listed in Table 3.1, most of our calculated frequencies and the PEDs are the same as Abe's [8]. We discuss here only the bands which are different from Abe's results and the bands which are important in order to analyze the TRSERS results in later sections. These bands also show the most significant changes in SERS spectra on going from (3N-H)FMN to (3N-

D)FMN upon deuteration.

The observed band of (3N-H)FMN at 1424cm^{-1} disappears upon deuteration in the (3N-D)FMN and (3N-D)LF SERS spectra. This band can be assigned to the calculated mode of 1421 cm^{-1} which is primarily the N_3-H bending mode coupled with ring III and a C=O stretching mode. Two new bands, 1172 cm^{-1} and 948 cm^{-1} which appear in (3N-D)FMN or (3N-D)LF SERS spectra, seem to correspond to calculated normal mode bands at 1154 cm^{-1} and 923 cm^{-1} which can be assigned to the N_3-D bending normal mode.

Observed bands which were shifted to higher wave number upon the deuteration are 1398 cm^{-1} to 1404 cm^{-1}, 1348 cm^{-1} to 1352 cm^{-1}, and 1260 cm^{-1} to 1290 cm^{-1}. There are bands above 900cm^{-1} which shift to lower wave number such as 1280 cm^{-1} to 1246 cm^{-1} and 1092 cm^{-1} to 1084 cm^{-1}. These bands which shift on deuteration are primarily assigned to ring II and ring III stretching vibrational modes. The band 1398 cm^{-1} most likely corresponds to the calculated mode at 1397 cm^{-1} which is attributed to a ring III, N_1-C_2-N_3-C_4 and N_3-H stretching mode, while on deuteration the corresponding up-shifted band at 1404 cm^{-1} is attributed to ring III, N_1-C_2-N_3-C_4 coupled with C_2=O stretching. The band at 1348 cm^{-1} which shifts to 1352 cm^{-1} upon deuteration corresponds to the calculated mode at 1354 cm^{-1}. This band is attributed to the ring II, N_{10}-C_{10a}, N_{10}-Me and C_{9a}-C_{5a} , stretching modes. The band at 1260 cm^{-1} which has a large isotopic shift to 1290 cm^{-1} upon deuteration, has been discussed by many authors. [8,9,11] This band is mainly attributed to a pure ring III stretching mode. This large wave number shift is explained as due to fact that the substitution of a heavier atom for hydrogen in this bending mode lowers the coupling of ring III stretching with N_3-H bending.

The band at 1280 cm^{-1} may be assigned to the calculated mode at 1281

cm^{-1}. This band is mainly attributed to ring II, C_{9a}-N_{10}-C_{10a} , coupled with ring III C_4-N_3 stretching mode. While the corresponding band at 1246 cm^{-1} upon deuteration, is attributed to ring II C_{9a}-N_{10}-C_{10a}-C_{4a} stretching. The band 1092 cm^{-1} was assigned to calculated mode at 1092 cm^{-1} which is attributed to the ring II stretching and C-H bending mode.

The normal mode calculations for photo-product I, the cationic enol form of either (3N-H)FMN or (3N-D)FMN, were carried out by reference to the work of Evans. [24] To execute the normal coordinate analysis for FMN photo-product I, we adjusted the geometrical parameters for FMN to reflect the changes of our proposed enol structure, applied the resulting force field from the FMN calculations and optimized. The geometrical parameter adjustments were the following: (1) The bond lengths on rings II and III were expected to change the most during enolization. The bonds N_{10}-C_{10a}, N_1-C_2, and N_3-C_4 were adjusted to double bond length, 1.310 Å, and bond N_1-C_{10a} was adjusted to single bond length, 1.380Å. (2) The C_2-O and C_4-O were adjusted to single bond length and the proton on N_3 shifted to the oxygen on C_2. The C-O single bond length, O-H bond length and the C-O-H angle were taken from phenol calculations[24], as 1.36Å, 0.96Å and 118^0, respectively.

After making these structural adjustments and their corresponding internal coordinate changes, we transferred the force constants from phenol calculations [24]. These force constants included the C-O stretches, C-O-H bending, C-C-O bending and the C····H, C····O non-bonding interactions. Without any modifications, these force constants reproduced fairly well the bands at 1200 cm^{-1} in PP-1 spectrum and the 926 cm^{-1} in deuterated PP-1. Since neither of these bands appear in the FMN spectra, the calculations confirmed that PP-1 does have an enol form. These results are not surprising since the calculated

frequencies of the C-O-H and C-O-D deformations in PP-1 are close to those of phenol. What the calculations actually prove is that coupling with other modes in PP-1 does not change the frequencies of the C-O-H and C-O-D deformations much. The final calculations for PP-1 reproduced the known fundamental frequencies with an average error of 0.38%. The results accounted for new peaks and for the relative shifts from steady state FMN frequencies and confirmed the expected changes in force constants. Table 3.3 and 3.4 shows the comparison of observed frequency shifts from FMN to PP-1 and those shifts based on the calculations. Table 3.5 shows force constant changes from FMN to PP-1.

3.3.4 Analysis of TRSERS Spectra of Photo-products

Detailed analysis of the vibrational modes of bands which undergo change on photo-initiation indicates that the bands 1092 cm^{-1} and 1348 cm^{-1} which shift to higher frequency at 75 ns belong to ring II stretching vibrational modes, while the band at 1260 cm^{-1} which also shifts to higher frequency at 75 ns is attributed to a pure ring III stretching mode. That these bands shift to higher frequency at short times implies an increase of bond order or aromaticity of the three member isoalloxazine ring at ring II and ring III of the photo-product I intermediate.

The bands at 1398 and 1424 cm^{-1} which we assign to the N_3-H bending mode disappear at 75 ns and a new band at 1196 cm^{-1} appears at this time. This 1196 cm^{-1} band is assigned to mixed C-O-H bending and stretching vibrational mode (calculated at 1200 cm^{-1}) in our normal mode analysis. The observation that these two bands are lost with time supports the conclusion that a proton

transfer is taking place within this time domain. The proton transfer is most likely direct from N_3-H to the adjacent carbonyl to form a new C-O-H bond within 75 ns.

At the longer time, 775 ns, the band at 1196 cm^{-1} which was assigned to C-O-H bending and stretching mode disappears, and a new band at 1326 cm^{-1} appears which are consistent with a new ring III secondary amine stretching mode. These changes indicate a de-enolization process of photo-product I on going to photo-product II under electrochemical control. Also the band at 1272 cm^{-1} which is attributed to a ring III stretching mode shifts to lower frequency at 1255 cm^{-1}, while a band at 1096 cm^{-1} which mainly involves a ring II stretching mode shifts only slightly to 1099 cm^{-1}. The other ring II and III stretching modes remain unchanged at times longer than 775 ns. Thus for photo-product II, one of the ring III stretching vibrational modes has shifted to lower frequency indicating a loss of some bond order or aromaticity. On the other hand, the ring II stretching vibrational modes remain at the same frequency as for photo-product I.

Some bands are observed for both photoproducts. For example, the band at 1540 cm^{-1} FMN which was assigned to N_5-C_{4a} and N_1-C_{10a} anti-symmetric vibrational modes by Abe's [8,9] and our normal mode calculations splits into two new bands at 1534 and 1554 cm^{-1} which appear in both photoproducts. The splitting of this band at 1540 cm^{-1} indicates electron density change at these two bonds on going from FMN to the photo-product intermediates.

Further experimental support for the photo enol-keto process comes from (3N-D)FMN TRSERS which was performed under the same experimental conditions as in the (3N-H)FMN TRSERS experiment. Comparing Figure 3.8a with Figure 3.8c, the most significant spectral shifts on going from the steady

state SERS of (3N-D)FMN to TRSERS of (3N-D)FMN at 75 ns are similar to those found in the TRSERS of PP-1 of (3N-H)FMN. These band shifts are listed in Table 3.2. The band at 1172 cm^{-1} which is attributed to the N_3-D bending mode disappears at the short time of 75 ns. New bands, which were attributed to the mixed C-O-D stretching and bending modes by our normal mode calculations for photo-product-1 of (3N-D)FMN, were observed at 1070 cm^{-1} and 926 cm^{-1} for the same delay time, 75 ns, Table 3.2b. Similar band shifts corresponding to ring II and ring III are also observed. The band 1084 cm^{-1} which is attributed to a ring II stretching mode shifts to 1092 cm^{-1}. The band at 1352 cm^{-1} which shifts to 1366 cm^{-1}, is attributed to a pure ring II stretching mode. These observations are additional evidence for the enol form for photo-product I and the aromaticity increase in ring II and ring III of this species.

New bands also are observed at 1592 cm^{-1}, 1540 cm^{-1} , 1522 cm^{-1}, 900 cm^{-1} and 848 cm^{-1} for (3N-D)FMN photo-product I. The band at 1592 cm^{-1} may correspond to the calculated band at 1602 cm^{-1} which was not SERS active in the FMN form, but may become SERS active in the photo-product I form. This band is attributed to ring II stretching. The 1540 and 1522 cm^{-1} bands can be assigned to the band calculated at 1545 and 1522 cm^{-1} which are new ring II and III stretching mode, respectively. These bands can be considered to result from a splitting of the 1538 cm^{-1} band of FMN. The bands at 900 cm^{-1} and 848 cm^{-1} can not be assigned with confidence since the PED calculation shows a dispersal of modes at these wave numbers. The 900 cm^{-1} band does not have a corresponding vibrational mode in our normal mode calculations. This band may belong to one of the out of plane vibration modes which are not included in our normal mode calculations.

The photoinduced spectral changes indicates the nature of the overall

photoinduced charge transfer mechanism. As shown above, at applied potential -0.4V, the photo-induced charge transfer from adsorbed FMN to Ag may occur at picosecond or even faster times. The slow charge transfer from the electrode back to FMN can be explained as follows; The electronic orbital overlap between FMN and metal is formed when FMN is adsorbed on the electrode. Likely coordination groups come from the lone pair electrons of nitrogen and oxygen on ring III. The nitrogen laser pulse excites an electron from an FMN orbital, possibly an n orbital, into empty states of the metal conduction band at or above the electrode Fermi level. Following this electron transfer step, the cation form of FMN undergoes a molecular geometry rearrangement with the proton at N_3 transferring to the C=O group to form the C-O-H group. This geometrical rearrangement may cause the cation of FMN to undergo electron density rearrangement on the isoalloxazine rings in order to minimize the system's total energy and to form a new electronic orbital overlap between the FMN cation and Ag sites on the electrode surface. A higher energy gap and a lower transition moment for electron transfer between the FMN cation, PP-1, and Ag sites is generated during the rearrangement process which prevents reverse charge transfer from the electrode to the cationic FMN molecules. Furthermore, the intermediates, photo-product I and II, are relatively stabilized by their structure and electron rearrangement which increases their aromatic character. Comparing the three rings of the isoalloxazine ring system of neutral FMN with photo-product II and photo-product I , neutral FMN has only one aromatic ring (ring I) , photo-product II has two aromatic rings (ring I and II) , whereas photo-product I has three aromatic rings in the isoalloxazine structure. It is likely that the aromatic character of the intermediates lowers the energy of the photo-products and stabilizes their life-time.

3.3.5 Relationship Between the Photo-Product Formation, Photon Energy, and Electrode Potential

The potential threshold experiments [10] for the stationary SERS spectra of photo-products as a function of exciting photon energy reveal that the SERS spectrum of photo-product I can *only* be observed at relatively *higher* photon energy. The wave lengths for this process fall in the FMN absorption band of 350 nm or shorter (in fact, under 350nm excitation, the observed stationary SERS spectra are a mixture of photo-product I, II and FMN). However, the SERS of photo-product II is observed using a *lower* exciting photon energy with wave lengths which fall in the lowest FMN absorption band at 460nm or longer. For the latter case, as long as the exciting photon energy and the Fermi level of the electrode satisfy the relationship:

$$h\nu \geq \kappa\,(E_F^{(0)} - eV) - E_{HOMO} \qquad (1)$$

photo-product II can be observed. Here $h\nu$ is the exciting photon energy, κ is a constant which depends on conditions at the electrode and the adsorbed FMN layer, such as the double layer conditions, adsorption geometry etc., E_{HOMO} is the HOMO energy level of FMN, $E_F^{(0)}$ is the Fermi level of the electrode in the absence of an electrostatic potential, and V is the Galvanic potential drop between the electrode and the adsorbed species. Strictly speaking, E_F is defined here as the electrochemical potential of the electron in the metal and E_{HOMO} as the difference in electrochemical potentials of the adsorbed FMN^+ and FMN species. A change in applied potential, E_{app}, between the Ag electrode and a

reference electrode will cause a change in V at the Ag/FMN interface. The energy required for photons to promote an electron from FMN to the electrode Fermi level depends on the energy gap between E_F and E_{HOMO} which can be controlled by E_{app}. A more positive applied potential and thus more positive V reduces the energy gap between the E_{HOMO} and the Ag metal Fermi level. Thus less photon energy is required to promote an electron from E_{HOMO} of FMN to E_F of the electrode. In a previously reported experiment [10], a linear plot of exciting photon energy vs. E_{app} (potential threshold for photo-product appearance) was observed in the photon energy range from 2.9eV to 2.0eV which corresponds to wave length from 450nm to 610nm and applied potential from -0.4V to +0.2V. A linear least squares curve fit of these points gives the equation:

$$h\nu = 2.309 - 1.332\, E_{app}$$

with correlation coefficient $r^2 = 0.998$. In this range, only photo-product II is observed which is the solvent relaxed FMN radical cation. An extrapolation of the plot of photon energy vs. potential threshold to 0.0 photon energy gives a potential of 1.73 V. This value represents the applied electrode potential which would be necessary to oxidize FMN to FMN^+ in the dark.

The observed results for photo-product production suggest that the charge transfer mechanism is different in different photon energy ranges. The longer wave length with lower photon energy may only excite a π orbital electron at the HOMO of FMN to the metal Fermi level to form photo-product II. A short wave length such as 337nm with higher photon energy may excite the FMN's n orbital electron [1] (located at the N_3 atom) to the metal Fermi level . The loss of an electron at the N_3 n orbital then would initiate the proton transfer enolization

process. Therefore photo-product I can only be observed with 337 nm light in TRSERS experiments or with 350 nm light in steady state SERS experiments.

3.3.6 Voltammetry Study of the FMN Adsorbate

In order to provide an accurate interpretation of the photoelectrochemical process, it is important to know the structure of the adsorbed film of FMN molecules on the roughened Ag electrode surface. For example, a monolayer or submonolayer structure would have different chemical and energy transfer properties than a multilayer adsorption structure. Thus we conducted linear sweep voltammetry (LSV) experiments to investigate whether there was possibly a multilayer structure on the Ag electrode surface. The voltammetry experiments were conducted at varying solution concentrations and scan rates. By comparing the electrochemical results for roughened and smoothed electrodes, we estimated the surface area of the roughened Ag electrode and the surface concentrations of adsorbed FMN. In dilute solutions ($1x10^{-6}$M to $1x10^{-4}$M), the cathodic and anodic peak current for an adsorbed layer can be described by [25]

$$i_{pa} = -i_{pc} = (n^2 F^2 / 4RT) A \Gamma \upsilon \qquad (2)$$

where Γ is the surface concentration of the redox active species (mol/cm^2), A is the electrode surface area (cm^2), υ is the potential scan rate (V/s), n is number of electrons transferred per elementary electrochemical step (n=2), F is Faraday constant (96,500C/mol), R is gas constant (8.31J/mol K), and T is temperature (293K). i_{pa} and i_{pc} stand for the anodic and cathodic peak current, in unit of

Amperes. The roughened surface area and the surface concentration of adsorbed FMN are contained in equation (2).

Concentration and Scan Rate Dependence.:

We investigated the concentration dependence of the LS response of FMN in the range from $1x10^{-6}$ M to $1x10^{-4}$ M. In this concentration region, all three types of Ag electrodes (see experimental section) present a linear relationship between peak current and scan rate which shows that the electrochemical process can be described by an equation with the sweep rate dependence of equation 2. Figure 3.9 shows peak current vs scan rate plots. The first four cases, (a) to (d), represent different electrode roughening conditions, but with the voltammetry carried out in cases (a), (b) and (d) with FMN at $1.0 x10^{-5}$ M concentration in 0.1M K_2SO_4 solution. Curve (a) represents a smooth electrode LS voltammetry experiment. Curve (b) shows the results for an electrode which was roughened in bulk 0.1M K_2SO_4 solution. Curve (c) is a different in that the electrode which was roughened in presence of FMN at a concentration of $1x10^{-5}$ M in 0.1M K_2SO_4 electrolyte solution, but the LSV experiments were made with only 0.1M K_2SO_4 electrolyte in the bulk solution. Curve (d) shows results for an electrode which was roughened in the presence of FMN in 0.1M K_2SO_4 electrolyte solution, at a concentration of $1x10^{-5}$M and where the LSV experiments were made in the same solution as used for electrode roughening. One does not observed a great deal of difference on comparing (b), (c) and (d), the three plots for the roughened electrodes. This suggests that the roughened electrodes have almost the same surface area and surface concentration and that the diffusion current contribution to peak current is negligible at $1x10^{-5}$M concentration. Comparing curve (a) with curves (b), (c) and

(d), a difference in peak current between smooth and roughened electrodes is evident which most likely comes from different surface areas, because the experiments were all carried out at the same concentration of FMN ($1x10^{-5}$ M). Cyclic voltammetry experiments indicate that FMN undergoes either reversible or quasireversible electrochemical reaction under our experimental conditions, and since all plots of peak current vs scan rate are linear, equation (2) was applied to these experiments.

Surface Concentrations on Smooth and Roughened Electrode:

The smooth Ag electrode with 1mm diameter is cut at 45° to the longitudinal direction, which makes an elliptical surface with geometric area of $0.0111cm^2$. Applying eq.(2) to smooth electrode LSV experiments, gives $\Gamma=5.7x10^{-11}mol/cm^2$ at concentration $1x10^{-5}M$, and $\Gamma=3.5x10^{-11}mol/cm^2$ at concentration of $5x10^{-6}M$.

In order to determine the roughened Ag electrode surface area, the LSV experiments for the roughened electrode were done in the same solution with the same concentration as for the smooth electrode. With the FMN concentration from $1x10^{-6}M$ to $1x10^{-5}M$, the ratio of $i_{Rpc} / i_{Spc} = A_R\Gamma_R/A_s\Gamma_s$ is constant at different concentrations and at different scan rates where i_{Rpc} and i_{Spc} stand for cathodic peak current of roughened and smooth electrodes, respectively. A_R and Γ_R and A_s and Γ_s refer to the roughened electrode surface area and surface concentrations and the smooth electrode surface area and surface concentrations, respectively. Because A_R and A_s should not change in these experiments (the roughened electrodes have the same pretreatment in all experiments and therefore should have the same roughened surface area), the value $A_R/A_s = B$ is a constant. Since the ratio of $i_{Rpc} / i_{Spc} = B(\Gamma_R/\Gamma_s)$ is constant,

the ratio (Γ_R/Γ_s) of surface concentration of FMN on roughened and smoothed electrodes does not change with change in concentration and the scan rates. Therefore, we make the assumption $\Gamma_R/\Gamma_s = 1$ for dilute solutions. Then $i_{Rpc} / i_{Spc} = A_R/A_s = B$ is the ratio of roughened and smoothed surface areas. These experiments give $B=A_R/A_s = 1.7$, or $A_R=1.7A_s$ for all experiments.

Applying eq.(2) to the roughened electrode, with $A_R = 1.7A_s$ the LSV experiments gives $\Gamma = 6.2\times10^{-11}$ mol/cm^2 at concentrations of 1×10^{-5}M, and $\Gamma=3.5\times10^{-11}$ mol/cm^2 at concentrations of 5×10^{-6} M. These results are in agreement with the smooth electrode results. For a FMN concentration of 1×10^{-4} M, the electrode was roughened in the presence of FMN solution, and the LS voltammetry experiments were done in bulk 0.1M K_2SO_4 solution. A linear i_p vs υ scan rate plot was found as shown in Figure 3.9(e). Applying the same surface area ratio $A_R=1.7A_s$ and equation.(2), gives $\Gamma=19.28\times10^{-11}$ mol/cm^2. Our SERS and TRSERS experiments which were discussed in the previous section, were carried out at this surface concentration.

Several research groups [6, 26-27] experimentally determined the cross-sectional area of DNI (7,8-dimethyl-3,10-dinonylisoalloxazine) as 0.47 nm^2 molecule^{-1}, FMN as 0.51nm^2 molecule^{-1} and FAD as 1nm^2 molecule^{-1}, and a monolayer adsorption density as $\Gamma=36\times10^{-11}$ mol/cm^2 for DNI and $\Gamma=17\times10^{-11}$ mol/cm^2 for FAD. They assumed these molecules to be adsorbed with the isoalloxazine ring toward the electrode surface. From their results, a monolayer of adsorbed surface concentration of FMN is $\Gamma=33\times10^{-11}$ mol/cm^2. On this basis the FMN surface concentration on roughened electrode in our SERS and TRSERS experiments is most likely monolayer or less.

3.3.7 FMN Modified Ag Electrode Photogalvanic Effect:

Photo-current vs time experiments were carried out as shown in Figure 3.10a, the FMN was adsorbed on a roughened Ag electrode by an ORC electrochemical pretreatment and only EDTA and $NaHSO_4$ were present in solution as reductant and electrolyte during the photogalvanic experiment. The photo-current was shown to last for hours and even days without changing current intensity. When the current decayed to zero after a long time experiment, if we added some fresh EDTA solution in the photogalvanic cell, the photocurrent resumed. In typical photogalvanic experiments, we used a 3 mm diameter Ag electrode which was cut at 45° to give a surface area of 0.1 cm^2. From voltammetry, the roughened electrode was found to have a surface area 1.7 times that of the smooth electrode which gives a roughened surface area of 0.17 cm^2. The same roughness pretreatment procedure was applied as in Section (e) with FMN present in K_2SO_4 solution with a concentration of $1x10^{-4}$ M which gives a surface concentration $\Gamma = 19.3x10^{-11}$ mol/cm^2. The total FMN molecules adsorbed on the electrode are given by $A_R\Gamma = 3.27x10^{-11}$ moles. A typical photogalvanic experiment on this electrode gave 21 μA of current (210 $\mu A/cm^2$ current density) which lasts for several hours without change in the current. In this experiment, during one hour $7.56x10^{-2}$ C of electricity flows which corresponds to $7.83x10^{-7}$ moles of electrons. The electrons passed were 24,000 times more than the total adsorbed FMN molecules which shows that every FMN molecule undergoes an oxidation-reduction cycle at least 24,000 times during one hour. Thus the FMN molecules must undergo a reversible reaction process. The photovoltage with white light from a Dolan-Jenner 150 W quartz-halogen lamp which behaves as 3000 K black body radiator was ca. 0.4V at 24 μA as

compared to ca. 0.8V for the same conditions at open circuit.

We also measured the so-called action spectrum of photocurrent vs. wavelength and compare it to the solution absorption spectrum in Figure 3.10b. The exciting light for the action spectrum was obtained from various discrete lines of a high power Ar^+ ion laser. This laser light was reflected off a glass surface and passed on the normal through the cell window before impinging on the Ag electrode surface, Figure 3.10a. The power of the laser light which passed through the glass reflecting plate was adjusted to the same value for each frequency used and about 0.7 mW was focused on the electrode surface. The solution absorption spectrum of FMN shows two broad peaks which were fit to Gaussian functions and these fits have maxima at 367nm and 450nm and widths (twice the standard deviation of the Gaussian) of 63.5 and 52.3 , respectively. In solution the absorbance decreases to a negligible value at wavelengths greater than about 520 nm. We have also measured the absorption spectrum of FMN adsorbed on SnO_2 and on quartz coated thin (transparent) Ag film surfaces and find nearly the same maxima but the spectra show an absorption tail which goes out beyond 700 nm. For the action spectrum, the Gaussian fits have maxima at 362 nm and 436 nm and widths (twice the standard deviation) of 42.8. and 63.4 , respectively. Thus the peaks are slightly shifted towards the blue in the action spectrum. We also see from Figure 3.10b that there is a reversal in the peak heights between the action spectrum and the absorption spectrum. The reason that the relative sensitivity of the band at 362 nm is higher than the band at 436 nm in the action spectrum may be that the transition moment for electron transfer between the molecule and metal is larger with UV excitation than with visible excitation.

The photo-current is a direct measure of the quantum conversion

efficiency (QCE) of the process (electron flux/ photon flux), since for monochromatic illumination, this conversion efficiency can be expressed by the relationship:

$$QCE = 1240 \times i_{photo} / P_w \times \lambda_L \qquad (3)$$

with the photo-current, i_{photo}, measured in microamps/cm^2 and the light power, P_W, measured in Watts/m^2 at wavelength λ_L in nm. For our Ag/FMN electrode systems, the QCE was found be around 2.0 % for typical runs which compares favorable with a dye sensitized TiO_2 / FMN electrode system [28] where a QCE of only 1% was found.

An advantage of the Ag/FMN/EDTA system over the classical photogalvanic effect with the photo-sensitive dye in solution is the transparency of the solution in the former system. Thus the illuminated compartment has only the sacrificial reductant solution, EDTA + $NaHSO_4$, instead of the reductant and photo-sensitive dye solution, FMN+EDTA+$NaHSO_4$, and there is no light absorption from FMN in solution. In the classical photogalvanic process with the dye sensitizer (FMN) in solution, the redox process comes from excited dye molecules which form triplets and react with the sacrificial reductant in solution producing the reduced form of the dye and an oxidized form of the reductant. The reduced dye is then oxidized at the illuminated electrode surface. Such a process has been proposed for the FMN, EDTA system with a semiquinone radical formed as the reduced product species in the homogeneous redox reaction. [29] From our TRSERS results and the other experimental results discussed, we believe that in the photogalvanic process the photo-process occurs directly at the metal/adsorbate interface. We could not observe the

semiquinone radical or anion form of FMN using SERS when EDTA was added to the electrolyte solution. Thus illumination of the Ag electrode produces, by direct charge transfer from FMN to the electrode, short lived intermediates in the form of flavin cations which are quenched by redox reaction with EDTA at the electrode surface. Therefore, we propose that the FMN/EDTA photogalvanic system works as follows:

At the illuminated anode:

$$FMN_{(ads)} + h\upsilon \rightarrow FMN^{+}_{(ads)} + e^{-}$$

$$FMN^{+}_{(ads)} + EDTA_{(aq)} \rightarrow FNM_{(ads)} + EDTA^{+}_{(aq)}$$

where direct charge transfer from adsorbed FMN to Ag to form a cationic FMN intermediate takes place and the cationic FMN intermediate then can be reduced to FMN by EDTA. The charge transfer process must be faster than nanoseconds since the fluorescence is quenched in the SERS experiment.

At the dark cathode:

$$2H^{+} + 2e^{-} \rightarrow H_2$$

The overall reaction of this photogalvanic cell is

$$h\upsilon + 2EDTA + 2H^{+} \rightarrow H_2 + 2EDTA^{+}$$

where EDTA acts as the sacrificial reductant. In practice the oxidized EDTA breaks down to further oxidized products. The photon energy may be converted to either electrical or chemical energy.

This mechanism is consistent with the results of H. Shinohara and M. Gratzel et al. [28] who conducted a similar experiment with an FMN/TiO_2 electrode system. They measured the photo-current of FMN or RF coated on TiO_2 electrodes and found electron injection from photo-excited flavin into the conduction band of TiO_2.

3.4 Conclusion

The TRSERS spectral results, potential threshold vs excited photon energy experiments, transient photo-current results vs. applied potential under 488 nm laser light, photo-potential vs incident photon energy experiments, as well as photo-current direction in the photogalvanic effect, all support the proposed photooxidation mechanism for FMN modified Ag electrodes. The photo-induced molecule to metal charge transfer occurs directly from adsorbed FMN to the Fermi level of the Ag metal electrode. At the relatively high photon energy of 337 nm or 350 nm laser light, it is suggested that the electron transfers from the FMN n orbital to Fermi level of the metal. At lower photon energy, the electron may transfer from π orbital of FMN to metal electrode. The 337 nm laser pulse photo-induced intermediate is a cationic form which undergone a chemical enolization process. This chemical process is responsible for the slow back electron transfer which allows photochemistry to occur directly at the metal electrode surface. As we pointed out earlier [10], the photochemistry is red shifted so that while 254 nm light is necessary to produce flavin radical cations in solution, only 488 nm light is necessary to give the cation with the interfacial system, a red shift of 2.4 eV. The proton transfers back from the enol to the keto

form within 775 ns after laser pulse initiation which gives a measure of the kinetics of proton transfer rate in this system. The photo-induced charge transfer process as revealed by TRSERS measurements provides a very consistent mechanism for the Ag/FMN/EDTA photogalvanic process.

Table 3.1 Observed and calculated SERS frequencies of (3N-H)FMN and (3N-D)FMN in cm^{-1}, and the assignments from P.E.D.

No.	[3N-H]FMN SERS	[3N-H]FMN Normal Mode Cal.	PED	[3N-D]FMN SERRS	[3N-D]FMN Normal Mode Cal.	PED
4		1713	$\upsilon(C_4{=}O)59$, $\upsilon(N_3{-}C_4)8$		1709	$\upsilon(C_4{=}O)59$
5		1677	$\upsilon(C_2{=}O)52$		1666	$\upsilon(C_2{=}O)51$
6	1630	1629	$\upsilon(C_8C_9)16$, $\upsilon(C_6C_7)8$ $\upsilon(C_{5a}C_6)9$, $\upsilon(C_9C_{9a})9$	1628	1630	$\upsilon(C_8C_9)16$, $\upsilon(C_9C_{9a})9$ $\upsilon(C_{5a}C_6)9$, $\upsilon(C_6C_7)8$
7		1609	$\upsilon(C_{5a}C_{9a})25$, $\upsilon(C_{4a}N_5)7$		1608	$\upsilon(C_{5a}C_{9a})25$, $\upsilon(C_{4a}N_5)7$
8	1576	1576	$\upsilon(N_1C_{10a})24$, $\upsilon(N_{10}C_{10a})17$ $\upsilon(C_{4a}N_5)16$	1576	1575	$\upsilon(N_1C_{10a})23$, $\upsilon(C_{4a}N_5)17$ $\upsilon(N_{10}C_{10a})16$
9	1540	1538	$\upsilon(N_1C_{10a})25$, $\upsilon(C_{4a}N_5)22$	1538	1538	$\upsilon(N_1C_{10a})26$, $\upsilon(C_{4a}N_5)21$
10	1506	1502	$\upsilon(C_{9a}N_{10})14$, $\upsilon(C_{4a}N_5)13$	1504	1501	$\upsilon(C_{9a}N_{10})14$, $\upsilon(C_{4a}N_5)13$
11	1464	1465	$\upsilon(C\,Me)21$, $\upsilon(C_7C_8)15$	1460	1465	$\upsilon(C_8\,Me)20$, $\upsilon(C_7C_8)15$
12		1437	$\upsilon(C_8C_9)17$, $\upsilon(C_6C_7)17$		1436	$\upsilon(C_8C_9)20$, $\upsilon(C_6C_7)19$, $\upsilon(C_7C_8)14$
13	1424	1421	$\delta(N_3{-}H)46$, $\upsilon(C_4{=}O)9$ $\upsilon(C_2N_3)9$, $\upsilon(C_2{=}O)7$	**1172** **948**	**1172** **940**	$\delta(N_3{-}D)17$, $\delta(C_4{=}O)7$, $\upsilon(N_1C_2)8$ $\delta(N_3{-}D)36$, $\upsilon(N_1C_2)7$, $\upsilon(C_2N_3)8$
14	1398	1397	$\upsilon(N_3{-}H)16$, $\upsilon(N_1C_2)14$, $\upsilon(C_2N_3)11$	1404	1401	$\upsilon(C_2N_3)23$, $\upsilon(C_2N_1)21$, $\upsilon(C_2{=}O)10$
15	1348	1354	$\upsilon(C_{9a}C_{5a})13$, $\upsilon(N_{10}C_{10a})11$ $\upsilon(N_{10}\,Me)9$	1352	1353	$\upsilon(C_{9a}C_{5a})12$, $\upsilon(N_{10}C_{10a})11$, $\upsilon(N_{10}\,Me)10$
16	1308	1310	$\upsilon(N_5C_{5a})28$, $\upsilon(N_{10}C_{9a})9$	1306	1313	$\upsilon(N_5C_{5a})21$, $\upsilon(C_8C_9)9$
17	1280	1281	$\upsilon(N_{10}C_{9a})12$, $\upsilon(N_{10}C_{10a})11$, $\upsilon(C_4N_3)11$	1290	1298	$\upsilon(C_4N_3)30$, $\upsilon(C_2{=}O)7$
18	1260	1251	$\upsilon(N_3C_4)20$, $\upsilon(C_4C_{4a})13$, $\upsilon(C_{4a}C_{10a})13$ $\upsilon(C_2N_3)10$, $\upsilon(N_1C_2)8$,	1246	1254	$\upsilon(C_{10a}C4a)16$, $\upsilon(N_{10}C_{10a})15$ $\upsilon(N_{10}C_{9a})10$
19		1199	$\upsilon(C\,Me)21$, $\upsilon(C_6C_7)11$, $\delta(C{-}H)13$		1199	$\upsilon(C\,Me)21$, $\upsilon(C_6C_7)11$, $\delta(C{-}H)12$
20		1179	$\delta(C{-}H)36$, $\upsilon(C_8C_9)7$		1187	$\delta(C{-}H)26$, $\upsilon(C_4C_{4a})9$

Table 3.1 continue

21	1150	1148	δ(C -H)42, υ(C Me)12	1148	1148	δ(C -H)41, υ(C M_e)12
22	1092	1092	δ(C -H)19, υ(N_5 -C_{5a})12	1084	1084	δ(C -H)17, υ(N_5-C_{5a})10, υ(C_{4a} C_{10a})5
23	1060 1018	1024	υ(N_1 C_2)18, υ(C_2 N_3)11			
24	992	1012	υ(N_{10} Me)31, υ(C_{5a} C_6)9	1020	1012	υ(N_{10} Me)27, υ(C_{5a} C_6)10
25	866	867	υ(C_{4a} C_{10a})6, υ(N_1 C_2)6	856	856	υ(N_1 C_2)8, δ(C N_3 C)5
26	834	834	υ(C_9 C_{9a})10, δ(C_2=O)6	830	829	υ(C_9 C_{9a})10
27	806	809	υ(C Me)6, υ(C_4 =O)7, υ(C_2 =O)5	798 786	782	δ(N_3 -D)11, υ(C M_e)8
28	742	741	υ(C_7 C_8)26, υ(C Me)13, δ(CC_6C)9	738	740	υ(C_7 C_8)26, υ(C Me)13, δ(CC_6C)10
29	662	690	δ(C_4 =O)10, δ(C_2=O C)10	656	682	δ(C_4 =O)11, δ(C_2=O)11
30	642	640	υ(C Me)13, δ(N_{10} Me)6	638	639	υ(C Me)13, δ(N_{10} Me)5
31	618	618	δ(CN_3C)10, δ(C Me)7	618 602	615	δ(CN_3C)10, δ(C Me)7
32	570 556	564	υ(N_{10} Me)19, δ(C N_{10} C)9	564 554	564	υ(N_{10} M_e)19, δ(CN_{10}C)9
33	534	530	δ(C -M_e)10, δ(C N_1 C)8, υ(C Me)8	528	529	δ(C -M_e)9, δ(CN_1C)8, υ(C Me)8
34	498	488	δ(C Me)21, υ(C Me)14	494	488	δ(C Me)21, υ(C Me)14
35		444	δ(C_2=O)17, δ(C_4=O)9		442	δ(C_2=O)17, δ(C_4=O)9
36		385	δ(C-Me)24, δ(C_2=O)10	368	385	δ(C-M_e)24, δ(C_4=O)10
37	312	311	δ(N_{10}-M_e)11, δ(C-M_e)9	304	311	δ(N_{10}-M_e)11, δ(C-M_e)9
38		295	δ(N_{10}-M_e)11, δ(C-M_e)9		295	δ(C-M_e)11, δ(N_{10}-M_e)9
39		243	δ(N_{10}-M_e)22, δ(C-M_e)16		242	δ(N_{10}-M_e)22, δ(C-M_e)16
40		222	δ(C-M_e)92	198	222	δ(C-M_e)92, υ(C_7-C_8)7
41		150	δ(C-M_e)16, δ($N_5$$C_{4a}$$C_4$)6		149	δ(C-Me)16, δ(C_4 C_{4a} N_5)6

Table 3.2. Comparision of band shifts from (3N-H)FMN to photo-product I in H_2O with the band shifts from (3N-D)FMN to photo-product I in deuterium solution.

Table 3.2(a). TRSERS in aqueous solution.

Band Assignment	ring II & III	$\upsilon(N_1\text{-}C_{10a})$ $\upsilon(N_5\text{-}C_{4a})$	$\delta(N_3\text{-}H)$	δ(C-O-H)	ring II	pure ring III	ring II
(3N-H)FMN	1576	1540	1424, 1398		1348	1260	1092
PP-I in H_2O	1580	1554, 1534		1196	1362	1272	1096

Table 3.2(b), TRSERS in deuterium solution.

Band Assignment	ring II & III	$\upsilon(N_1\text{-}C_{10a})$ $\upsilon(N_5\text{-}C_{4a})$	$\delta(N_3\text{-}D)$	δ(C-O-D)	ring II	pure ring III	ring II
(3N-D)FMN	1576	1538	1172		1352	1404	1084
PP-I in D_2O	1578	1540, 1522		1070, 926	1366	1411	1092

υ ----- stretch; δ ----- bending

Table 3.3 Experimental and calculated SERS frequencies of FMN and photo-product I in H_2O solution. The FMN band assignments are also included.

Expt. (3N-H)FMN SERS (cm^{-1})	Calc. (3N-H)FMN SERS (cm^{-1})	Expt. PP-1 TRSERS (cm^{-1})	Calc. PP-1 TRSERS (cm^{-1})	Expt. Shift (cm^{-1})	Calc. Shift (cm^{-1})	(3N-H)FMN Assig.
1630	1629	1630	1628	0	-1	Ring I
1576	1576	1580	1578	+4	+2	Ring II & III
		1554	1546			$\upsilon(N_1\text{-}C_2)$
1540	1538					$\upsilon(N_1\text{-}C_{10a}, N_5\text{-}C_{4a})$
		1534	1522			$\upsilon(N_1\text{-}C_2, N_3\text{-}C_4)$
1424	1421					$\delta(N_3\text{-}H)$
1348	1354	1362	1364	+14	+12	Ring II
1308	1310	1308	1308	0	-2	Ring II & I
1260	1251	1272	1273	+12	+22	Ring III
		1196	1200			δ(C-O-H)
1092	1092	1096	1098	+4	+6	Ring II & I

υ--- Stretch; δ---Bending.

Table 3.4 Experimental and calculated SERS frequencies of FMN and photo-product I in D_2O solution. The FMN band assignments are also included.

Expt. (3N-D) FMN SERS (cm^{-1})	Calc. (3N-D) FMN SERS (cm^{-1})	Expt. PP-1 in D_2O TRSERS (cm^{-1})	Calc. PP-1 in D_2O TRSERS (cm^{-1})	Expt. Shift (cm^{-1})	Calc. Shift (cm^{-1})	(3N-D)FMN Assig.
1628	1630	1628	1628	0	-2	ring I
	1608	1592	1602			ring II
1576	1575	1578	1576	+2	+1	ring II, III
1538	1538	1540	1545	+2	+7	ring II, III
		1522	1522			ring III
1404	1401	1411	1419	+7	+8	ring III
		1397	1397			ring III
1352	1353	1366	1364	+14	+11	ring II
1306	1313	1301	1307	-5	-6	ring I, II
		1228	1228			ring II, III
1172	1172					N_3-D bending
1084	1084	1092	1094	+8	+10	ring II
		1070	1074			C-O-D bending
948	940					N_3-D bending
		926	930			C-O-D bending
		900				

υ--- Stretch; δ---Bending.

Table 3.5 Force constants optimized in the photo-product I calculations.*

FMN (mdyne/Å)	PP-1 (mdyne/Å)	Type
4.826	4.987	$K(N_{10}\text{-}C_{9a})$
4.209	4.176	$K(N_5\text{-}C_{5a})$
6.904	5.798	$K(N_5\text{-}C_{4a})$
3.170	3.458	$K(C_{10a}\text{-}C_{4a})$
6.397	5.672	$K(N_1\text{-}C_{10a})$
3.341	4.430	$K(C_4\text{-}C_{4a})$
4.276	4.472	$K(N_1\text{-}C_2)$
4.237	4.625	$K(N_3\text{-}C_4)$
4.295	5.581	$K(N_3\text{-}C_2)$
4.826	5.245	$K(N_{10}\text{-}C_{10a})$
	3.532	$K(C_2\text{-}O)$
	3.798	$K(C_4\text{-}O)$
	0.669	H(-C-O)
	0.456	H(C-O-H)
	1.518	F(...O)
	0.660	F(C(O)H)
0.306	0.410	ortho interaction

* K: stretch, H: bend, F: non-bonded interaction.

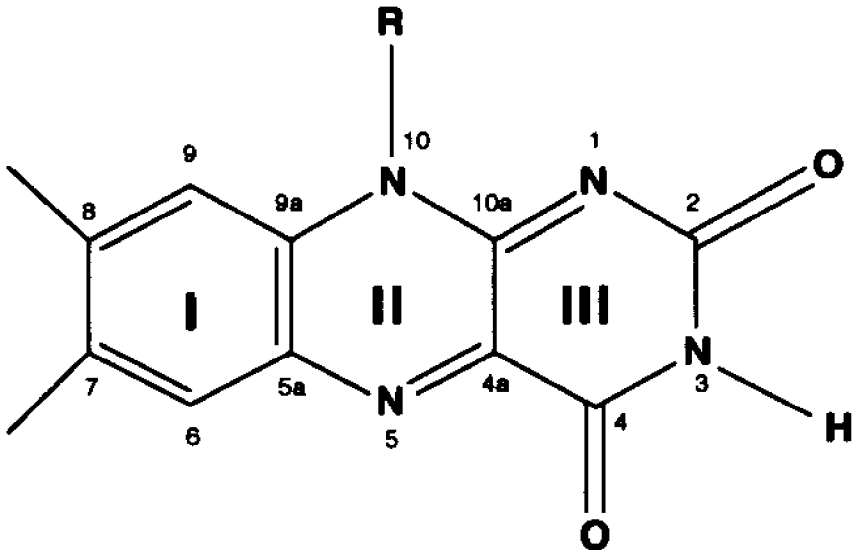

FMN: $R = CH_2\text{-}CH(OH)\text{-}CH(OH)\text{-}CH(OH)\text{-}CH_2(H_2PO_4)$

LF: $R = CH_3$

Figure 3.1 The structure and atomic numbering of the isoalloxazine ring of flavin.

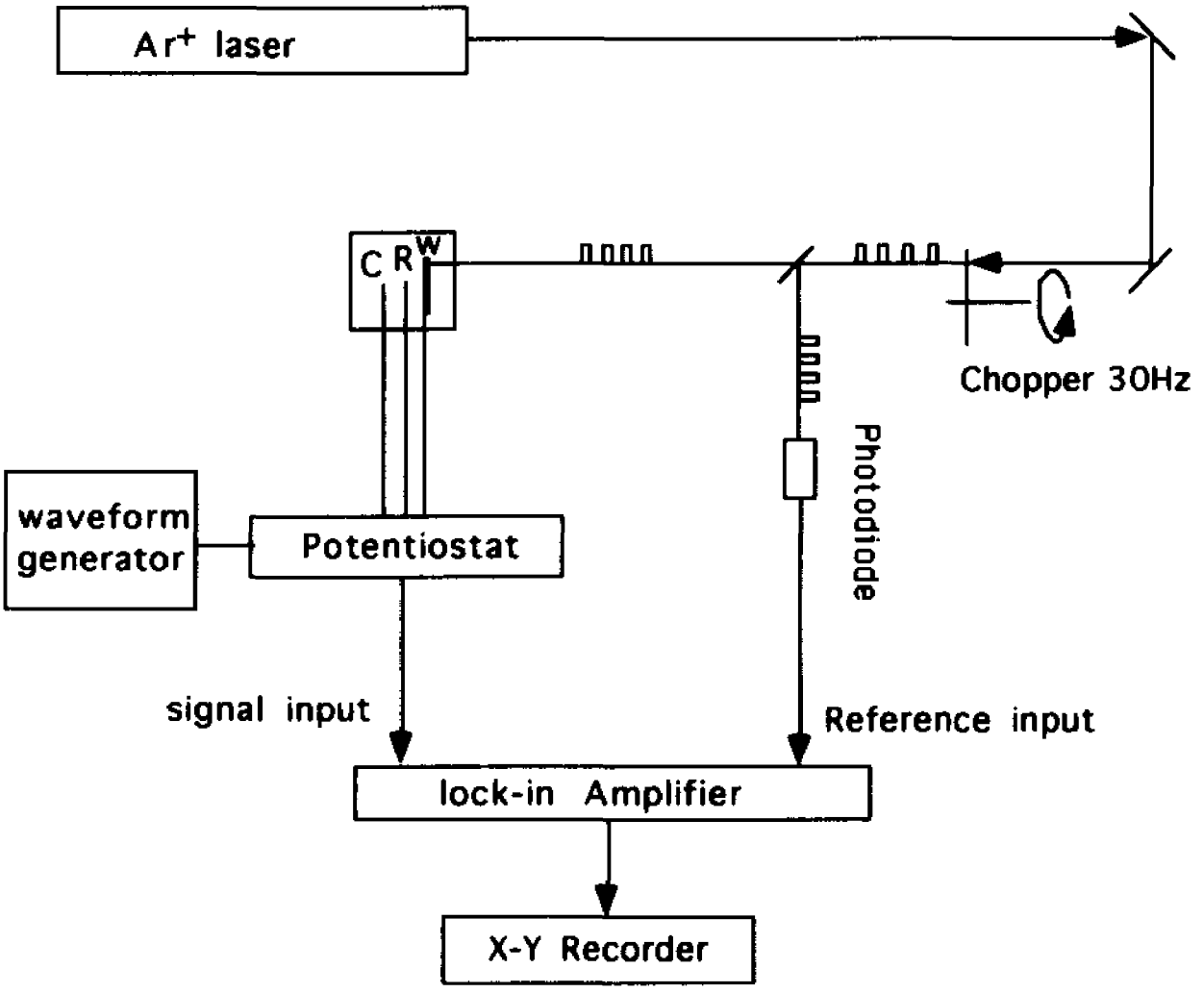

Figure 3.2 Experimental set-up for transient photocurrent studies. A CW Ar ion laser line at 488nm was used as an excitation light source with a light chopper and lock-in amplifier to eliminate the non photocurrent background

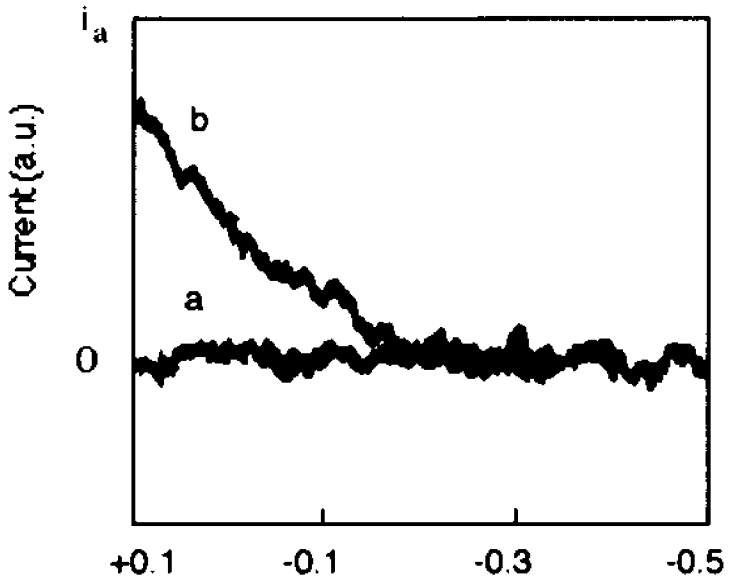

Figure 3.3 Transient photocurrent as a function of applied potential vs. SCE, recorded by using the set-up in Figure 3.2 during a positive-going potential sweep.
Curve (a) Photocurrent in the dark.
Curve (b) Photocurrent generated by 488nm laser light.

Figure 3.4 SERS spectra of FMN adsorbed on roughened Ag electrode at an applied potential -0.4V vs. SCE in pH 7.2 K_2SO_4 electrolyte solution. 488nm Ar^+ laser line used as excitation. (a) FMN in H_2O solution; (b) FMN in D_2O solution.

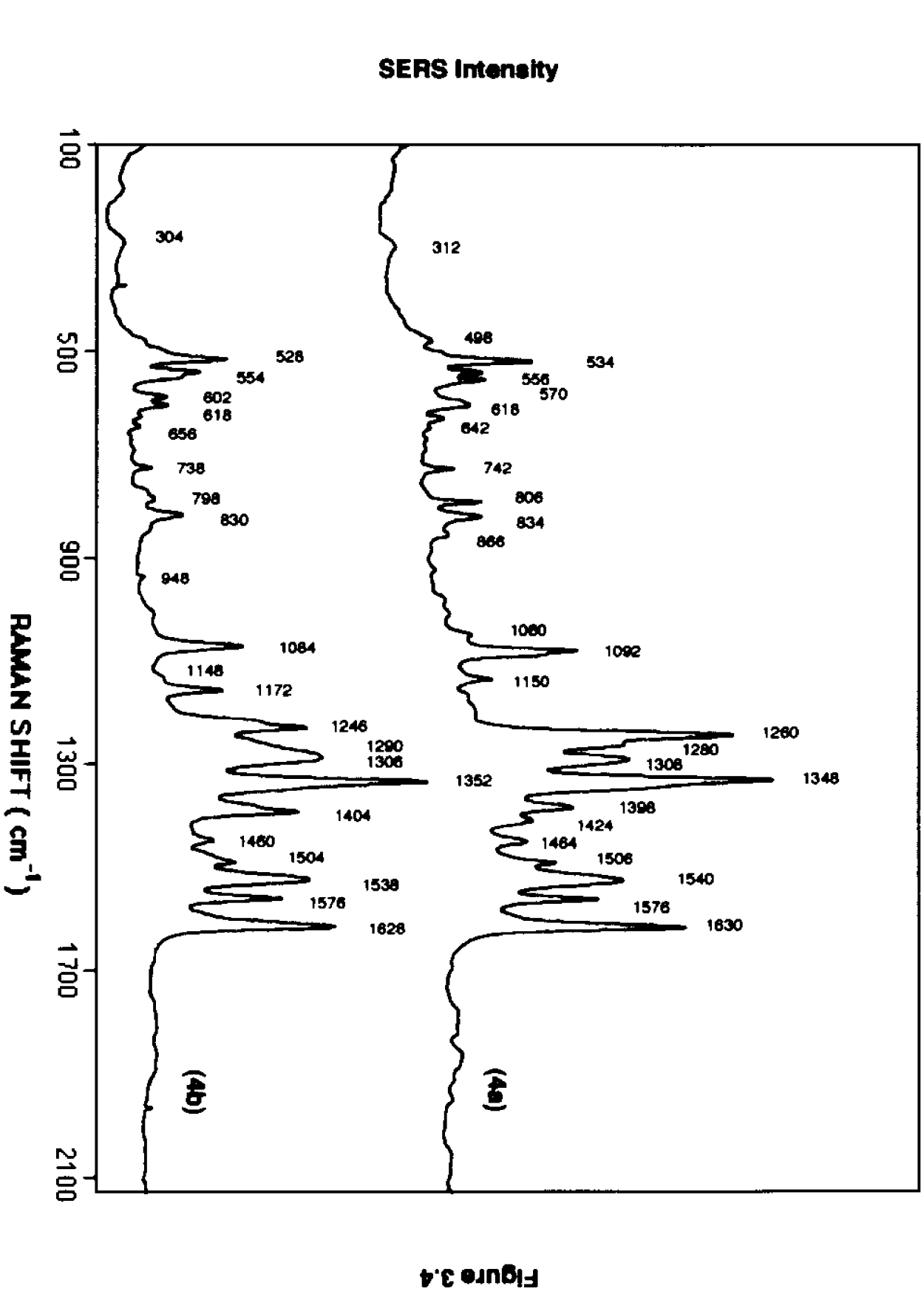
SERS Intensity
RAMAN SHIFT (cm-1)
100
500
900
1300
1700
2100
304
526
554
602
618
656
738
798
830
948
1084
1148
1172
1246
1290
1306
1352
1404
1460
1504
1538
1576
1628
(4b)
312
498
534
556
570
618
642
742
806
834
866
1060
1092
1150
1260
1280
1308
1348
1398
1424
1464
1506
1540
1576
1630
(4a)

Figure 3.4

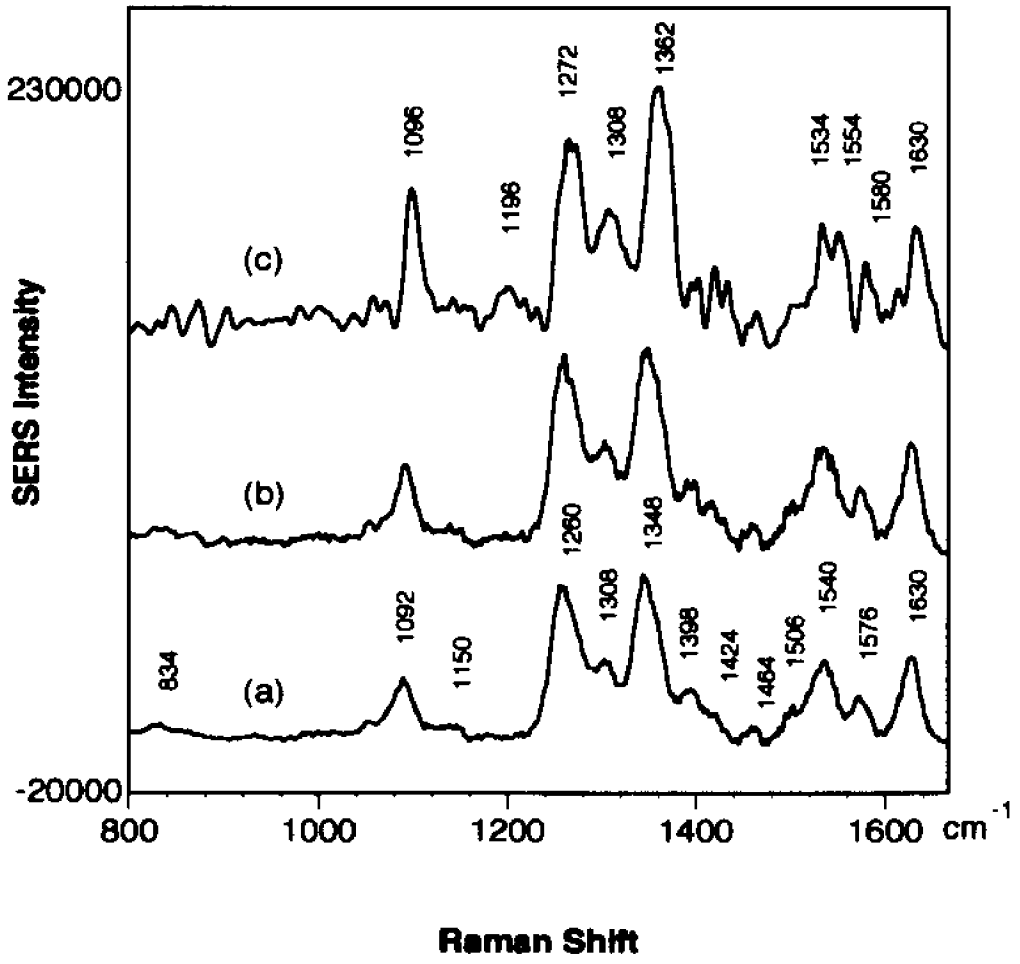

Figure 3.5 Time-resolved SERS spectra of flavin mononucleotide (FMN) at -0.4V vs. SCE on a roughened Ag electrode. Acquisition time: 200ns

(a): Spectrum detected by 488nm laser light alone;

(b): Spectrum detected by 488nm laser light with 75 ns time delay after 337nm nitrogen laser excitation;

(c): The difference spectrum of curve (b) and curve (a)x4

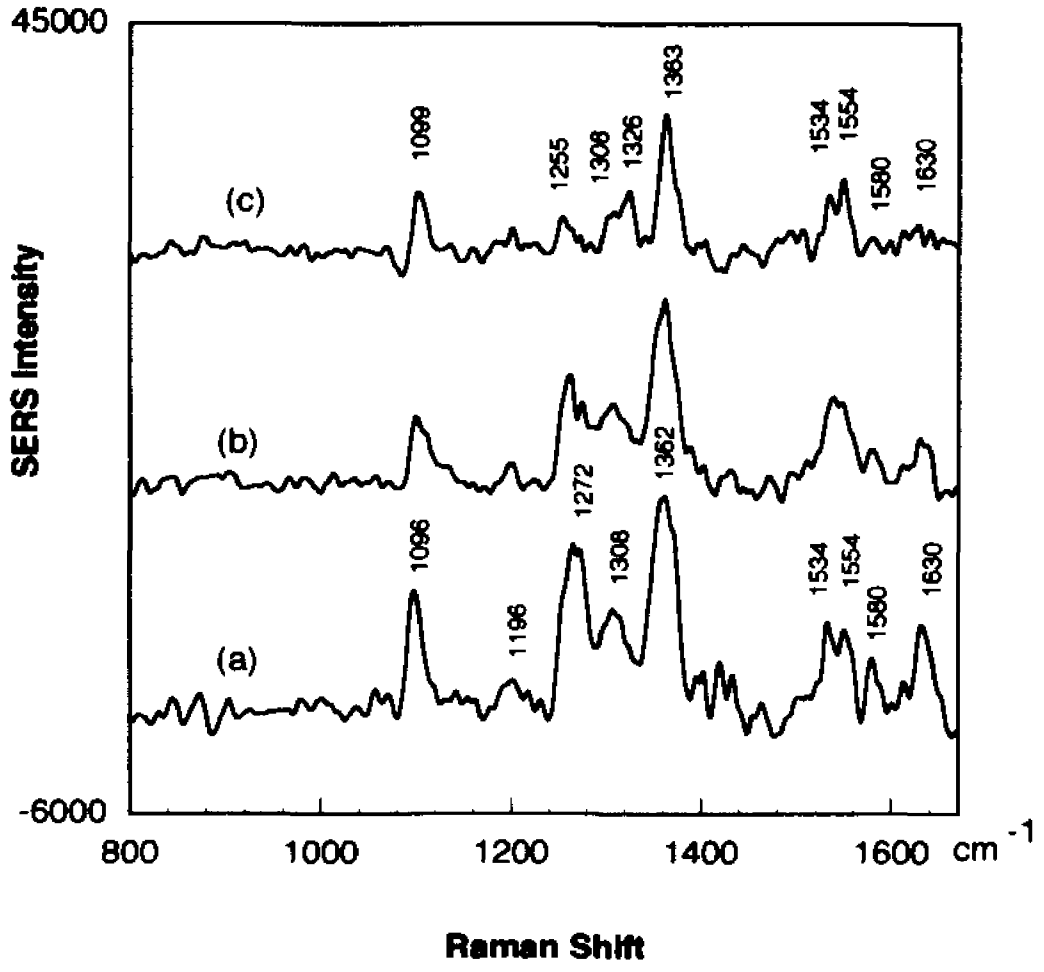

Figure 3.6 Time-resolved SERS spectra of FMN as a function of delay time with 337nm pulsed excitation. 488nm cw laser light as a probe beam. Acquisition time: 200ns
Delay time: (a) 75ns; (b) 375ns; (c) 775ns.

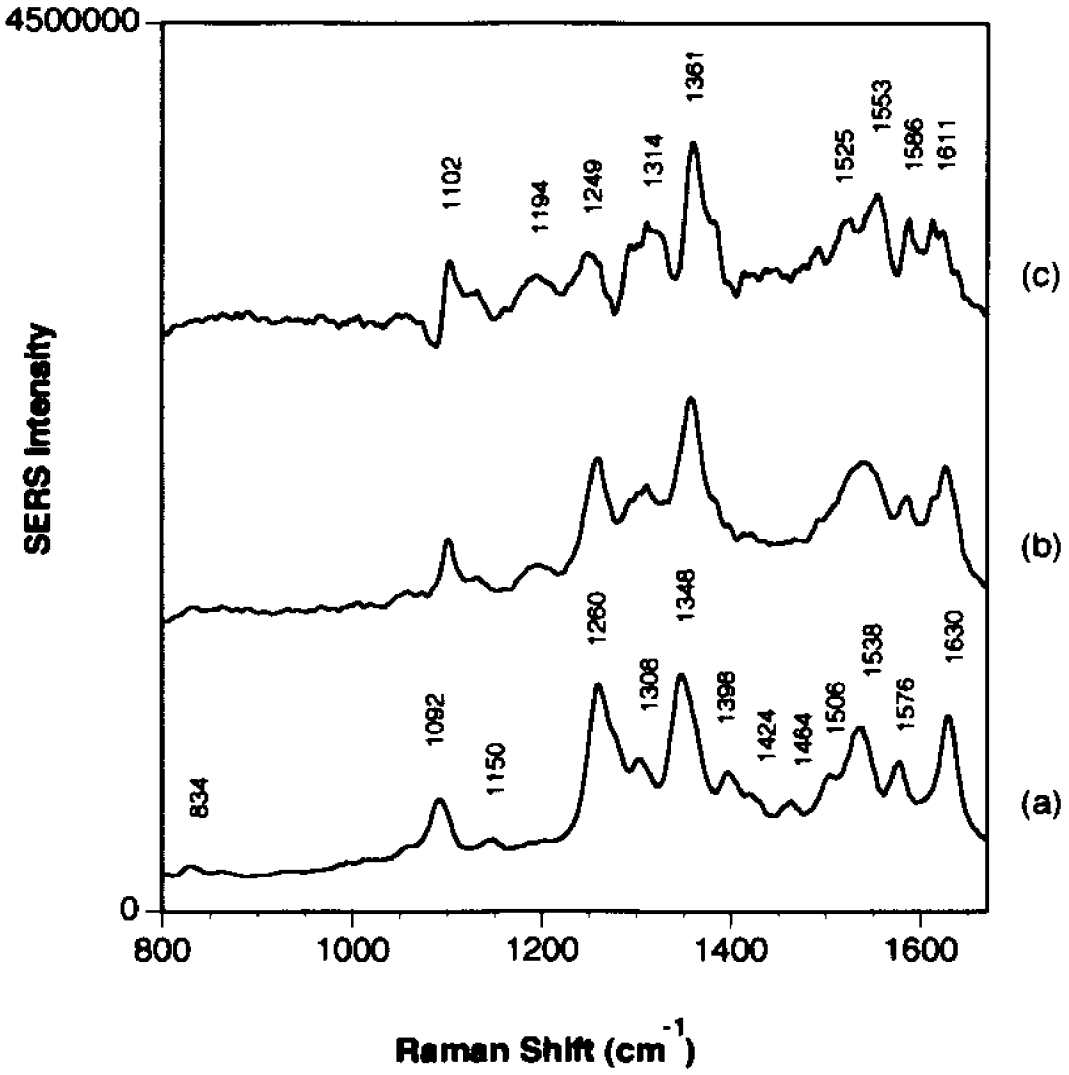

Figure 3.7 Steady state SERS spectra of photoproducts on a Ag electrode at -0.4V vs. SCE. 350nm excitation laser light was overlapped with the 488nm cw probe laser light on the Ag electrode surface.

(a) SERS of FMN with 488nm laser light probe only;

(b) FMN was excited by 350nm cw laser light and SERS of photo-proucts were probed by 488nm cw laser light;

(c) Normalized difference spectrum of (b)-(a); (c)=3.2x(b)-(a).

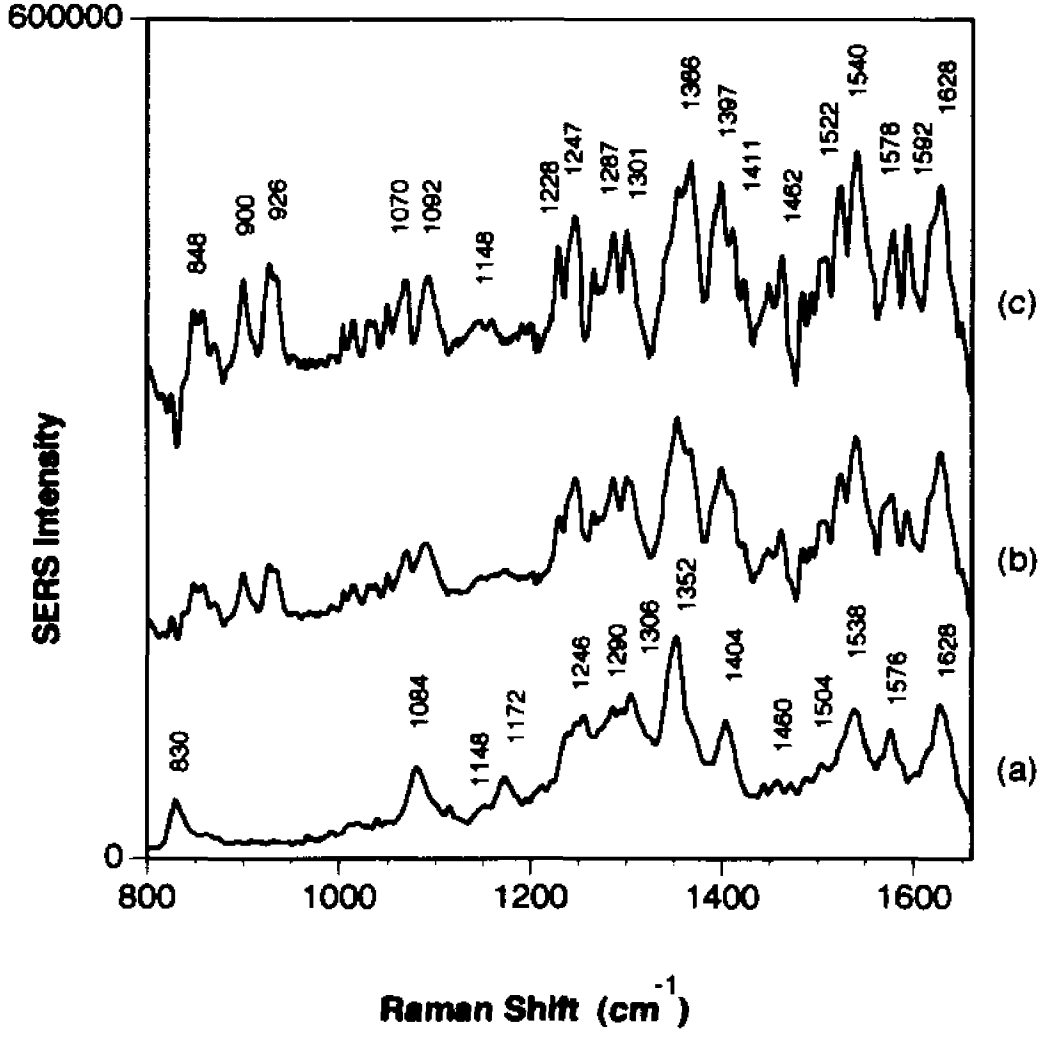

Figure 3.8 Time resolved SERS spectra of FMN in D_2O solution at -0.4V vs. SCE on a roughened Ag electrode.
Acquisition time 500ns.

(a) Spectrum detected by 488nm laser light only;

(b) Spectrum detected by 488nm laser light with 75 ns time delay after 337nm N_2 laser pulse excitation.

(c) Difference spectrum of (b) and (a), i.e., (c)=2.4x(b)-(a).

Figure 3.9 Peak current vs. potential curves for different solution conditions and electrode preparation conditions. (a) For a smooth electrode, linear sweep voltammetry (LSV) experiments carried out with FMN presents at $1x10^{-5}$ M in 0.1M K_2SO_4 solution. (b) For an electrode roughened in 0.1M K_2SO_4 bulk solution, LSV experiments carried out with FMN ($1x10^{-5}$ M) present in 0.1M K_2SO_4 electrolyte. (c) For an electrode roughened with FMN ($1x10^{-5}$ M) present in 0.1M K_2SO_4 solution, LSV experiments carried out with 0.1M K_2SO_4 solution only in the bulk. (d) For an electrode roughened with FMN ($1x10^{-5}$ M) present in 0.1M K_2SO_4 solution, LSV experiments carried out with FMN ($1x10^{-5}$ M) present in 0.1M K_2SO_4 electrolyte. (e) For an electrode roughened with FMN ($1x10^{-4}$ M) present in 0.1M K_2SO_4 solution, LSV experiments carried out with 0.1M K_2SO_4 solution only in the bulk.

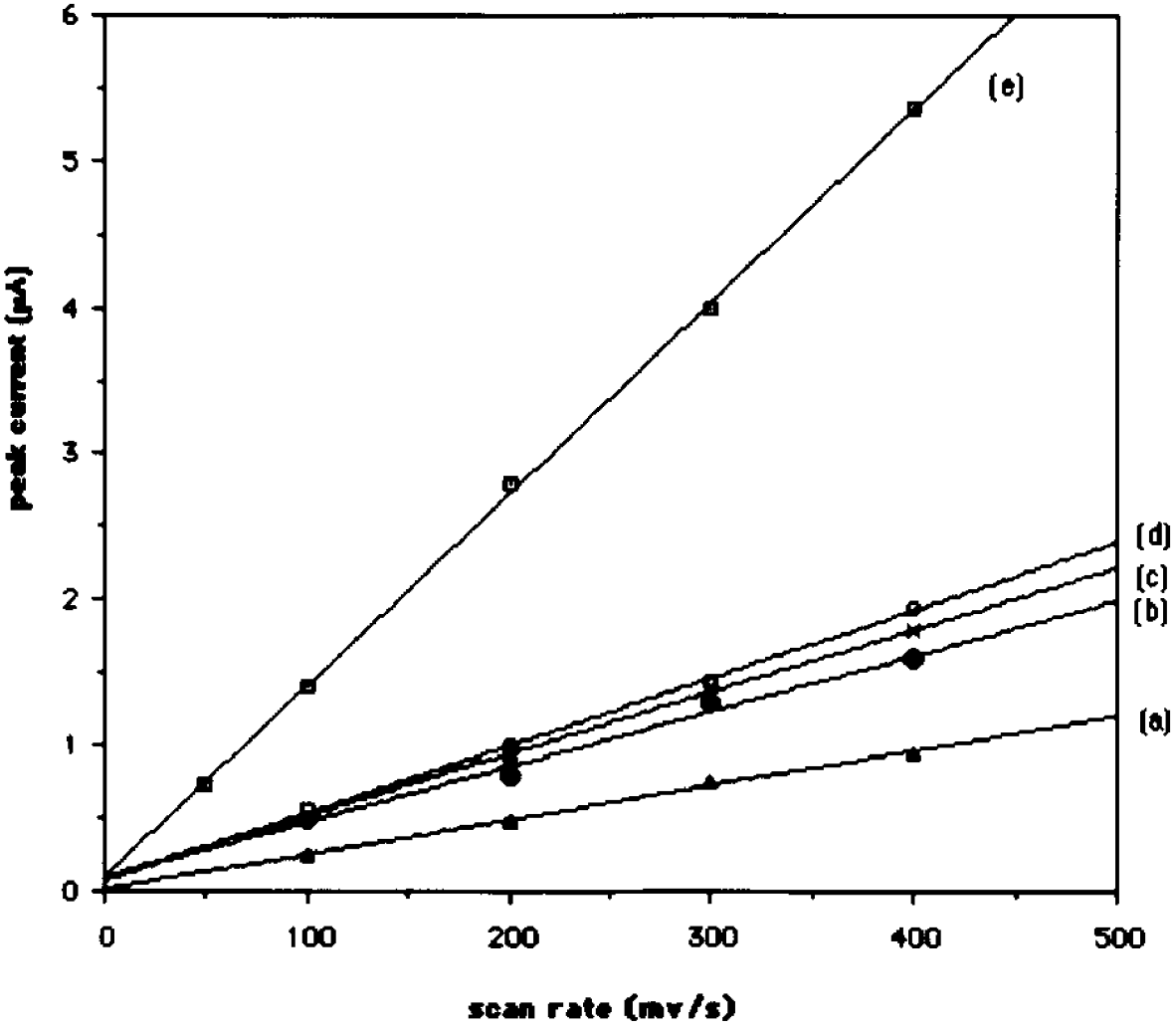
peak current (μA)
scan rate (mv/s)
0
1
2
3
4
5
6
0
100
200
300
400
500
(e)
(d)
(c)
(b)
(a)

Figure 3.9

Figure 3.10. (a) Experimental setup for photogalvanic effect studies. The light source was either a quartz-halogen 150 W lamp or a discrete line from a laser source. (b) Photocurrent action spectrum (open circles) with adsorbed FMN on the electrode and $NaHSO_4$ (0.1M) with EDTA (0.2M) in the bulk aqueous solution at pH=3 and the solution absorption spectrum (solid black circles) for FMN ($1x10^{-4}$ M) in $NaHSO_4$ (0.1M) with EDTA (0.2M) in aqueous solution, pH=3. For the photocurrent action spectrum, the monochromatic light power impinging on the electrode surface was 0.7 mW at each wavelength measured. Dotted and dashed lines are Gaussian fits to the spectral bands. Absorption spectrum of FMN was measured with a Carry Model 14 spectrophotometer.

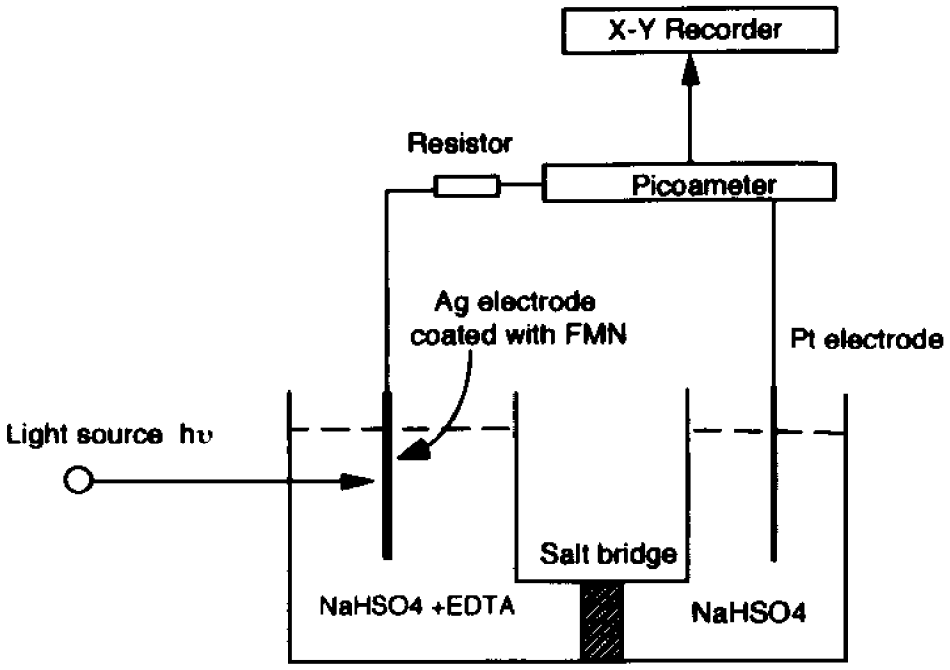

Figure 3.10 a

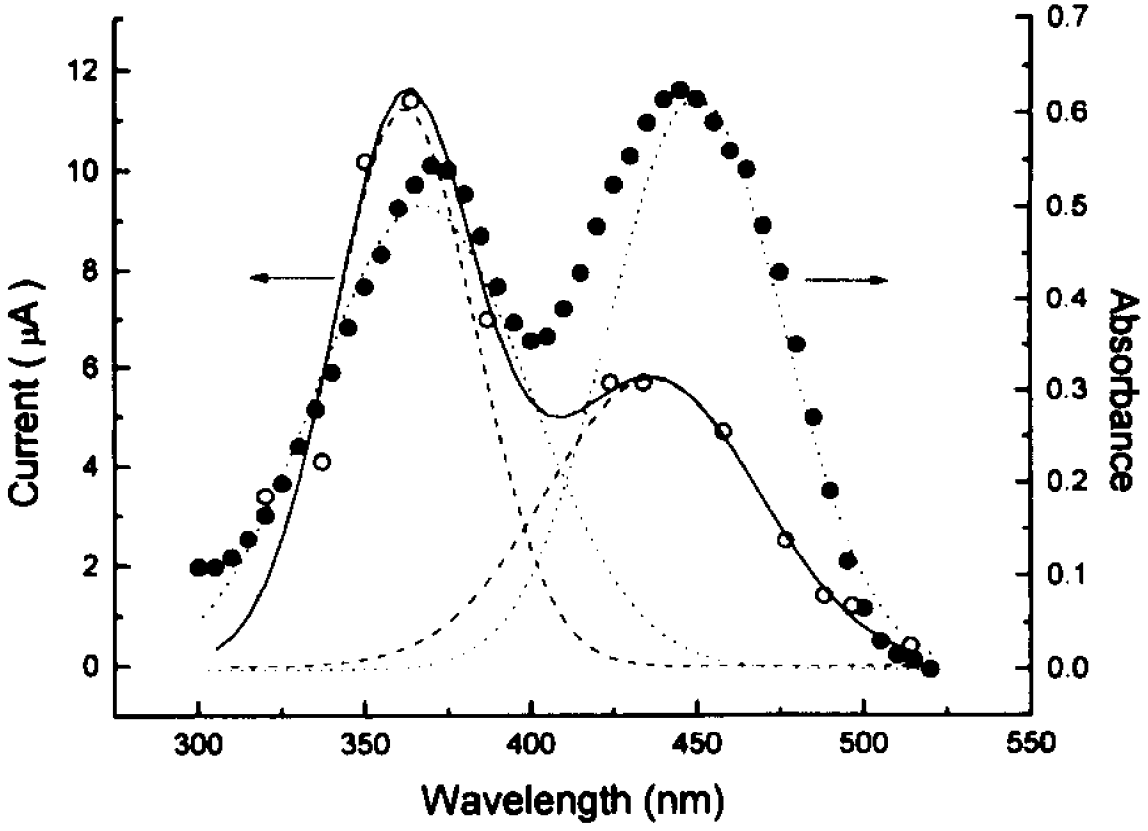

Figure 3.10b

Chapter 4 SERS Studies of Adsorption of Flavin Mononucleotide and Its Hydroquinone and Cation on a Ag Electrode

4.1 Introduction

Flavins play a key role as redox cofactors in biology.[1] Figure 4.1 shows the structural diagram for the common flavin cofactors, all based on the isoalloxazine chromophore, which is capable of facile one and two electron reductions.[2-3] Due to their biological importance, flavins and their interactions with different substrates have been extensively studied by different techniques. Among them, the resonance Raman (RR) and surface enhanced Raman scattering (SERS) methods give very valuable information on molecular structure. As examples, the interactions of flavin-proteins were studied by RR spectra [4] and the interactions of flavins-Ag colloid were studied by SERS spectra [5-6] in recent years. The studies of interactions of flavins with different substrates are useful for the following reasons:

(1) Biomolecular behavior is strongly affected by the surrounding environment. The study of interactions of biomolecules with their surroundings is important for understanding biological processes. For example, the studies of interactions of a molecule-substrate may provide information on bonding sites, bonding strength, molecular orientation, charge redistribution and change of molecular structure and conformation of the adsorbed molecule. This information may be key for answering why the adsorbed molecules change their physical and chemical properties and to elucidate a reaction mechanism. It is also important to know whether the band frequency shifts and intensity changes observed in SERS spectra as compared to free flavin RR spectra indicate denaturation of adsorbed biomolecules or molecule-surface interaction.[7-9]

(2) The interaction of biomolecules adsorbed on different substrates may

serve as models of biomolecule-metal ion or biomolecule-protein systems. For example, the adsorption behavior of biological molecules at an electrode may be related to their physiological functions *in vivo* which usually appears at charged biological interfaces such as cell membranes. [10] The metal ion-flavins, such as Ag(I)-FMN and Ru(II)-FMN, were studied by resonance Raman spectroscopy as possible models for metal-flavin interactions in biological environments. [11-12]

(3) The interactions of chromophore molecules with different substrates can not be avoided in many RR and SERS experiments. Most of the chromophore organic compounds fluoresce very strongly when excited by UV or visible light, and the strong fluorescence obscures Raman spectra. Therefore, fluorescence quenching methods have to be applied to these chromophore molecules in order to obtain Raman spectra. Bonding flavins to protein in RR spectroscopy and adsorbing flavins to Ag electrodes in SERS spectroscopy are examples of quenching methods.

(4) The study of interactions between adsorbates and substrates has general applications in the studies of interfacial electrochemistry and in elucidating SERS mechanisms. [13-16]

An important method for studying flavin-substrate interactions is to analyze the Raman spectral differences between free flavin and the flavin adsorbed on different substrates with the help of normal mode calculations. However, systematic studies of interactions of flavins with different substrates have not been reported. The origins of the SERS spectral differences between flavin adsorbed on a Ag electrode and on Ag colloid surfaces have not been thorouggly addressed. Analyzing the spectral differences may reveal the important interaction properties of flavin-substrate systems.

In this study, we investigated adsorption properties of FMN on a Ag

electrode by SERS experiments and normal mode calculations. We also analyzed spectral differences from previous studies, to propose a new adsorption mechanism and to provide new information about the interactions of flavins with a Ag electrode. We compared our SERS spectra of flavins adsorbed on a Ag electrode with the SERS spectra of flavins adsorbed on a Ag colloid, with the RR spectra of the free flavin in solution, and with the RR spectra of flavin-metal ion complex. We also carried out normal mode calculations to fit and interpret SERS experimental data by testing different bonding sites and interaction parameters between the flavin and Ag electrode. The proposed bonding sites, adsorption orientation and interaction parameters have been determined. The assignment of SERS bands of FMN by normal mode calculation was also carried out.

We also report UV/Vis absorption studies and SERS studies of hydroquinone which was electrochemically generated from flavin by a two electron reduction. The UV/Vis absorption spectra of such electrochemically generated hydroquinone were investigated by a UV/VIS spectroelectrochemistry system. The SERS spectroscopy study of hydroquinone is reported for the first time. We found that a correlation between the SERS of flavin and the SERS of hydroquinone was not available.

4.2 Experimental Section

Flavin mononucleotide (FMN), riboflavin (RF), and Lumiflavin were purchased from Sigma Chemical Co. and used as received. Reagent grade K_2SO_4 served as supporting electrolyte. The solutions were prepared with deionized distilled water and deaerated by nitrogen bubbling for 20 min. before

each experiment. For the isotopic effect studies, D_2O (99.98 percent) was purchased from Sigma Co. and solution was prepared in a nitrogen gas bag. The pH of solution was adjusted by adding reagent grade H_2SO_4 or NaOH and measured with an Orion Research Model 720 digital ionalyzer (Orion Research Inc.).

The SERS experimental setup was similar to that described elsewhere .[17] A spectra Physics Model 164 argon ion laser at 488nm was used as an excitation source. The laser power at the electrode was approximately 30mW. Spectra were recorded with a Spex Model 1401 double monochromater with a wave number resolution of $2cm^{-1}$, and photon counting detection was used.

The sample cell was made of quartz and its window was cut as 45° in order to reduce the absorption of the incident excitation light and Raman scattering light by electrolyte solution in the sample cell. The sample cell consisted of a silver working electrode with $1.11mm^2$ surface area, a Pt counter electrode, and a saturated calomel electrode (SCE) as the reference. All electrode potentials in this study are quoted vs. SCE. The oxidation reduction pretreatment was accomplished in the presence of FMN ($1x10^{-4}$ M) in 0.1 M K_2SO_4 electrolyte by applying a potential step from -0.4V to 0.5V for one second. Under this pretreatment, a monolayer of adsorbed FMN was formed. SERS experiments were with only K_2SO_4 support electrolyte in the bulk solution.

The absorption spectra of neutral FMN and hydroquinone product of FMN were carried out with a Model Lambda 4 UV/VIS spectrophotometer (Perkin Elmer) combined with spectroelectrochemical set up, a Model 173 potentiostat (EG & G PARK) and a Model 175 wave form generator (EG&G PARK). The sample cell for carrying out electrochemistry and absorption spectra measurement simultaneously is shown in Figure 4.2. The sample cell consists of

two parts, a solution reservoir compartment, within which a Pt counter electrode and Ag/AgCl reference electrode are emerged, and a detection area which is made of a gold grid film serving as an electrochemical working electrode with two quartz windows which are separated by Teflon film with distance of 300Å. The sample solution in the detection area undergoes electrochemical reaction under electrode potential control. This thin layer electrochemical cell enables the sample solution in the working electrode area to be electrolyzed under equilibrium conditions. Therefore, the cyclic voltammetry and corresponding absorption spectrum gives accurate information of the redox states of the sample solution.

4.3 Results and Discussions

4.3.1 A comparison of Raman spectra of FMN

Table 4.1 lists our SERS spectrum bands of FMN adsorbed on a Ag electrode at an applied potential of -0.4V and those of FMN / riboflavin (RF) adsorbed on Ag colloid [5-6]. The resonance Raman spectra of free FMN [18], and FMN-Ag^+ complex [12] in solution are also listed in this table. In order to avoid spectra differences caused by different excitation wavelengths [18], all of the experimental data were adopted from the results with the same excitation wavelength, the 488nm laser line. The following band shifts are observed.

The SERS spectra of FMN adsorbed on a Ag electrode at applied potential -0.4V showed some differences from the RR spectra of free flavin in solution. The following bands shift to lower frequencies from the RR to SERS spectrum. The 1584cm^{-1} band shifted to 1576cm^{-1}, the 1550cm^{-1} band to

1540cm^{-1}, the 1355cm^{-1} band to 1348cm^{-1} and the 1162cm^{-1} band to 1150cm^{-1}. The 1412cm^{-1} band disappeared and new bands at 1424cm^{-1} and 1398cm^{-1} were observed. These band changes can be considered as a consequence of flavin adsorption on the Ag electrode.

The SERS spectra of FMN adsorbed on a Ag electrode at applied potential -0.4V also showed obvious differences from the SERS spectra of FMN adsorbed on Ag colloid. The SERS bands of FMN adsorbed on the Ag electrode at 1424cm^{-1}, 1398cm^{-1} and 1260cm^{-1} can not be observed in the SERS of FMN adsorbed on Ag colloid, while the bands observed at 1409cm^{-1} and 1235cm^{-1} in the SERS of FMN on Ag colloid can not be observed in the SERS of FMN on the Ag electrode. Bands at 1260cm^{-1} and 1150cm^{-1} in the SERS of FMN on a Ag electrode may correspond to bands at 1287cm^{-1} and 1160cm^{-1} in SERS of FMN on Ag colloid respectively. However, several band shifts from the RR spectra to the SERS spectrum of FMN on Ag colloid are similar to the band shifts from RR spectra to SERS of FMN on Ag electrode. Those band shifts are from 1584cm^{-1} to 1576cm^{-1}, 1550cm^{-1} to 1536cm^{-1} and 1355cm^{-1} to 1349cm^{-1}.

The SERS spectra of adsorbed flavin on a Ag electrode at applied potential -0.4V also showed significant differences from the RR spectra of FMN-Ag^+ complex. We only mention here some of bands which we will be discussed in later sections. The SERS band of FMN at 1630cm^{-1} shifts to 1625cm^{-1}, the 1540cm^{-1} band disappeared and instead new bands at 1554cm^{-1} and 1530cm^{-1} appear. The band at 1260cm^{-1} disappeared and a new band appeared at 1293cm^{-1}. The RR spectra of FMN-Ag^+ are also quite different from the RR spectra of free FMN. These differences will be discussed later.

4.3.2 The proposed adsorption site of FMN on Ag electrode:

Since the adsorption site of flavin adsorbed on a substrate strongly affects the behavior of the flavin's biological function, the adsorption site of flavin bound to different substrates and ions has been discussed by many groups.

It has been proposed for studies on colloids that the flavin adsorbs in its deprotonated anion form through the N(3) position at ring III [5-6]. This conclusion was based on the SERS spectral pH dependence, the absence of SERS signals from N(3)-substituted compounds, and the absence of deuterium isotope effects. Recently, further research by the same N. S. Lee and coworkers [19-20] and others [21] indicated that the carbonyl groups, C(2)=O and C(4)=O may be also involved in the adsorption to a Ag colloidal surface. From the observation of down shift of Raman bands of the stretching vibrational mode of the C=O groups on ring III by exciting at wavelength 647nm, far from absorption band, they concluded that the flavin may adsorb on Ag colloid surface through the negatively charged N(3) as well as through C(2)=O and C(4)=O groups.

The site of the FMN bond to Ag^+ ion were studied by Benecky et al.[11-12, 22-24]. It was proposed that N(5) and C(4)=O are bonding sites for the FMN-Ag^+ complex from RR [11-12], FT-Raman [22] and X-ray experiments [23-24]. However, N(5) and C(4)=O were not proposed as adsorption sites for either FMN on colloidal Ag or on a Ag electrode surface by Copeland [12] or by Holt [25] from enzyme activity measurements of glucose oxidase (GO) adsorbed on Ag surfaces. The Ag^+ ions which were bonded between N(5) and C(4)=O in flavin-Ag^+ complex are known to be potent inhibitors of the enzyme [26]. These studies showed that the enzyme adsorbed on Ag electrode and Ag colloidal surfaces remains more than 86% active. Therefore, the N(5), C(4)=O was not proposed as adsorption site in SERS experiments. Further experimental evidence for this

proposal is the fact that the RR and SERS spectra of FMN-Ag^+ are significantly different from SERS of FMN adsorbed on Ag electrode or Ag colloid surface. The Ag^+ ion which is covalently bonded to the N(5), C(4)=O position in the FMN-Ag^+ complex strongly affects all three ring vibrational modes of FMN, but the adsorption of FMN on Ag surfaces in SERS experiments only affects the vibrational modes of rings II and III. For example, the band observed at 1630 cm^{-1} in the RR spectra of free FMN which is attributed to ring I stretch mode shifts to 1625cm^{-1} in the RR or SERS of FMN-Ag^+ complex, but this band has no shift in the SERS spectra of FMN adsorbed on a Ag electrode or on a Ag colloid surface. The shift of this band indicates that the ring I vibrational mode was strongly influenced by the bonding of Ag^+ ion to N(5), C(4)=O, but it is not affected by adsorption of FMN on a Ag electrode or a Ag colloid surface. The band at 1550cm^{-1} in RR the of free FMN, which was assigned to N(5)-C(4a), C(10a)-N(1) out-of-phase stretching mode, splits into two bands at 1554cm^{-1} and 1530cm^{-1}, but this band only shifts to 1540cm^{-1} in the SERS of FMN adsorbed on a Ag electrode and to 1536cm^{-1} in the SERS of FMN on Ag colloid. The differences of the 1550cm^{-1} shift between complexion and adsorption may also indicate different bonding sites or bonding characteristics between the complex-ion and adsorption. The splitting of this band may indicate a stronger influence at N(5) and C(4)=O upon complex-ion formation than on adsorption.

The N(1), C(2)=O sites have not been proposed as an adsorption site for any substrates so far, due to the consideration of steric strain from the R group on the N(10).

Our SERS experimental results, however, do not suggest that the deprotonated N(3) anion, or N(3) along with C(2)=O and C(4)=O is the adsorption site for flavin adsorbed on a Ag electrode, since our SERS spectra of FMN

adsorbed on Ag electrode are quite different from that of FMN adsorbed on Ag colloid as discussed in section (a). Further experimental evidence supporting this conclusion is provided by following observations: (1) In our experiments, significant band shifts of SERS spectra were observed when N(3) was deuterated. Our SERS band shifts upon deuteration have parallel a pattern to those in RR experiments. But these SERS spectral band shifts were not observed upon deuteration in Lee's experiments [5] since the N(3) deprotonated anion adsorbed on Ag colloid surface cannot be deuterated, and therefore, no bands shift was observed. (2) The 1424cm^{-1} band observed in our SERS spectra which was assigned mainly to N(3)-H bending mode was observed in SERS of Ag colloid. (3) The band at 1260cm^{-1} has no band shift in our SERS experiments, but it shifts to 1287cm^{-1} in SERS of Ag colloid which was explained as a result of N(3) deprotonation and N(3) adsorption. These observations lead to the conclusion that negative charged N(3) is not the adsorption site of FMN adsorbed on the Ag electrode in our SERS experiments.

Our SERS results also neither suggest that the N(5), C(4)=O is an adsorption site of FMN adsorbed on a Ag electrode, since our SERS spectra showed significant differences from RR spectra of FMN-Ag$^+$ complex [12] as well as SERS of the FMN-Ag$^+$ complex on a Ag electrode [25] . Furthermore, as discussed above, the SERS and RR as well as the enzyme activity studies of FMN adsorbed on different surfaces indicated that N(5), C(4)=O is not the adsorption site of flavin adsorbed on a Ag electrode.

Based on the above observations, and with the assistance of our normal mode calculations, we therefore propose that the flavin is adsorbed flat on the Ag electrode mainly through the electron lone pairs at N(3) and N(10) nitrogen atoms with the possible participation by π electrons on the FMN rings II and III, because

N(3) and N(10) are SP^3 hybrids with electron lone pairs perpendicular to the FMN ring plane as well as the π electrons. But N(1) and N(5) as well as the oxygen at C(4) and C(2) are SP^2 hybrids with electron lone pairs on the plane of FMN.

4.3.3 The normal mode calculations: Force constants and SERS bands assignment of FMN adsorbed on a Ag electrode

Normal mode calculations of flavin have been carried out by several groups [27-28]. However, these normal mode calculations have focused primarily on the free flavin and have rarely addressed the broader question of a flavin interaction with its environment. Our work provides the first calculations designed to elucidate the factors from adsorption which influences its vibrational modes as well as its structure.

As reported in our recent publication, [29] by using Abe's force constants as initial values, [27] we fitted Copeland and Spiro's resonance Raman frequencies [18] as well as isotopic band shifts reported by Kitagawa et al. [30] with a SIMPLEX program developed by A. Vivoni in our group. [31] All bands observed by Copeland and Spiro occurred above 1000 cm^{-1} and were mainly ring stretching vibrations. To keep a low ratio of frequencies being fitted to adjustable parameters, only ring II and ring III stretching force constants were allowed to vary during the optimization. Ring I stretching force constants were not varied during the optimization because ring I bands do not show differences between the IR, resonance Raman or SERS spectra. The resulting force constants were then used as the initial force constants for optimizing the SERS frequencies. The same force constants optimized in the resonance Raman calculation were optimized in the SERS calculation. The force constants obtained from the SERS optimization reproduced the frequency shifts between the resonance Raman and

SERS spectra. The force constant differences between the resonance Raman and the SERS calculation will be analyzed below in terms of the orientation of flavin on the surface.

Table 4.2 lists the band shifts of the experimental results from the RR of FMN in solution to the SERS of FMN on a Ag electrode. The band shifts for the normal mode calculations of FMN from RR to SERS on a Ag electrode are also listed in this table. The calculated force constant changes from free FMN to adsorbed FMN are listed in Table 4.3. From Table 4.2 and 4.3, one notices that most of the changes of FMN vibrational modes and force constants are found from ring II and III. This may indicate that the adsorption of FMN on Ag mainly involvs these two rings.

Based on our normal mode calculations, all bands which were assigned to ring I stretching vibration modes do not change frequencies from RR to SERS experiments. These bands are 1630cm^{-1} and 1464cm^{-1}. The assignment for these bands are normally in agreement with most other research groups. Many of the bands assigned to ring II and ring III vibrational modes were shifted to lower frequencies in the SERS spectra of FMN adsorbed on a Ag electrode. The RR band at 1584cm^{-1} is shifted in SERS to 1576cm^{-1}. The 1550cm^{-1} band of RR spectrum shifted to 1540cm^{-1} in SERS. These two bands at 1584cm^{-1} and 1550cm^{-1} are attributed to N(10)-C(10a), C(10a)-N(1) and C(4a)-N(5) stretching. Their down shifts may indicate delocalization of π electron density in this region. The RR band at 1412cm^{-1} which was assigned mainly to N(3)-H bending mode, disappears in the SERS on the Ag electrode but new bands at 1424cm^{-1} and 1398cm^{-1} which were assigned mainly to same bending modes appeared in this region. The above band changes may indicate that N(10) and N(3) are both involved in the adsorption on Ag electrode. The RR band at 1355cm^{-1} which was

attributed to ring II, N(10)-C(10a), N(10)-R stretching mode was found to shift to lower frequency, 1348cm^{-1}, in the Ag electrode SERS. This band shift further indicates that N(10) and electron density delocalization at ring II were involved in the adsorption of FMN on a Ag electrode. The RR band of free FMN at 1262cm^{-1} has a small shift on the Ag electrode SERS, but it shifts to 1287cm^{-1} in Ag colloid SERS. This band was attributed to pure ring III stretching coupled with the N(3)-H bending mode. The larger frequency shift of this band in the case of Ag colloid SERS indicated that the deprotonation and adsorption processes occurred through N(3) atom, which causes decoupling of the ring III stretching vibration with the N(3)-H bending, which in turn causes frequency up shift of this band similar to the high shift of FMN upon deuteration. The RR band at 1162cm^{-1} shifts to 1150cm^{-1} in the Ag electrode SERS but has no shift in the Ag colloid SERS. This band is mainly attributed to the C-H in plane bending mode. The shift of this band to lower frequency may indicate some interactions between the H atoms at ring I and the Ag atoms of the Ag electrode connected with N(10) at FMN ring II. The N(3) anion adsorption mode, however would not affect this C-H in plane bending mode. As indicated in SERS of Ag colloid experiments, no frequency shift can be observed for this band.

Based on above experimental observations and our normal mode calculations, we therefore suggest that the FMN is adsorbed flat on Ag electrode mainly through N(10) and N(3) lone pair electrons. Furthermore investigation of changes of force constants from FMN to adsorbed FMN on a Ag electrode indicated that all changes are involved in ring II and III. The force constants that significantly decreased are $S(N_1\text{-}C_{10a})$ and $S(N_{10}\text{-}C_{10a})$ and those that significantly increased are $S(N_5\text{-}C_{4a})$ and $S(N_5\text{-}C_{5a})$. One possible explanation for the frequency down shifts and force constant changes could be the orientation

effect at rings II and III on adsorption. At an applied potential of -0.4V, the Ag electrode is negatively charged acting as an electron donor. Based on the orientation effect, the flat adsorption of FMN on the Ag electrode through N(10) and N(3) will increase the electron density significantly at N(5) which may reduce the force constants of $S(N_1\text{-}C_{10a})$ and $S(N_{10}\text{-}C_{10a})$, but increase force constants of $S(N_5\text{-}C_{4a})$ and $S(N_5\text{-}C_{5a})$. The partially negative charge at N(5) and C(10a) will reduce the conjugation of FMN due to the adsorption. Therefore, the bands assigned to ring II and III stretching modes shift to lower frequencies.

The flat adsorption of FMN through the isoalloxazine ring on a Ag electrode was also proposed for SERS experiments by Taniguchi [32] and Brabec et. al. [33], and was supported by electrochemical results by Takamura [34], Verhagen [35], Ueyama [36], Gorton [37], and Muller [38]. However, there was no clear experimental evidence presented by these authors.

Possible adsorption sites of FMN through N(3), N(3) with C(2)=O and C(4)=O as well as N(5) with C(4)=O were also tested by our normal mode calculations. Since these adsorption models only involved one or two adatoms with the FMN molecular plane perpendicular to Ag electrode surface, we adjusted force constants and interaction parameters between adsorbed atoms of FMN and Ag atoms of substrates by referring to the work of Vivoni et al.[39]. The normal mode calculations for these FMN-Ag electrode adsorption models were carried out based only on these modifications. However, the calculations for the N(3), N(3) with C(2)=O and C(4)=O as well as N(5) with C(4)=O as selected adsorption sites did not reproduce our SERS spectra. Therefore, our normal mode calculations do not suggest that N(3), N(3) with C(2)=O and C(4)=O as well as N(5), or C(4)=O are the adsorption sites of SERS of FMN on Ag electrode. These results might be another indirect indication for the flat adsorption model.

4.3.4 Interpretation of different adsorption sites of FMN on substrates

The different adsorption sites of FMN on a Ag electrode and on Ag colloidal surface can be explained through a bonding interaction that is dependent upon the potential of the surface, the pH of the solution, and the nature of the anions in solution which was demonstrated recently by Koglin [40] and Lu et al. [41]. It is not surprising that the FMN changes adsorption sites from Ag electrode to Ag colloid surface, since the surface potential, size and shape of Ag particles in the Ag colloid solution and the properties of the solution, such as pH value, cation and anion concentrations are quite different on a Ag electrode. The adsorption of flavin on the Ag electrode depends on the pretreatment of the Ag electrode and the applied potential at which the SERS experiment is carried out. In order to investigate the dependence of adsorption on potential, we carried out potential dependent SERS studies. Figure 4.3 shows the potential dependence of the SERS spectra of FMN adsorbed on a Ag electrode. Experimental conditions were established to avoid photochemistry during SERS experiment. In this experiment, the Ag electrode was pretreated in bulk 0.1M K_2SO_4 electrolyte by applying a potential step from -0.4V to 0.5V for one second and then was immersed in a $1x10^{-4}$ M FMN solution for 10 minutes. Figure 4.3(a) shows the SERS spectrum taken at open circuit which is identical to that of SERS on Ag colloid solution reported by Lee et. al. [5-6]. With a potential change in the positive to negative direction, the spectrum changes. At an applied potential of -0.4V, the SERS spectrum as shown in Figure 4.3(d) becomes identical to that in which the Ag electrode is pretreated in FMN+K_2SO_4 solution

and the SERS spectrum is taken under applied potential of -0.4V. The above experimental results indicated that at a potential more positive than 0V, the FMN adsorbed on the Ag electrode surface through N(3) anion or N(3) anion along with C(4)=O and C(2)=O of FMN ring III. At a potential more negative than -0.2V, the FMN adsorbed on the Ag electrode surface through nitrogen atoms with the main contributions from N(3) and N(10) in a flat adsorption configuration. The potential dependence of adsorption may indicate that a positive surface potential favors anion or oxygen atom adsorption, while a negative surface potential favors nitrogen or π electron adsorption.

4.3.5 The UV/Vis studies of FMN hydroquinone

Our experiments which combined UV/Vis absorption spectrophotometry with electrochemistry provided possibilities to generate the hydroquinone electrochemically and to obtain the corresponding absorption spectrum simultaneously. From the electrochemistry of FMN in solution at pH 7, one observes that the FMN is in its neutral form at applied potential more positive than -0.5V, while at applied potential more negative than -0.5V, the FMN is in its semiquinone or hydroquinone forms. Figure 4.4(a) and 4.4(b) show the UV/Vis absorption spectra of FMN at applied potential of -0.4V and -0.7V, respectively. Figure 4.4(a) reveals an identical spectrum as that of neutral FMN in aqueous solution and that of neutral FMN at more positive potential from -0.5V to +1.5V in our experiments. This result may indicate that the FMN does not change its oxidation state at applied potential from -0.5V to +1.5V. As shown in Figure 4.4(b), the spectra obtained at applied potentials more negative than -0.5V may correspond to either the semiquinone or hydroquinone forms. Our experiments also showed that the electrochemically generated hydroquinone can be

reoxidized to neutral FMN when the applied potential returns back from -1.0V to a potential more positive than -0.5V.

The absorption spectrum of neutral FMN, Figure 4.4(a), shows a strong absorption band at 266nm, a band at 370nm and the lowest transition band at 445nm, while the absorption spectrum of hydroquinone in Figure 4.4(b) is quite different from that of neutral FMN. In Figure 4.4(b), a strong absorption band was found at 256nm and two shoulders were found around 290nm and 340nm, respectively. The absorption bands of FMN at 370nm and 445nm disappeared in Figure 4.4(b). The missing band at 445nm which is attributed to the lowest π–π^* transition of FMN means that this lowest π–π^* transitions of FMN originating from rings II and III does not exist in the electrochemically generated new species. The shoulder at 340nm of the new species may correspond to the band of FMN at 370nm which shifts 30nm to shorter wavelength. The 370nm band of FMN contributes to a mixture of the n-π^* and the second π–π^* transition. This band shift may indicate redistribution of the π electrons and non-bonding lone pair electrons of nitrogen at rings II and III. Therefore, the shoulder at 290nm may be due to a new n-π^* transition of the new species. The band at 256nm may be the shifted 266nm band of FMN.

The electrochemically generated new species can be easily identified as neutral hydroquinone, FMN-H_2, by comparing the absorption spectrum with the spectra of flavins, semiquinones and hydroquinones. The complete set of absorption spectra of cation, neutral and anion flavins and the radical cation, anion and neutral semiquinones were reported by Heelis and Land et al. [42-45]. The reported absorption spectra of the flavins and semiquinones are significantly different from that of Figure 4.4(b). Therefore, the species at applied potential of -0.7v in our experiment is neither a flavin nor flavin semiquinone. It most likely is

one of hydroquinone forms. The absorption spectra of cation, neutral and anion hydroquinones also have been reported by Ishikawa and Lei et. al. [45-47]. The reported absorption spectrum of the cation hydroquinone is also significantly different from those of the neutral and anion hydroquinones. However, the absorption spectra of neutral and anionic hydroquinones are similar to each other. The spectrum of Figure 4.4(b) reveals the same UV/Vis absorption features as that of neutral and anion hydroquinone chemically prepared by Lei et al reported. Therefore, at solution of pH7 and potential -0.7V in our experiment, the electrochemically generated species is most likely the neutral hydroquinone. The two electrons, two proton reduction of FMN changed the electronic structure and caused the transitions to shift towards the red region. Therefore, a RR spectrum of flavin hydroquinone is not available in the UV/Vis region.

The absorption spectrum of the one electron oxidized cation FMN cannot be observed from our UV/Vis-electrochemical experiments since too high an oxidation potential is required. As we previously reported [48], the potential for one electron oxidation of FMN should be about 1.70 V vs. SCE without photo assistance. This potential for oxidation of FMN is in a region where water begins to be oxidized. In our experiment, we did not observe a change in FMN absorption spectra up to an applied potential +1.5V at which a strong water oxidation wave was observed in a cyclic voltammetry experiment. This experiment provides additional evidence that FMN cannot be oxidized at applied potential more negative than +1.5V vs SCE at Ag electrode without a photo assisted process.

4.3.6 SERS studies of FMN hydroquinone

With improvement of our instrumental sensitivity, we were able to

observed SERS spectra of fully reduced FMN adsorbed on a Ag electrode for the first time. Figure 4.5(a) shows SERS spectrum of FMN at an applied potential -0.4V vs SCE and Figure 5.5(b) shows the hydroquinone spectrum of FMN at an applied potential -0.7V vs SCE. At potential -0.7V, as indicated by UV/Vis spectrophotometry and cyclic voltammetry experiments, the FMN was fully reduced (two electron reduced) to the neutral hydroquinone form, FMN-H_2. Figure 4.5(c) shows the difference spectra between Figure 4.5(b) and Figure 4.5(a). Figure 4.5(c) represents the SERS spectra of FMN hydroquinone. In Figure 4.5(b), for frequencies higher than 1000cm^{-1}, new bands at 1184cm^{-1}, 1214cm^{-1}, 1292cm^{-1}, 1484cm^{-1} and 1554cm^{-1} were clearly observed without doing difference spectra and the bands of the hydroquinone below 1000cm^{-1} were significantly enhanced. In Figure 4.5(c) the intensity increase of bands at 1344cm^{-1}, 1278cm^{-1}, 1090cm^{-1} as well as for bands below 1000cm^{-1} may reflect the molecular orientation change from FMN to hydroquinone, since hydroquinone has lost its planar configuration. At pH values of electrolyte solution from 4 to 10 in our SERS experiments, the hydroquinone should be in its dihydrogen neutral form. The two hydrogens are bonded to N(1) and N(5) atoms. The hydrogen bonding weakens the N(5)-C(4a), C(10a)-N(1) bonds, and changes the lone pair electron direction on N(5) and N(1). The N(5) and N(1) hybridization changes from SP^2 to SP^3. These lone pair electron directional changes may cause a change in the adsorption of FMN on the Ag electrode from N(3), N(10) lone pair electrons as well as the π electron of isoalloxazine to N(1), N(3), N(5) and N(10) lone pair adsorption interactions. The loss of N(5)-C(4a), C(10a)-N(1) double bonds characteristically causes a loss of conjugation of these bonds and makes ring II and ring III become a more non-planar configuration. The non-planar configuration of the hydroquinone may be adsorbed on the Ag electrode with

some degree of angle orientation to the electrode. Therefore, it may enhance the SERS intensity of some bands which belong to the in plane vibrational modes of the hydroquinone. Therefore, the increase intensity of the in planar stretching vibration modes of SERS spectra bands at 1344cm^{-1}, 1278cm^{-1}, 1090cm^{-1} as well as the bands below 1000cm^{-1} is quite reasonable. At very negative applied potential, -1.0V, the pure FMN hydroquinone SERS spectra appear without the need for difference spectra. However, its intensity became relatively very weak. This may be attributed to the negative electrode having higher electron density which repulses the hydroquinone electron lone pair from the electrode. The repulsion weakens the adsorption between electrode and hydroquinone and reduces the enhancement of SERS intensity.

4.3.7 Observation of SERS spectra of cation FMN

In this section we report that the stationary SERS spectrum of FMN cation is formed under an applied potential more positive than -0.2V at excitation wavelength of 488nm.

Figure 4.6(a) shows the SERS spectrum of cation FMN adsorbed on a roughened silver electrode at applied potential -0.2V vs SCE when excited by 488nm laser light. Figure 4.6(b) shows difference spectra between Figure 4.6(a) and Figure 4.5(a) which shows new bands of the SERS spectrum of cation FMN. As confirmed by transient photocurrent and photopotential measurements, [29, 48] a cation form of FMN will be formed on the electrode at this potential under photon assistance of the 488nm laser excitation.

The difference spectrum of Figure 4.6(b) clearly shows band shifts, such as band 1540cm^{-1} shifting to higher wave number, 1552cm^{-1}; 1348cm^{-1} shifting to higher wave number, 1360cm^{-1}; 1260cm^{-1} shifting to lower wave number,

1250cm^{-1}; and the 1092cm^{-1} band shifting to higher wave number, 1104cm^{-1}. Investigating these bands shifts by comparing band assignments in section 4.3.3, one could conclude that these band shifts indicate increasing aromaticity of ring II and decreasing aromaticity of ring III in the FMN cation form. Similar band shifts to this stationary SERS spectrum of cation FMN can also be observed in TRSERS which corresponds to the photo product II [29, 48]. These previous studies indicated that the cation form of FMN was formed by transferring one electron from its π orbital to the metal Fermi level at applied potential -0.2V under photon assistance of 488nm laser light, and it was stabilized by rearrangement of the isoalloxazine's three rings to make both ring I and ring II conjugated (or aromatic) in order to reduce the total energy.

Thus the band at 1540cm^{-1} which was predominantly assigned as an out of phase stretching of C(4a)=N(5) and C(10a)=N(1) by Abe and Bowman as well as our normal mode calculation shifts to higher wave number, 1552cm^{-1}, in the cation form due to the increasing ring II aromaticity. The same explanation can be made for bands at 1348cm^{-1} and 1092cm^{-1} which are assigned to ring II stretching vibrations and shift to higher wave numbers 1360cm^{-1} and 1104cm^{-1} due to the increasing ring II double bound character. On the other hand, the band 1260cm^{-1} which belongs to a ring III stretching vibration mode loses its double bond character and shifts to a lower wave number, 1250cm^{-1}. The new bands at 1620cm^{-1} and 1328cm^{-1}, may be explained as new ring II,III vibrational modes due to the structural changes.

4.4 Conclusions

By analysis of Raman spectra of FMN and with the help of normal mode calculations, we have proposed that FMN was adsorbed flat on Ag electrode at an applied potential of -0.4V vs SCE. Interaction of adsorbed FMN with Ag electrode in our SERS experiment was represented as force constant changes as given by our normal mode calculations. The potential dependence of SERS spectra of FMN indicates that the adsorption sites change with applied potential. We also reported the SERS spectrum of the hydroquinone and cation FMN. UV/Vis absorption spectrophotometry studies indicate that the hydroquinone is in the neutral from.

Table 4.1. Comparison of Raman Bands of FMN; (units of cm^{-1})

RR of Free FMN[a]	SERS of FMN on Ag Electrode at -0.4V[b]	SERS of RF / FMN on Ag Colloid[c]	RR /SERS of FMN-Ag^+ Complex[d]
1630	1630	1630	1625
1584	1576	1576	1576
1550	1540	1536	1554 1530
1503	1506	1507	
1464	1464	1465	1486 1461
	1424		
1412			
		1409	1401
	1398		1374
1355	1348	1349	1351
1303	1308	1303	1316
1282	1280		1293
1262	1260	1287	
1229		1235	1220
1183			
1162	1150	1160	1154
1085	1092	1092	

Data Adopted from:

(a) R. A. Copeland, and T. G. Spiro; J. Phys. Chem.; **1986,** 90, 6648

(b) Our results, SERS of FMN adsorbed on Ag electrode at applied potential -0.4V vs SCE. Excitation 488nm Ar^+ laser line, power at electrode is about 30mw.

(c) N. S. Lee, Y. Z. Hsieh, M. D. Morris, and L. M. Schopfer; J. Am. Chem. Soc.; **1987,** 109, 1358

(d) M. Beneck, T. J. Yu, K. L. Watter, and J. T. McFarland; Biochim. Biophys. Acta; **1980,** 626, 197

Table 4.2. Comparison of calculation and exeprimental Raman Band shifts of FMN from RR to SERS; (Unit of cm^{-1})

Calculation band frequency of FMN RR spectrum	Calculation band frequency of FMN SERS on Ag Electrode at -0.4V	Calculation band shifts	Expt. band shifts
1633	1634	1	0
1584	1572	-12	-8
1538	1526	-12	-10
1490	1491	1	3
1473	1473	0	0
	1424		
1409			
	1398		
1347	1343	-4	-7
1326	1327	1	5
1287	1283	-4	-2
1253	1250	-3	-2
1160	1156	-4	-12
1101	1101	0	7

Table 4.3. List of force constants changes of FMN from RR to SERS; (unit of mdyne / Å)

Type of force constants	Calculation force constants of FMN from RR spectrum	Calculation force constants of FMN from SERS on Ag Electrode at -0.4V	Changes of force constants
$S(N_{10}\text{-}C_{9a})$	4.8473	4.8709	0.0236
$S(N_5\text{-}C_{5a})$	4.8982	4.9852	0.0870
$S(N_5\text{-}C_{4a})$	6.8829	6.9905	0.1076
$S(C_{4a}\text{-}C_{10a})$	3.2566	3.2147	-0.0419
$S(N_1\text{-}C_{10a})$	6.6441	6.1998	-0.3443
$S(C_{4a}\text{-}C_4)$	3.0103	3.0045	-0.0058
$S(N_1\text{-}C_2)$	4.2144	4.2609	0.0465
$S(N_3\text{-}C_4)$	4.5030	4.4767	-0.0263
$S(N_3\text{-}C_2)$	4.2144	4.2513	0.0369
$S(N_{10}\text{-}C_{10a})$	4.6972	4.5100	-0.1872

S: Streching

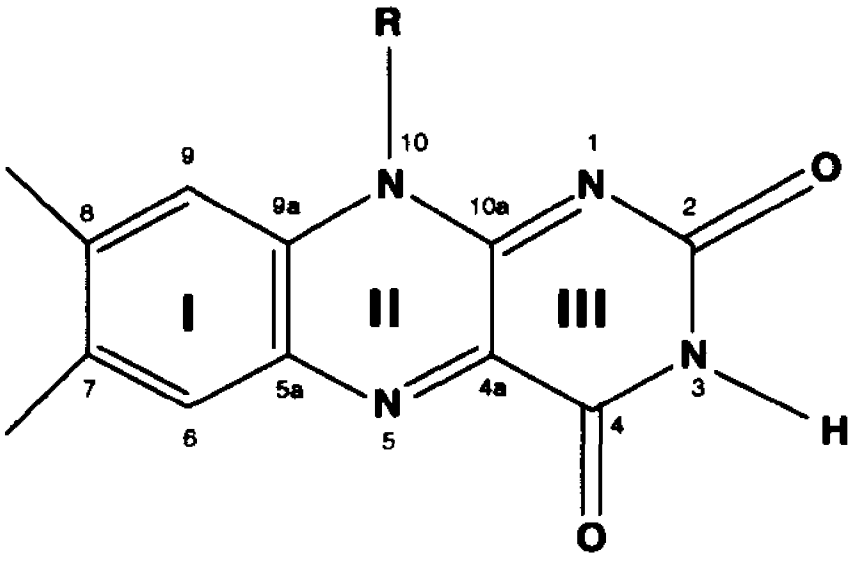

FMN: $R = CH_2\text{-}CH(OH)\text{-}CH(OH)\text{-}CH(OH)\text{-}CH_2(H_2PO_4)$

LF: $R = CH_3$

Figure 4.1 The structure and atomic numbering of the isoalloxazine of flavin.

Figure 4.2. The configuration of UV/Vis-electrochemical cell which consists of two parts, the UV/Vis detection area (function as working electrode) and the sample solution bath; (a) Front view of the cell. (b) Top view of the UV/Vis detection area. This detection area consists of gold grid working electrode and two quartz windows which were separated by 300Å Teflon thin film. This configuration enables probe light to pass through the gold grid working electrode and the solution in this area to be completely electrolysis.

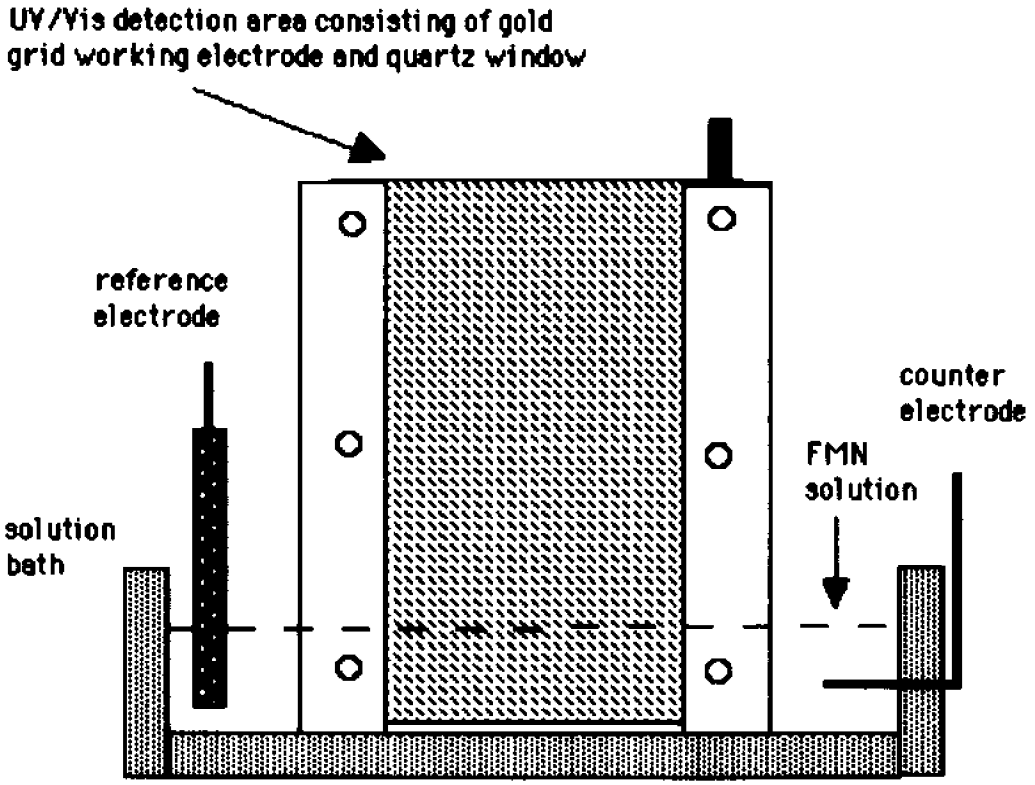

Figure 4.2(a) Front view of UV/Vis spectroelectrochemical cell

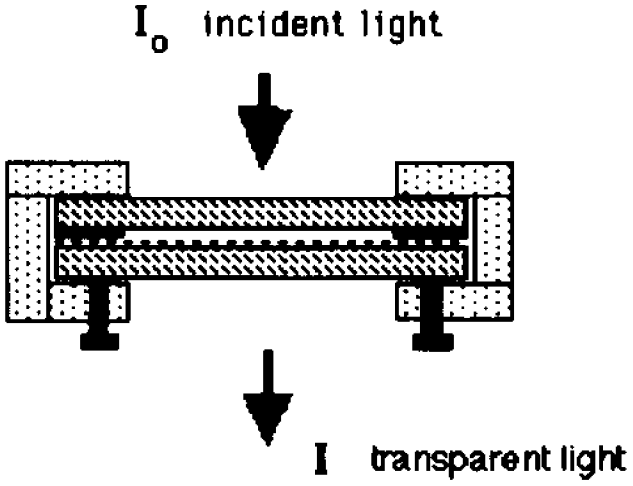

Figure 4.2(b) Top view of UV/Vis detection area, the working electrode

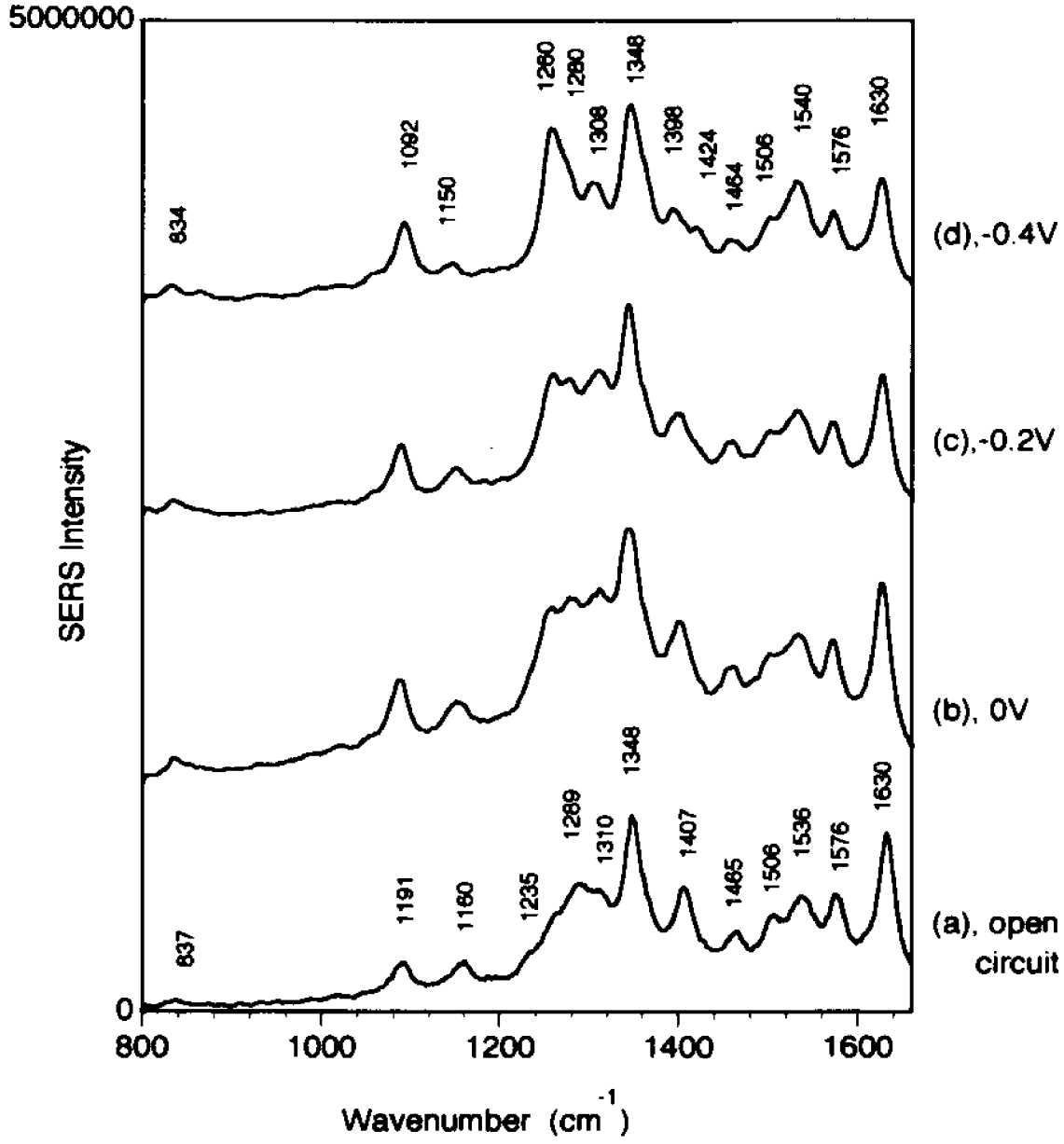

Figure 4.3 Potential dependence of SERS spectra of FMN adsorbed on roughened Ag electrode in pH 7 K_2SO_4 electrolyte solution; (a) open circuit, (b) 0V, (c) -0.2V, (d) -0.4V. Excitation of 488nm Ar^+ laser light with power of 30mW at Ag electrode. Experimental details were considered to avoid photochemical reactions due to 488nm laser light. Exposure time of the Ag electrode to laser light is only 0.3s during which spectrum was taken. Each spectrum was taken at a new spot on the Ag electrode area.

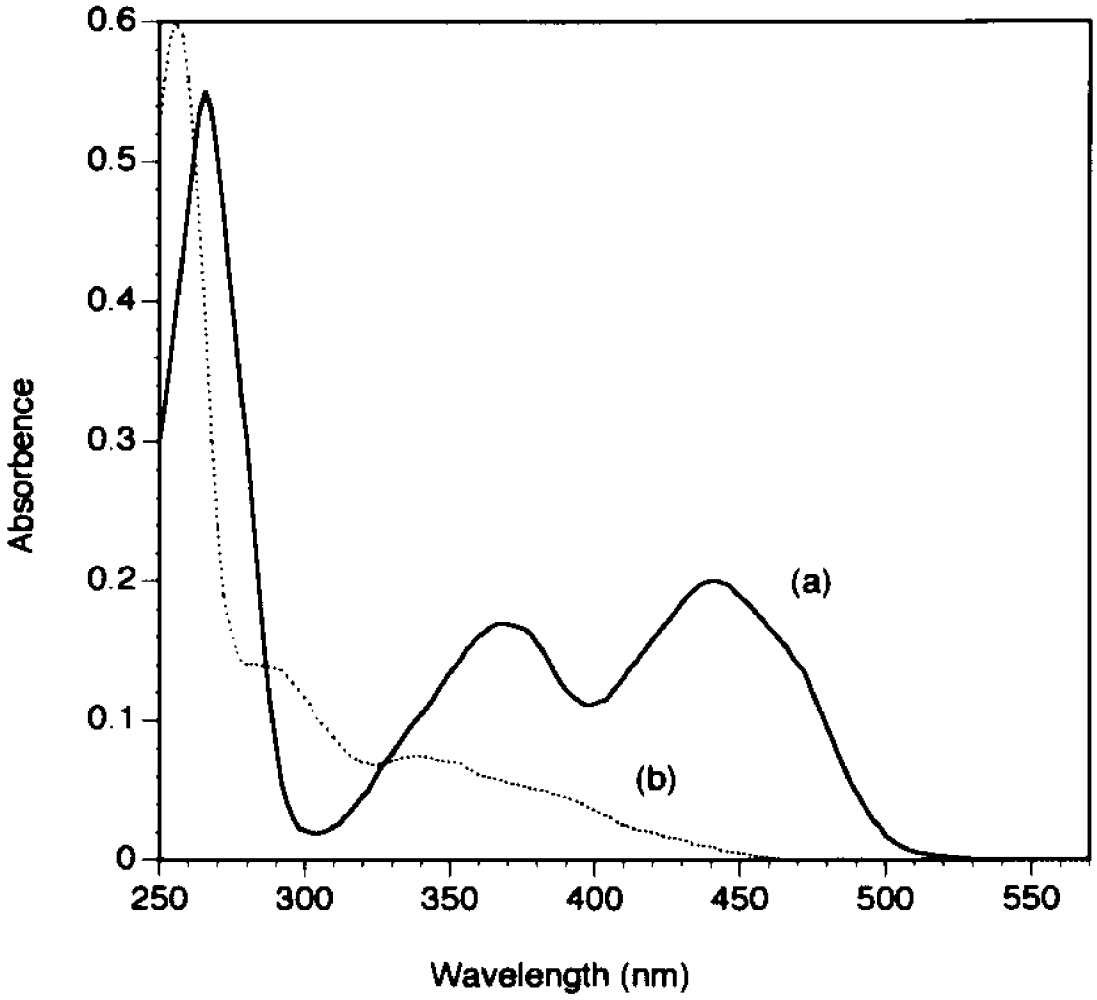

Figure 4.4 Absorption spectra of FMN at different applied potential obtained by using UV/Vis-electrochemical cell system of Figure 4.2.
(a) At applied potential of -0.4V, spectrum is the same as FMN in aqueous solution.
(b) At applied potential of -0.7V, spectrum is the same as chemical produced neutral FMN hydroquinone in aqueous solution.
Concentration of FMN is ($1x10^{-3}$) in 0.1M K_2SO_4 aqueous solution pH 7.

Figure 4.5 SERS spectra of FMN adsorbed on Ag electrode in pH 7 K_2SO_4 electrolyte solution; (a) -0.4V, (b) -0.7V, and (c) differential spectrum of (a) and (b); (c) = (b) - (a) with band 1630 cm^{-1} as a normalization band. Spectrum (c) shows new bands of the hydroquinone. Laser excitation 488nm line.

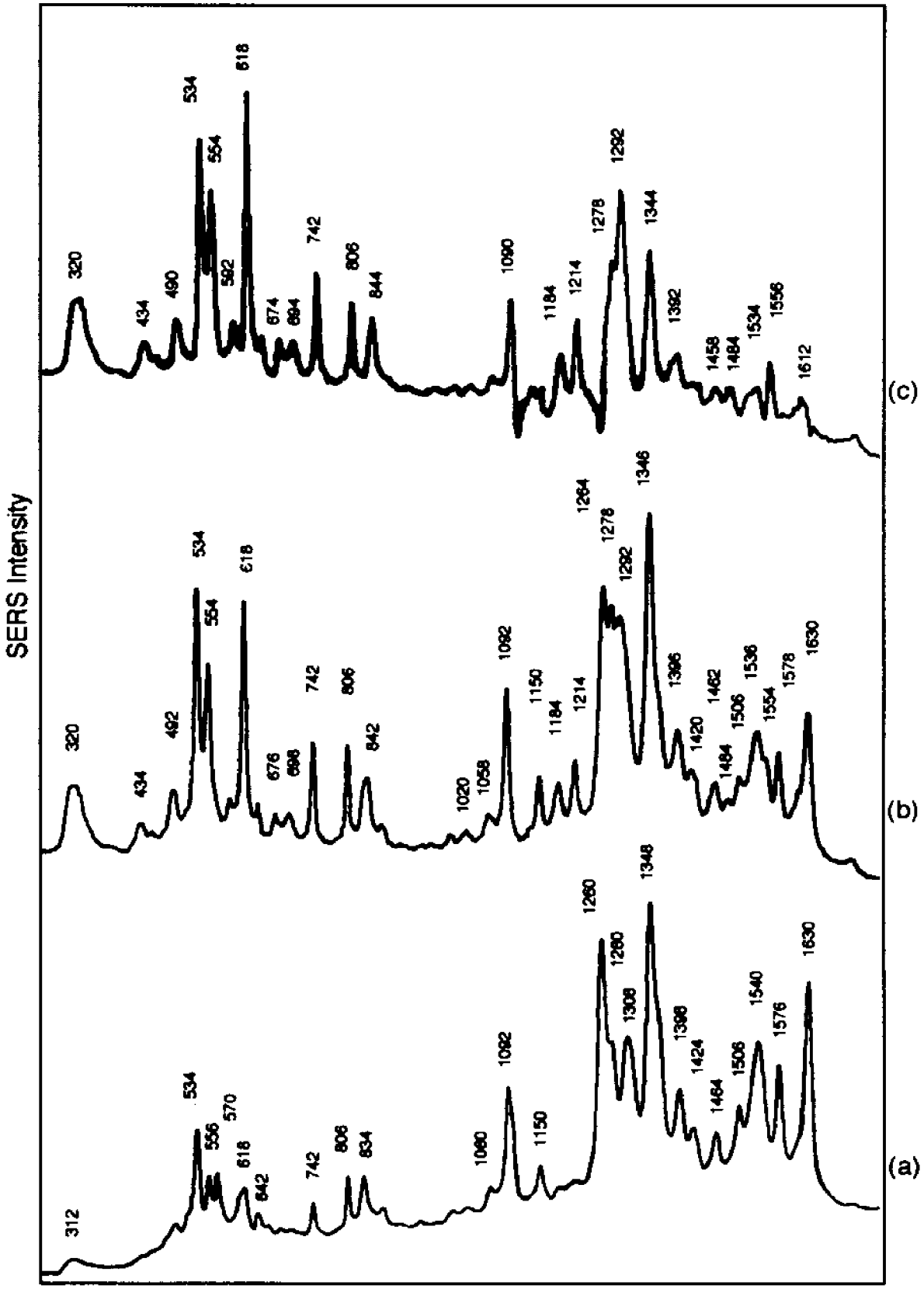
SERS Intensity
(c)
320
434
490
534
554
582
618
674
694
742
806
844
1090
1184
1214
1278
1292
1344
1392
1458
1484
1534
1556
1612
(b)
320
434
492
534
554
618
676
696
742
806
842
1020
1058
1092
1150
1184
1214
1264
1278
1292
1346
1396
1420
1462
1484
1506
1536
1554
1578
1630
(a)
312
534
556
570
618
642
742
806
834
1060
1092
1150
1260
1280
1308
1348
1398
1424
1464
1506
1540
1576
1630
wavnumber (cm-1)

Figure 4.5

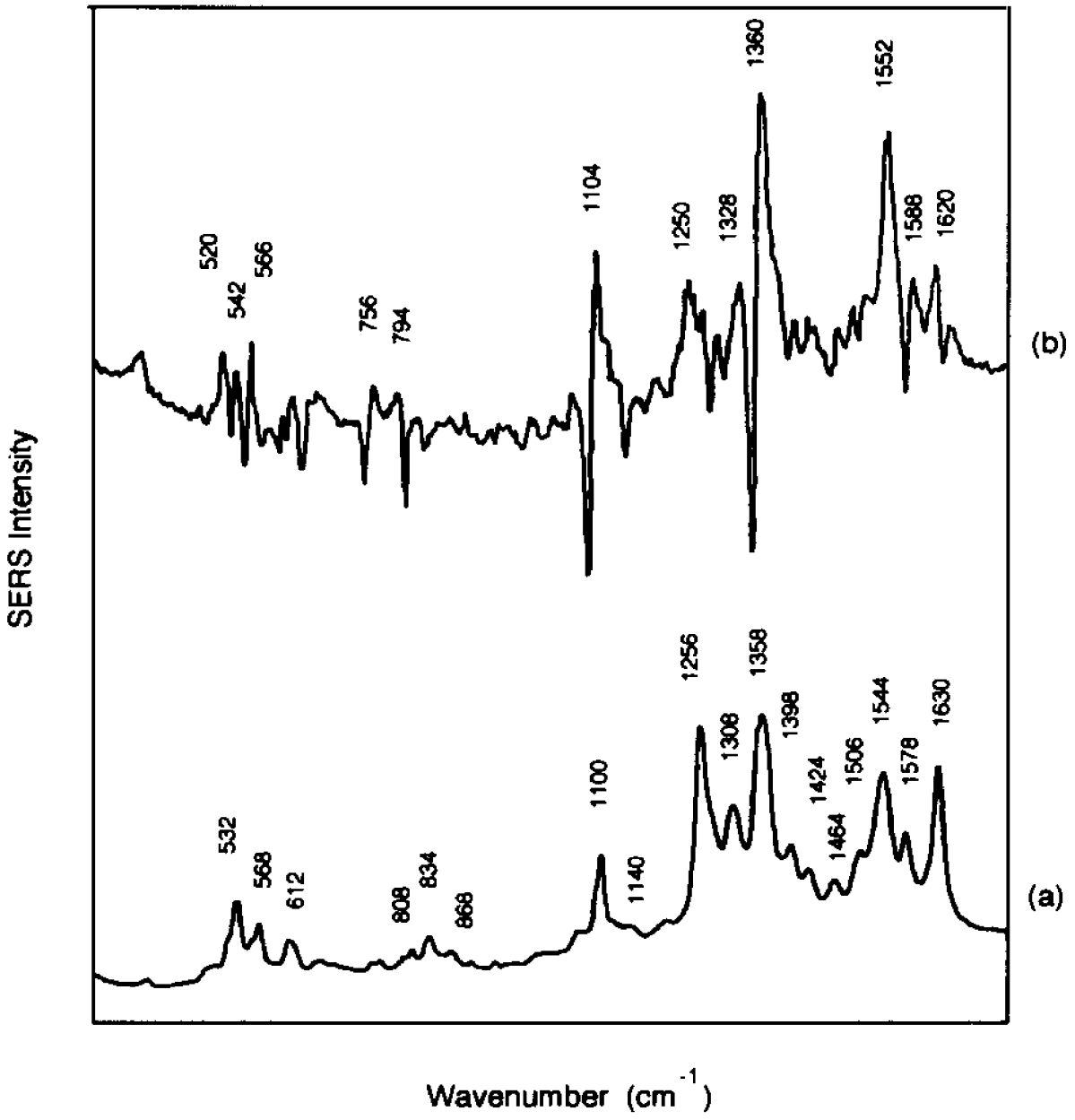

Figure 4.6 SERS spectra of cation FMN adsorbed on a Ag electrode in K_2SO_4 electrolyte solution.

(a) Spectrum obtained at applied potential of -0.2V,
(b) Differential spectrum of (4.6a) and (4.5a); (b) = (4.6a) - (4.5a). The band at 1630cm^{-1} is used as a normalization band. Spectrum (b) shows new SERS bands of cation FMN generated by 488nm laser photo-assistance.

Chapter 5 Detection of Short-Lived Intermediates in Electrochemical Reactions Using Time-Resolved Surface-Enhanced Raman Spectroscopy

5.1 Introduction

The development of surface-enhanced Raman scattering (SERS) spectroscopic methods for studying species on electrode surfaces has enabled detection of molecules heretofore inaccessible through normal high-resolution means. [1,2] The vast majority of SERS measurements have been applied to stable species, although the technique should be capable of investigating transient phenomena at very short times. Early studies of fast time -resolved SERS, in the millisecond region, involved measuring the scattering intensity at fixed wave number vs. time. [3,4] However, coupling the surface enhancement with optical multichannel devices capable of scanning entire spectral regions in milliseconds allows the possibility of examining the structure of relatively short-lived species during the process of electrochemical oxidation or reduction. An optical multichannel analyzer (OMA) has previously been used to record a time-resolved resonance Raman scattering (TR^3S) signal on a millisecond time scale for a species generated electrochemically; [5] However, it was shown that transient measurements using a RR process at an electrode is not straight-forward because of the distortion of the signal by self-absorption. [6] With SERS this distortion is eliminated because the scattering, in most cases, comes from a layer of molecular dimensions at the surface. Although TR^3S studies from milliseconds to nanoseconds have been accomplished in solution [7,8] there has been a marked lack of such measurements using SERS. [9] In this thesis we report detection of a short-lived intermediate with a lifetime of less than 100 ms in the electrochemical oxidation of p-(hydroxylamino)-benzoic acid. We believe this is the first time a transient intermediate has been detected by time-resolved

SERS (TRSERS) recording of a succession of spectra with a multichannel detection system.

5.2 Experimental Section

The experimental apparatus used in these experiments is identical with that previously described [10] with the addition of an electronically controlled shutter with a response time of 7 ms, used to initiate the detection procedure, which itself is illustrated in Figure 5.1. A potential pulse (-0.9 V vs. SCE) is applied to the electrode for a period of 200 ms reduce PNBA to the hydroxylamine compound, and the potential is relaxed to -0.2 V during which the time-resolved surface-enhanced Raman spectrum is recorded by means of a gated detection scheme, which samples the spectrum by a optical multichannel analyzer (OMA) at various intervals (Figure 5.1).

The p-nitrobenzoic acid (PNBA) was reagent grade and used without further purification. Solutions of PNBA were made up in 0.1 M Na_2SO_4 , and NaOH was used to adjust the pH to 11 so that PNBA is in the form of a carboxylate anion. p-(Hydroxylamino) benzoic acid (PHABA) was synthesized according to the literature [11] and the product recrystallized three times in distilled water. p-Nitrosobenzoic acid (PNSBA) was prepared [12] by using Tollens' reagent to oxidize PHABA with a molecular ratio 5:2. After acidification with concentrated HCl, the product was extracted into ether and from ether into a basic aqueous solution. Polished silver electrodes were pretreated by two successive oxidation-reduction cycles where the electrode potential was jumped from 0.0 V to -0.5 V for 2 s and returned to 0.0 V. All electrode potentials in this

paper are quoted versus the saturated calomel electrode, SCE.

5.3 Results and Discussion

The electroreduction of arylnitro compounds is a complicated process which has received much attention in the literature. [13-19] These studies indicate that reduction of PNBA should produce p-nitrosobenzoic acid (PNSBA) as an intermediate which does not accumulate but is further reduced to p-(hydroxylamino)benzoic acid (PHABA). [18] Depending on electrode material and pH, the final reduced product is p-aminobenzoic acid (PABA) which typically occurs in a separate reduction step at very negative potentials. [18] In addition, in basic media a chemical coupling reaction between the nitroso and hydroxylamine compounds can occur forming an azoxy compound. [16,18] Cyclic voltammetry on Ag [10] of 1 mM PNBA solution shows that two cathodic waves are found at approximately -0.6 and -1.2 V and a single anodic wave, at -0.3 V on reversing the scan. The first cathodic peak at -0.6 V corresponds to a four-electron reduction from PNBA to the arylhydroxylamine, PHABA (reaction 1) and the

$$Ar\text{-}NO_2 + 4e^- + 3H_2O \xrightarrow{k} Ar\text{-}NHOH + 4OH^- \qquad (1)$$

second cathodic wave at -1.2 V has been attributed to the formation of PABA in a two-electron-reduction step. [10] The anodic wave on the reverse sweep at -0.3 V corresponds to a reoxidation of the hydroxylamine, formed on the cathodic sweep, to the nitroso compound, PNSBA, with a two-electron-transfer step (reaction 2). Furthermore, there is the possibility [10] that the coupling reaction of

$$Ar\text{-}NHOH + 2OH^- \rightleftharpoons Ar\text{-}NO + 2H_2O + 2e^- \qquad (2)$$

the nitroso compound with the hydroxylamine compound occurs according to (reaction 3) to give the arylazoxy compound

$$Ar\text{-}NHOH + Ar\text{-}NO \rightleftharpoons Ar\text{-}N(\rightarrow O)=N\text{-}Ar + H_2O \qquad (3)$$

Thus in a potential reversal experiment as described in the Experimental Section when the potential is returned from -0.9 V to -0.2 V both reactions 2 and 3 are possible.

The SERS spectrum [10] of the starting compound, the PNBA anion, at a potential of -0.2 V shows only four major bands at 866, 1115, 1350, and 1600 cm^{-1} (see Table 5.1). The 1600cm^{-1} band is assigned to the benzene ring stretching mode, υ_8. The other three bands belong to vibrations of the nitro group [10] with the 1350 and 1115cm^{-1} bands assigned to the symmetric stretch, υ_s (NO_2), and antisymmetric stretch, υ_a (NO_2), respectively. The 866cm^{-1} band represents the deformation of the nitro group, $\delta(NO_2)$. Exsitu pretreatments in 0.1 M Na_2SO_4, 0.1 M KCl solutions yield the same spectra as the in situ pretreatment.

SERS spectra from authentic compounds which may appear as intermediate products have been measured and their major bands are also listed in Table 5.1. The SERS spectrum of the authentic hydroxylamine compound taken in 0.1 M Na_2SO_4 at pH 11 and -0.5 V shows only two major bands at about 1364 and 1600cm^{-1}. When the authentic hydroxylamine compound in 0.1 M Na_2SO_4 at pH 3.7 is electrochemically oxidized on a Ag electrode surface at -0.1

V bands appear which can be attributed to the nitroso compound. These bands which appear in acidic medium are listed under the entry PNSBA [b], while the spectral bands in Table 5.1 labeled PNSBA [c] are obtained in basic media from species generated both chemically [12] and electrochemically by oxidation of authentic hydroxylamine. It can be seen from the table that the latter system, PNSBA [c], shows two very strong bands at 1277 and 1329 cm^{-1} and a medium strength band at 1095 cm^{-1}. However, in acidic medium (pH 3.7) the 1277 and 1329cm^{-1} bands become very weak and the 1095cm^{-1} and totally disappears. According to many authors, [13-21] the chemical coupling reaction between the nitroso and hydroxylamine compounds proceeds very quickly in basic media but it proceeds only slightly in acidic media. Thus the spectrum of PNBA in acidic medium should represent the nitroso compound and that of PNSBA in basic medium a mixture of nitroso and azoxy compounds.

Figure 5.2 shows the time-resolved SERS spectra for the potential excitation experiment in 0.05 M PNBA with 0.1 M Na_2SO_4 as supporting electrolyte at pH 11. The electrode potential is jumped from zero to -0.9 V for 200 ms and then back to -0.2 V. The time-dependent SERS were taken at t_1 , when the potential returned from -0.9 V to -0.2 V (see Figure 5.1). The time interval between successive spectra was 10 ms. At the pumping potential, -0.9 V, the main species on the Ag electrode surface should be the hydroxylamine compound according to our proposed cyclic voltammetry reduction scheme.[10] The first spectrum obtained after the potential pulse returns to -0.2 V shows one intense band at 1364 cm^{-1} and two weaker bands at 866 and 1600 cm^{-1}. These same bands are also found at -0.9 V during the potential excitation and are nearly identical with those listed in Table 5.1 for the authentic hydroxylamine compound, PHABA, confirming that PHABA is formed at -0.9 V. Several new

peaks at 996, 1095, 1115, 1130, 1145, 1175, 1233, 1277, 1325, 1350, 1395, 1454 and 1580cm^{-1} start to appear 30 ms later. The final spectrum corresponds to a mixture including nitro, nitroso, and azoxy compounds. Some of these bands at 866, 1115 and 1350cm^{-1} belong to the nitro compound which continues to diffuse onto the surface of the electrode after the electrochemical process ceases. The bands at 1130, 1145, 1395 and 1454 cm^{-1} represent the formation of the nitroso compound (see Table 5.1), while the bands at 1095, 1277 and 1325cm^{-1} are close to bands at 1098, 1273 and 1325cm^{-1} found in the literature [21,22] in the spectrum of azoxybenzene. These bands represent the product which develops from the chemical coupling reaction between the nitroso and the hydroxylamino compounds. The bands representing the azoxy compound appear nearly at the same time and the same rate as those of the nitroso compound (see Figure 5.3a). This result is consistent with the conclusion drawn from electrochemistry that a rapid chemical reaction, which consumes the nitroso molecules, follows the formation of nitroso compound. However, the assignment of all of the bands due to the azoxy compound is difficult because some of the bands assigned to the nitroso compound overlap with the azoxy compound.

Transient bands are found at 966, 1233 and 1580cm^{-1}. These bands appear slightly earlier than those bands for the final products and then disappear about 70 ms later. The experimental curves of the intensities of the transient 1233 and 1580cm^{-1} bands versus time are shown in Figure 5.3b. These transient bands must correspond to some kind of intermediate. A reasonable interpretation suggests that this intermediate is a free-radical anion, Ar-NO$^{-\bullet}$, produced during the electrochemical oxidation of the hydroxylamine compound:

$$\text{Ar-NHOH} + 2\text{OH}^- \rightleftharpoons \text{Ar-NO}^{-\bullet} + 2\text{H}_2\text{O} + e^- \qquad (4)$$

$$Ar\text{-}NO^{-\cdot} \rightleftharpoons Ar\text{-}NO + e^{-} \qquad (5)$$

The lifetime of this species on the Ag electrode surface is about 70 ms. ESR studies provide evidence for the existence of nitroso radical anion but the lifetime of this free radical in solution is much longer, about 2 min. [19] The shorter lifetime in our experiment is understandable since the species is not free in solution but is situated in the electrical field of the double layer at Ag surface. The 1580cm^{-1} band of the transient species may be assigned as the benzene ring stretching mode. The resonance effect of the free radical with the benzene ring would tend to stabilize the radical and thus cause a shift of the ring stretch band from 1600 to 1580cm^{-1}. Furthermore, the transient band at 1233cm^{-1} may be related to the carbon-nitrogen vibration since the resonance effect favors the double-band structures and the carbon-nitrogen single-bond vibration band is located at about 1145cm^{-1}.

5.4 Conclusion

It is clear from the results presented that time-resolved surface-enhanced Raman spectroscopy can provide a valuable tool for detailed studies of short-lived intermediates in electrode processes. Further time-resolved SERS studies of the PNBA electrochemistry are presented in our another publication. [23]

Table 5.1: SERS Bands of PNBA and Its Reduction Products

PNBA[a]	PNSBA[b]	PNSBA[c]	PHABA[d]
866 s	847 m[e]	847 m	847 w
	926 m	926 m	
1115 s		1095 m	
	1130 vs[e]	1130 vs	
	1145 vs	1145 vs	
	1175 m	1175 m	
	1277 w[e]	1277 vs	
1350 vs	1329 w	1329 vs	
	1372 s[e]	1372 w	1364 s
	1395 vs	1395 vs	
	1454 vs	1454 vs	
1600 vs	1600 vs	1600 vs	1600 s

[a] pH 11, excitation at 609nm with 20 mW power to prevent photochemistry.[10]

[b] pH 3.7, excitation at 488nm with 100 mW power.

[c] pH 11, excitation at 488nm with 100 mW power.

[d] pH 3.7 or 11, excitation at 488nm with 100 mW power.

[e] vs, very strong; s, strong; m, medium; w, weak.

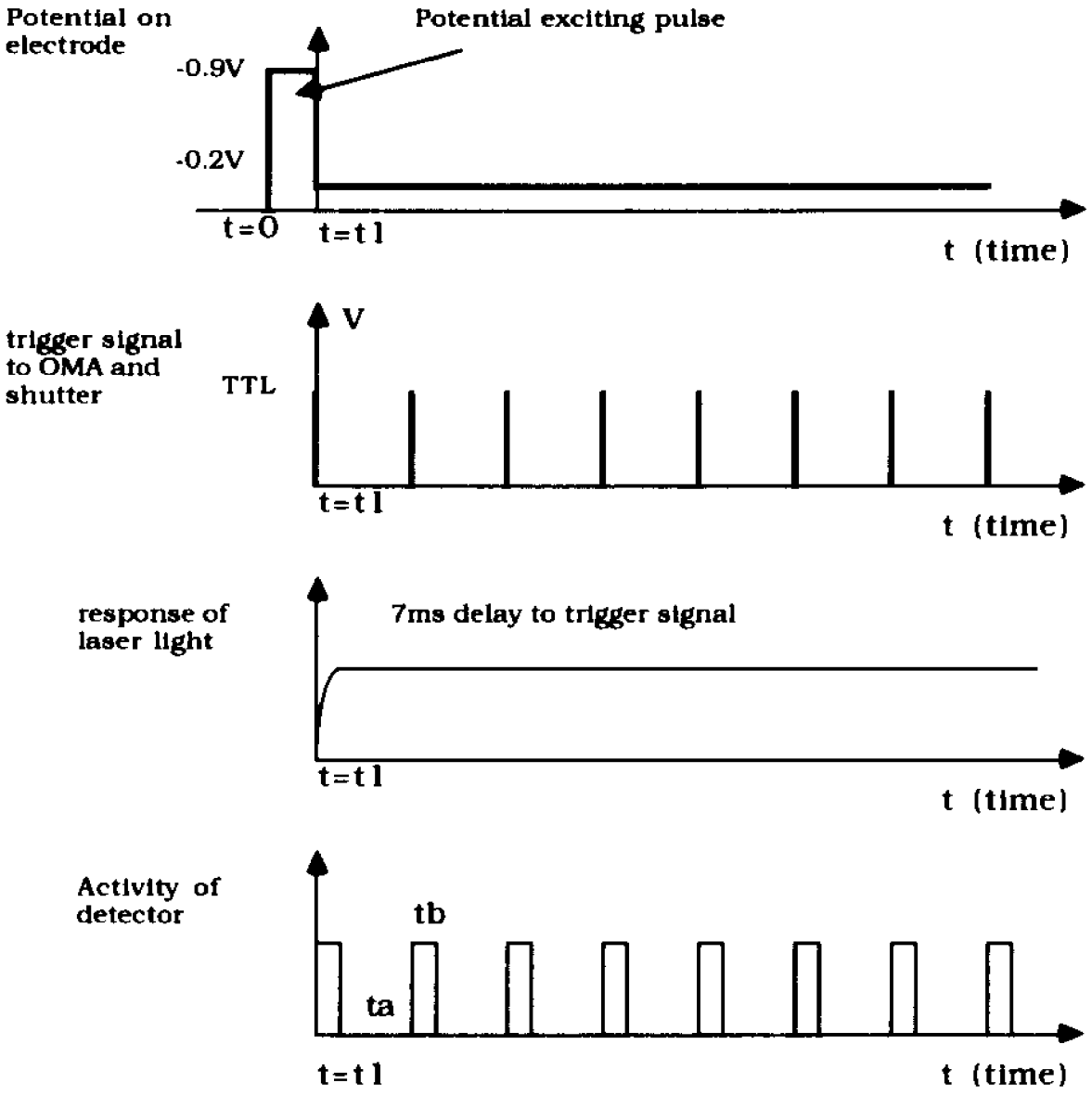

Figure 5.1 Time resolved SERS detection process for an electrochemical excitation experiment. A potential pulse (-0.9V) is applied to the electrode for a period t_1 (200 ms) to reduce PNBA to its hydroxylamine compound, the first product. Then the potential is returned to -0.2V and an unstable intermediate is generated during this process. Following the exciting potential pulse, each TTL trigger generated by a waveform generator enables a SERS detection. t_a is delay time between spectra and t_b is integration time of SERS spectrum.

Figure 5.2 Time resolved SERS spectra of PNBA on a roughened Ag electrode. Excitation potential pulse from 0.0V to 0.9V with 200ms pulse width duration followed by a step to -0.2V. Irradiation with 120mW of 488nm laser light.

Figure 5.2(a) Time 0-90 ms.

Figure 5.2(b) Time 120-150 ms.

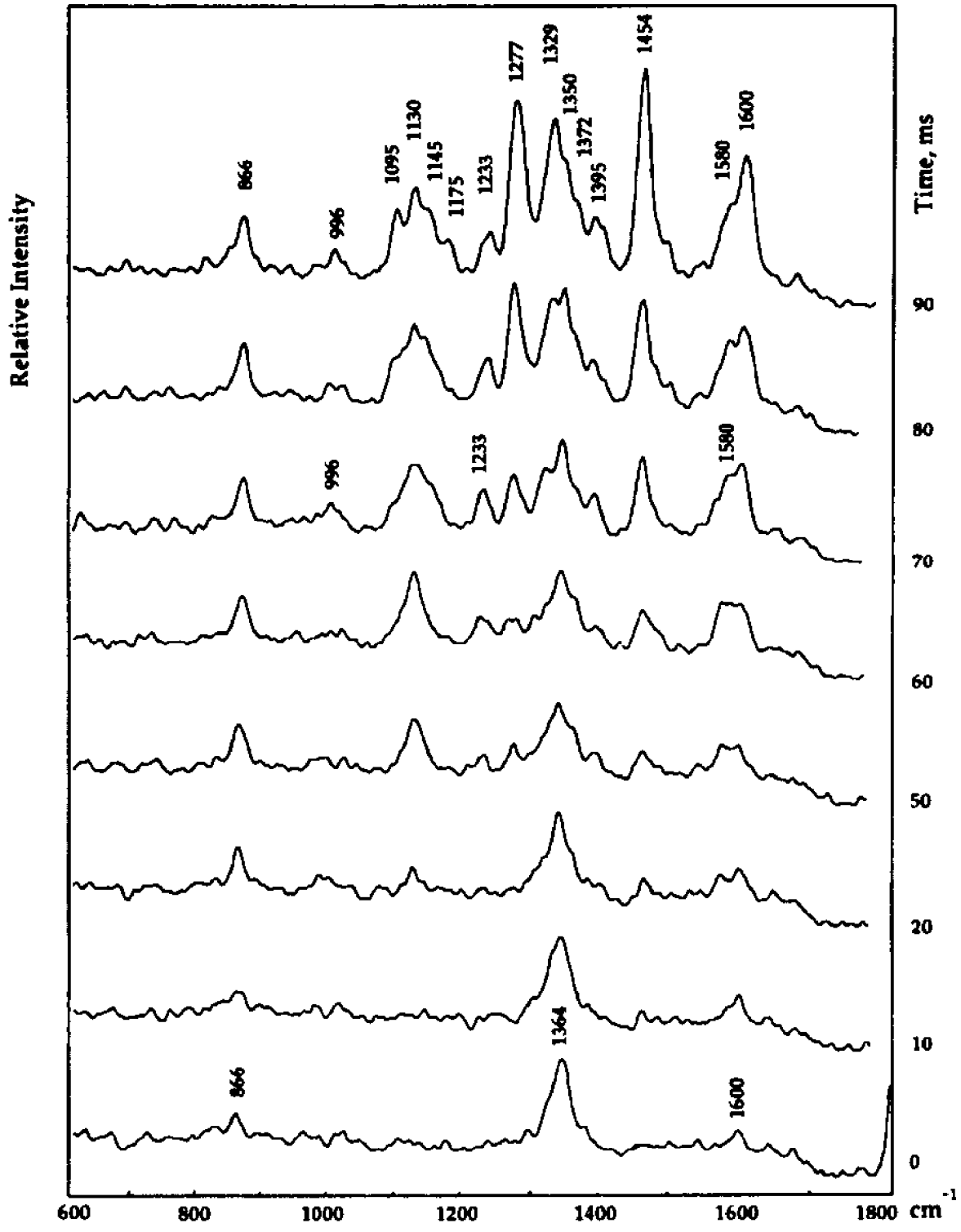
Relative Intensity
Time, ms
866
996
1095
1130
1145
1175
1233
1277
1329
1350
1372
1395
1454
1580
1600
1364
90
80
70
60
50
20
10
0
600
800
1000
1200
1400
1600
1800
cm -1

Figure 5.2a

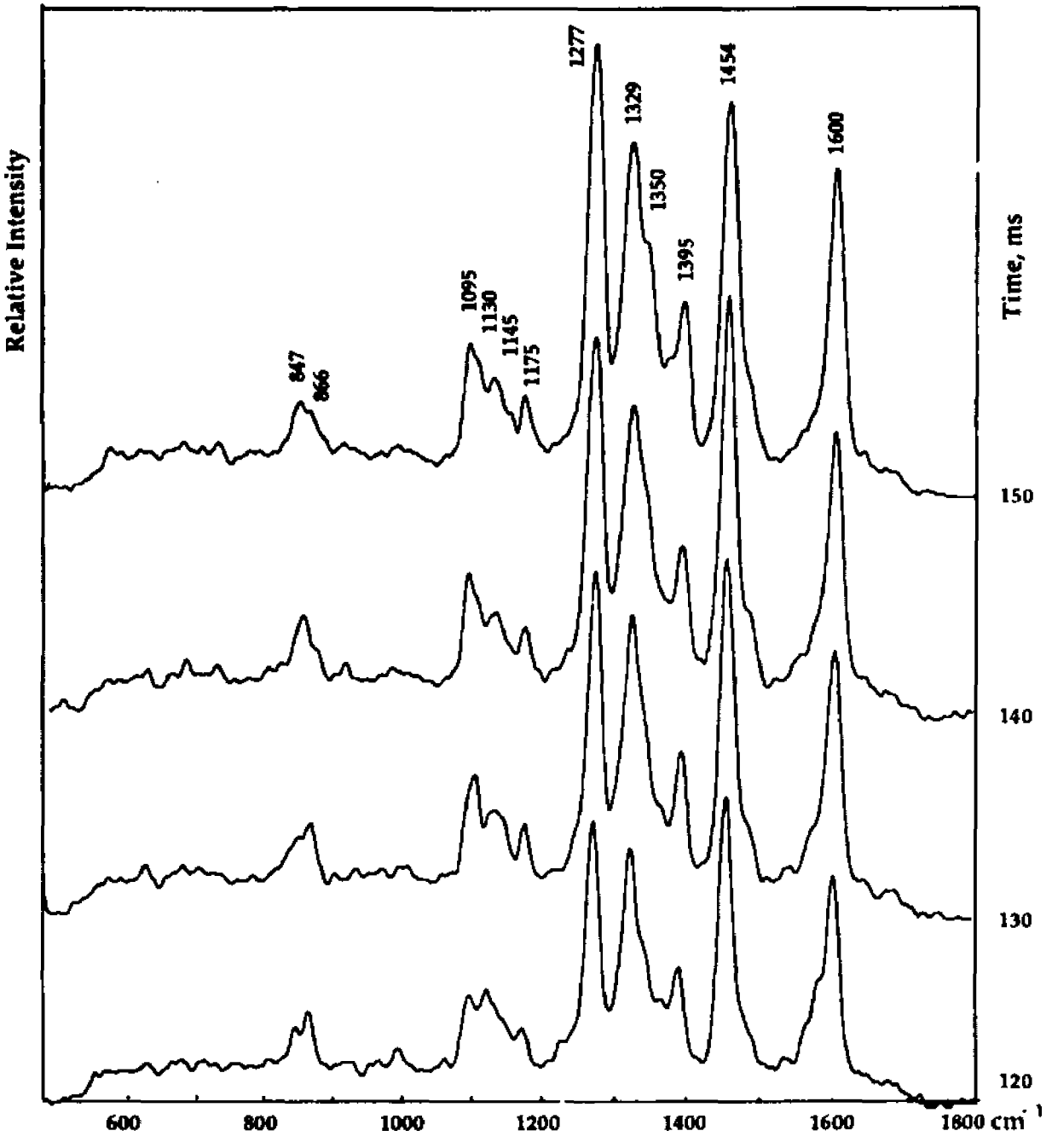
Relative Intensity
847
866
1095
1130
1145
1175
1277
1329
1350
1395
1454
1600
Time, ms
150
140
130
120
600
800
1000
1200
1400
1600
1800 cm⁻¹

Figure 5.2b

Figure 5.3 Time dependence of intensities of some SERS bands in a potential pulse excitation.

(5.3a) Bands plotted: Δ ···· 1277 cm^{-1}, O ···· 1395 cm^{-1}, □ ···· 1454 cm^{-1}.

(5.3b) Bands plotted: O ···· 1233 cm^{-1}, Δ ···· 1580 cm^{-1}.

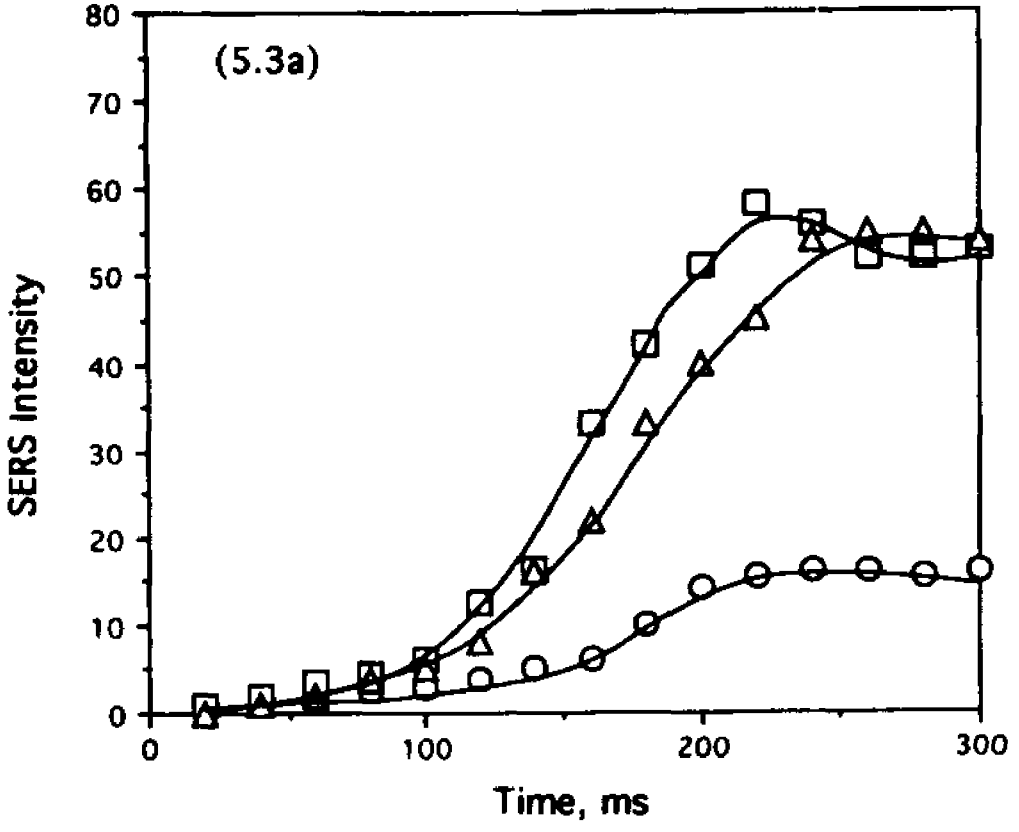
(5.3a)
SERS Intensity
Time, ms
0
10
20
30
40
50
60
70
80
0
100
200
300

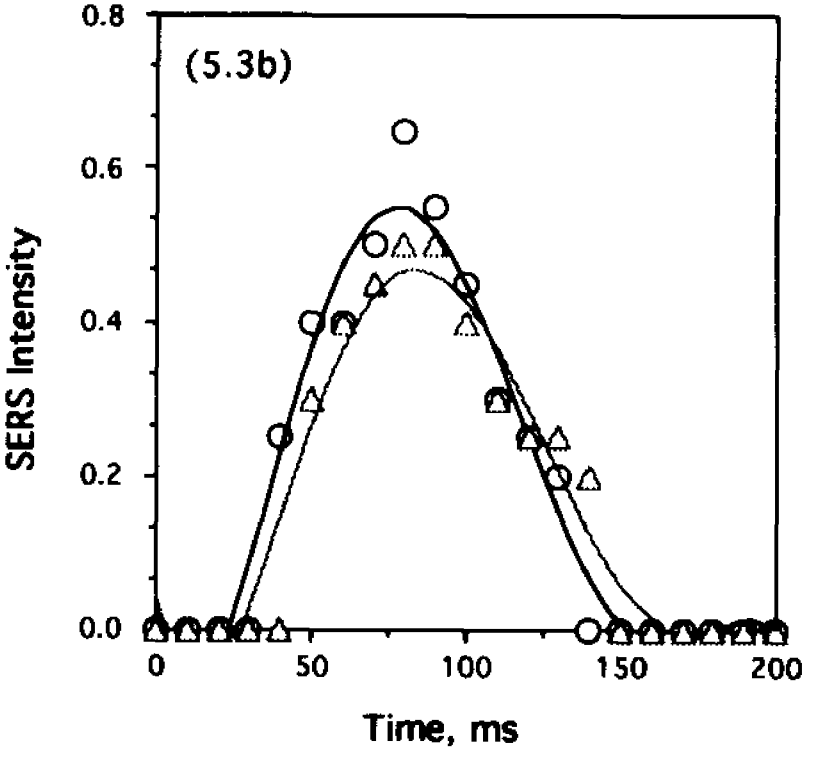
(5.3b)
SERS Intensity
Time, ms
0.0
0.2
0.4
0.6
0.8
0
50
100
150
200

APPENDIX (A)

Literature Search for SERS and TRSERS publications:

Years	# of SERS papers	# of TRSERS papers
1972-1976	22	
1977-1981	200	3
1982-1986	704	3
1987	117	
1988	119	3
1989	111	
1990	128	
1991	134	2
1992	138	2
1993	118	4
Jan. 1994-Jun. 1994	88	
Total of Papers	1879	17

The literature search is based on Chemical Abstracts. Search under titles of:

(1) Raman spectra--resonance surface enhanced
(2) Raman spectra--surface enhanced
(3) Raman spectrometry--resonance surface enhanced
(4) Raman spectrometry--surface enhanced
(5) Raman spectra--adsorbed on

The TRSERS papers were restricted by following worlds: time resolved, time dependent (dependence, development), real time, kinetics, dynamics, transient, monitoring, probe (probing).

The literature search may not accurately reflect all papers published during last twenty years, but it gives a relative comparison of the number of papers for SERS and TRSERS.

BIBLIOGRAPHY

Chapter 1

(1) G. A. Somorjai; J. Phys. Chem., 1990, 94, 1013

(2) J. B. Hudson; Surface Science: An Introduction; Butterworth-Heinemann, 1991

(3) Interaction of Atoms and molecules with Solid Surfaces; V. Bortolani, N. H. March, and M. P./ Tosi, Eds.; Plenum Press, New York, 1990

(4) Concepts in surface physics; Springer Series in Surface Science, Vol.30; M. C. Desjonqueres, D. Spanjaard Eds., Springer-Verlag, Berlin, New York, 1993

(5) Atomic and Electronic Structure of Surface: Theoretical Foundations; Springer Series in Surface Science, Vol. 16; M. Lannoo, P. Friedel, Eds.; Springer-Verlag, Berlin, New York, 1991

(6) Diffusion at Interface: Microscopic Concepts, Springer Series in Surface Science, Vol. 12; M. Grunze, H. J. Kreuzer and J. J. Weimer, Eds.; Springer-Verlag: Berlin, 1988

(7) Chemistry and Physics of Solid Surface VIII, Springer Series in Surface Science, vol. 22; R. Vanselow, R. Howe, Eds.; Springer-Verlag: Berlin, New York, 1990

(8) Chemistry and Structure at Interfaces, New Laser and Optical Techniques; R. B. Hall, A. B. Ellis, Eds.; VCH Publishers, Inc.; Deerfield Beach, Florida, 1986

(9) R. Sh. Mikhail, E. Robens; Microstructure and Thermal Analysis of Solid Surfaces; John Wiley & Sons, 1983

(10) Interactions on Metal Surfaces, V; R. Gomer, Ed.; Springer-Verlag, Heidelberg, 1975

(11) Advances in Catalysis; D. D. Eley, H. Pines and P. B. Weisz, Eds.; Academic Press, Inc.; Orlando, 1985

(12) J. Kijenski and A. Baiker; Catalysis Today, 1989, 5, pp1-107

(13) Adsorption and Catalysis on Transition Metals and Their Oxides; Springer Series in Surface Sciences, vol.9; V. F. Kiselev, O. V. Krylov Eds., Springer-Verlag, Berlin, New York, 1989

(14) Laser-Controlled Chemical Processing of Surfaces, Materials Research

Society Symposia Proceedings, V29; A. W. Johnson, D. J. Ehrlich and H. R. Schlossberg, Eds.; North Holland, New York, 1984

(15) S. R. Morrison; Electrochemistry at Semiconductor and Oxidized Metal Electrodes; Plenum Press, New York, 1980

(16) Advances in Corrosion Science and Technology, Vol. 7; M. G. Fontana and R. W. Staehle, Eds.; Plenum Press, New York, 1980

(17) G. Wranglen; An Introduction to Corrosion and Protection of Metals; Chapman and Hall, London, 1985

(18) Corrosion Mechanisms, a Series of Reference Books and Textbooks, Vol.28; F. Mansfeld, Ed.; Marcel Dekker, New York, 1987

(19) X. L. Zhou and J. M. White; Surf. Sci., 1988, 194, 438 (AES)

(20) M. E. Levin, M. Salmeron, A. T. Bell and G. A. Somorjai; Surf. Sci., 1988, 195, 429 (XPS)

(21) X. Y. Zhu, S. Akhter, M. E. Castro and J. M. White; Surf. Sci., 1988, 195, L145 (SIMS)

(22) Low Energy Electron Diffraction: Experiment, Theory and Surface Structure Determination; Springer Series in Surface Sciences, Vol. 6; M. A. Van Hove, W. H. Weinberg, C. M. Chan, Eds., Springer-Verlag, 1986, Berlin, New York, 1986 (LEED)

(23) J. Dericbourg; Surf. Sci., 1992, 269/270, 1157 (TEM)

(24) Scanning Tunneling Microscopy I: Springer Series in Surface Sciences, Vol. 20; D. Anselmetti, et. al. Eds., Springer-Verlag, Berlin, New York, 1992 (STM)

(25) G. Bracco, M. Canepa, P. Cantini, F. Fossa, L. Mattera, S. Terreni and D. Truffelli; Surf. Sci., 1992, 269/270, 61 (ISS)

(26) A. Ausmees, M. Elango, A. Kikas, E. Nommiste and A. Saar; Surf. Sci., 1992, 269/270, 583 (UPS)

(27) H. Ibach, M. Balden, D. Bruchmann and S. Lehwald; Surf. Sci., 1992, 269/270, 94 (HREELS)

(28) Vibrational Spectroscopies for Adsorbed Species, ACS Symposium Series, 137; A. T. Bell and M. L. Hair, Eds.; American Chemical Society; Washington, D. C., 1980 (FTIR, Raman)

(29) D. A. Stern, E. Wellner and G. N. Salaita; L. Laguren-Davidson, F. Lu, N.

Batina, D. G. Frank, D. C. Zapien, N. Walton, A. T. Hubbard; J. Am. Chem. Soc.; 1988, 110, 4885

(30) J. Y. Gui, B. E. Kahn, C. H. Lin, F. Lu, G. N. Salaita, D. A. Stern, D. C. Zapien and A. T. Hubbard; J. Electroanal. Chem. ; 1988, 252, 169

(31) T. E. felter and A. T. Hubbard; J. Electroanal. Chem.; 1979, 100, 473

(32) Advances in Electrochemistry and Electrochemical Engineering, Vol. 9; P. Delahay and C. W. Tobias, Eds., Wiley, New York, 1973

(33) W. R. Heineman and J. F. Goelz; J. Electroanal. Chem., 1978, 89, 437

(34) Non-Traditional Approaches to the Study of the Solid-Electrolyte Interface, Proceedings of an International Conference, Snowmass, Colorado, 1979; T. E. Furtak, K. L. Kliewer and D. W, Lynch, Eds., North-Holland Publishing Co., Amsterdam, 1980

(35) K. M. Kunimatsu, G. Samant, H. Seki and M. R. Philpott; J. Electroanal. Chem., 1988, 243, 203

(36) D. E. Aspnes; Surf. Sci., 1980, 101, 84

(37) J. T. Maloy and A. J. Bard; J. Am. Chem. Soc., 1971, 5968

(38) L. R. Faulkner; J. Electrochem. Soc., 1977, 124, 1725

(39) P. A. Christensen, A. Hamnett; in New Techniques for the Study of Electrodes and Their Reactions, Comprehensive Chemical Kinetics Series, Vol.29, Chapter 1; R. G. Compton, A. Hamnett, Eds., Elsevier, Amsterdam, 1989

(40) M. Fleischmann, P. J. Hendra and A. J. McQuillan; J. C. S. Chem. Comm., 1973, 80

(41) H. B. mark and B. S. Pons; Anal. Chem.; 1966, 11938

(42) H. Neugebauer, G. Nauer, N. Brinda-Konopik and G. Gidaly; J. Electroanal. Chem., 1981, 122, 381

(43) A. Bewick and K. Kunimatsu; Surf. Sci.; 1980, 101, 131

(44) T. Davidson, S. pons, A. Bewick and P. P. Schmidt; J. Electroanal. Chem., 1981, 125, 237

(45) J. K. Foley, C. Korzeniewski, J. L. Daschbach and S. Pons; in Electroanalytical Chemistry, A Series of Advances, Vol. 14; A. J. Bard, Ed., M. Dekker, New York, 1986, pp309

(46) A. Bewick and S. Pons; in Advances in Infrared and Raman Spectroscopy, Vol.12, R. J. H. Clark and R. E. Hester eds., Wiley Heyden, New York, 1985, Chapter 1

(47) M. Fleischmann, P. J. Hendra and A. J. McQuillan; J. Chem. Phys. Lett., 1974, 26, 163

(48) D. L. Jeanmaire and R. P. VanDuyne; J. Electroanal. Chem., 1977, 84, 1-20

(49) M. G. Albrecht and J. A. Creighton; J. Am. Chem. Soc., 1977, 99, 5215

(50) R. P. Van Duyne; in Chemical and Biochemical Applications of Lasers; C. B. Moore Ed.; Academic Press, New York, 1979, Vol. 4, pp101-184

(51) C. A. Murray, D. L. Allara and M. Rhinewine; Phys, Rev. Lett., 1981, 46, 57

(52) D. S. Corrigan, P. Gao, L. W. H. Leung and M. J. Weaver; Lamhmuir, 1986, 2, 744

(53) D. S. corrigan, J. K. Foley, P. Gao, S. Pons and M. J. Weaver; Langmuir, 1985, 1, 616

(54) D. S. corrigan and M. J. Weaver; J. Phys. Chem., 1986, 90, 5300

(55) R. L. Birke and J. R. Lombardi; 'Surface Enhanced Raman Scattering', in Spectroelectrochemistry: Theory and Practice; J. R. Gale Ed., Plenum Press, New York, 1988, pp263-348

(56) T. E. Furtak; Optical and Electronic Resonances: 'The underlying Sources of Surface Enhanced Raman Spectroscopy' in Advances in Laser Spectroscopy; B. Garetz and J. R. Lombardi, Eds., John Wilew and Son, Chichester, 1984, vol.2, pp175-205

(57) R. K. Chang and B. L. Laube; 'Surface Enhanced Raman Scattering and Nonlinear Optics Applied to Electrochemistry', in CRC Critical Reviews in Solid State and Materials Science; CRC Press, Inc., Boca Raton, 1984, Vol.12, pp1-73

(58) H. Seki; J. Electron Spectroscopy and Related Phenomena, 1986, 39, pp289-310

(59) M. Moskovits; Reviews of Modern Physics, 1985, 57, 783

(60) M. Kerker; Acc. Chem. Res., 1984, 17, 271

(61) G. C. Schatz; Acc. Chem. Res., 1984, 17, 370

(62) A. Otto; in Light Scattering in Solids IV, Topics in Applied Physics; M. Cardona, G. Guntherodt, Eds.; Springer-Verlag, Heidelberg, 1984, Vol. 54, 289

(63) K. Arya and R. Zeyher; in Light Scattering in Solids IV, Topics in Applied Physics; M. Cardona, G. Guntherodt, Eds.; Springer-Verlag, Heidelberg, 1984,Vol. 54, 419

(64) T. E. Furtak; J. Electroanal. Chem., 1983, 150, 375

(65) Surface Enhanced Raman Scattering; R. K. Chang, T. E. Furtak, Eds.; Plenum Press, New York, 1982

(66) T. E. Furtak and J. Reyes; Surface Science, 1980, 93, 351

(67) R. P. VanDuyne; in Chemical and Biochemical Applications at Lasers; C. B. Moore, Ed.; Academic Press, New York, 1979, Vol. 4, pp101-184

(68) D. S. Wang, H. Chew and M. Kerker; Applied Optics, 1980, 19, 2256

(69) M. Kerker, D. S. Wang and H. Chew; Applied Optics, 1980, 19, 4159

(70) P. K. Aravind, A. Nitzan and H. Metiu; Surface Science, 1981, 110, 189

(71) N. Liver, A. Nitzan and J. I. Gersten; Chem. Phys. Lett., 1984, 111 449

(72) P. K. Aravind, E. Hood and H. Metiu; Surface Science, 1981 109, 95

(73) P. K. Aravind and H. Metiu; Chem. Phys. Lett., 1980, 74, 301

(74) U. Laor and G. C. Schatz; Chem. Phys. Lett., 1981, 82, 566

(75) E. J. Zeman and G. C. Schatz; in Dynamics on Surfaces; B. Pullman, et al. Eds. 1984, pp413-424

(76) E. J. Zeman and G. C. Schatz; J. Phys. Lett., 1987, 91, 634

(77) M. Moskovits; Solid State Commun., 1979, 32, 59

(78) C. A. Murray and D. L. Allara; J. Chem. Phys., 1982, 76, 1290

(79) C. A. Murray, D. L. Allara and M. Rhinewine; Phys. Rev. Lett., 1981, 46, 57

(80) P. F. Liao, J. G. Bergman, D. S. Chemla, A. Wokaun, J. Melngailis, A. M. Hawryluk and N. P. Economou; Chem. Phys. Lett., 1981, 82, 355

(81) M. Kerker, O. Siiman, L. A. Bumm and D. S. Wang; Applied Optics, 1980,

19, 3253

(82) O. Siiman, L. A. Bumm, R. Callaghan, C. G. Blatchford and M. J. Kerker; J. Phys. Chem., 1983, 87, 1014

(83) M. Kerker, O. Siiman and D. S. Wang; J. Phys. Chem., 1984, 88, 3168

(84) M. Moskovits; J. Chem. Phys., 1978, 69, 4159

(85) D. P. DiLella, A. Gohin, R. H. Lipson, P. McBreen, M. J. Moskovits; J. Chem. Phys., 1980, 73, 4282

(86) J. A. Creighton; in Surface Enhanced Raman Scattering; R. K. Chang and T. E. Furtak, Eds., Plenum Press, New York, 1982, pp315-338

(87) M. Moskovits; in Surface Enhanced Raman Scattering; R. K. Chang and T. E. Furtak, Eds., Plenum Press, New York, 1982, pp243-274

(88) E. Burstein, Y. J. Chen, C. Y. Chen, S. Lundquist, and E. Toastti; Solid State Commun., 1979, 29, 567

(89) J. R. Lombardi, R. L. Birke, T. Lu, J. Xu; J. Chem. Phys., 1986, 84, 4171

(90) J. I. Gersten, R. L. Birke, J. R. Lomardi; Phys. Rev. Lett., 1979, 43, 147

(91) A. Otto, J. Billmann, J. Eickmans, U. Erturk and C. Pettenkofer; Surface Science, 1984, 138, 319

(92) A. Otto, J. Timper, J. Billmann, G. Kovacs and I. Pockrand; Surface Science, 1980, 92, L55

(93) E. Burstein, S. Lundqvist and D. L. Mills; in Surface Enhanced Raman Scattering; R. K. Chang and T. E. Furtak, Eds., Plenum Press, New York, 1982, pp67-88

(94) H. Ueba; J. Chem. Phys., 1980, 73, 725

(95) B. N. Persson; J. Chem. Phys., 1981, 82, 561

(96) S. Efrima and H. Metiu; J. Chem. Phys., 1979, 70, 1602

(97) S. Efrima and H. Metiu; J. Chem. Phys., 1979, 70, 1939

(98) R. L. Birke, T. Lu and J. R. Lombardi; Surface Enhanced Raman Spectroscopy, in Techniques for Characterization of Electrodes and Electrochemical Processes; R. Varma and J. R. Selman, Eds., John Wiley & Sons, Inc., 1991, chapter 5, pp211-277

(99) J. R. Lombardi, R. L. Birke, L. A. Sanchez, I. Bernard and S. Sun; Chem. Phys. Lett., 1984, 104, 240

(100) J. R. Lombardi, E. A. Shields Knight and R. L. Birke; Chem. Phys. Lett., 1981, 79, 214

(101) D. Schmeisser, J. E. Demuth and Ph. Avouris; Chem. Phys. Lett., 1982, 87, 324

(102) J. E. Demuth and P. N. Sanda; Phys. Rev. Lett., 1981, 47, 57

(103) P. N. Sanda, J. M. Warlaumont, J. E. Demuth, J. C. Tsang, K. Christmann and J. A. Bradley; Phys. Rev. Lett., 1980, 45, 1519

(104) M. Moskovits and D. P. DiLella; J. Chem. Phys., 1980, 73, 6068

(105) R. Dornhaus, M. B. Long, R. E. Benner and R. K. Chang; Surface Science, 1980, 93, 240

(106) C. Pettenkofer, J. Eickmans, U. Erturk and A. Otto; Surface Science, 1985, 151, 9

(107) J. Billman and A. Otto; Surface Science, 1984, 138, 1

(108) J. Billman and A. Otto; Solid State Commun., 1982, 44, 105

(109) A. Otto, J. Timper, J. Billmann and I. Pockrand; Phys. Rev. Lett., 1980, 45, 46

(110) J. Billmann and A. Otto; Appl. Surf. Sci., 1980, 6, 356

(111) I. Pockrand and A. Otto; Appl. Surf. Sci., 1980, 6, 362

(112) H. Seki; J. Vac. Sci. Technol., 1981, 18, 633

(113) H. Seki; J. Chem. Phys., 1982, 76, 4412

(114) B. Pettinger, H. Wetzel; in Surface Enhanced Raman Scattering; R. K. Chang and T. E. Furtak, Eds., Plenum Press, New York, 1982, pp293-314

(115) T. E. Furtak and S. H. Macomber; Chem. Phys. Lett., 1983, 95, 328

(116) S. H. Macomber and T. E. Furtak; Solid State Commun., 1983, 45, 267

(117) R. L. Birke and J. R. Lombardi; Investigation of Radical Ions with Time Resolved Surface Enhanced Raman Spectroscopy, in Molecular Engineering; Kluwer Academic Publishers, Netherlands, 1994, vol. 4, pp277-310

(118) M. Moskovits; Reviews of Modern Physics, 1985, 57, 783

(119) A. Otto; in Light Scattering in Solids IV, Topics in Applied Physics, M. Cardona and G. Guntherodt, Eds.; Springer-Verlag, Heidelberg, 1984, Vol. 54, 289

(120) E. Koglin and J. M. Sequaris; in Analytical Problems; Springer-Verlag, Berlin Heidelberg, New York, Tokyo, 1986, Vol.134, pp1

(121) T. M. Cotten; in Surface and Interfacial Aspects of Biomedical Polymers, J. D. Andrade, Ed.; Plenum Press, New York, 1985, Vol.2, pp161-187

(122) Y. J. Chen, G. M. Carter and S. K. Tripathy; Solid State Commun., 1985, 54, 19

(123) R. Aroca and D. Battisti; Langmuir, 1990, 6, 250

(124) R. Aroca and U. Guhathakurta-Ghosh; J. Am. Chem. Soc., 1989, 111, 7681

(125) J. H. Kim, T. M. Cotton, R. A. Uphaus and D. Mobius; J. Phys. Chem., 1989, 93, 3713

(126) T. M. Cotton, R. A. Uphaus and D. Mobius; J. Phys. Chem., 1986, 90, 6071

(127) G. J. Kovacs, R. O. Loutfy and P. S. Vincett; Langmuir, 1986, 2, 689

(128) M. Takahashi, M. Goto and M. Ito; J. Electroanal. Chem., 1988, 251, 177

(129) P. Gao, D. Gosztola and M. J. Weaver; J. Phys. Chem., 1989, 93, 3753

(130) L. W. H. Leung and M. J. Weaver; Langmuir, 1988, 4, 1076

(131) S. Farquharson, K. L. Guyer, P. A. Lay, R. H. Magnuson and M. J. Weaver; J. Am. Chem. Soc., 1984, 106, 5123

(132) R. P. Van Duyne, K. L. Haller and R. I. Altkorn; Chem. Phys. Lett., 1986, 126, 190

(133) R. P. Van Duyne, R. I. Altkorn and K. L. Haller; IEEE Circuits and Devices, 1986, 2, 61

(134) R. P. Van Duyne and J. P. Haushalter; J. Phys. Chem., 1984, 88, 2446

(135) J. M. Bello and T. Vo-Dihn; Appl. Spectrosc., 1990, 44, 63

(136) J. M. Stencel; Raman Spectroscopy for Catalysis, Van Nostrand Reinhold

Catalysis Series, Chapter 5; Van Nostrand Reinhold, New York, 1990

(137) P. B. Dorain, K. U. Von Raben, R. K. Chang and B. L. Laube; Chem. Phys. Lett., 1981, 84, 405

(138) R. E. Holt and T. M. Cotton; J. Am. Chem. Soc., 1989, 111, 2815

(139) P. J. Tarcha, T. E. Rohr, J. J. Markese and T. Cotton; Surface Enhanced Raman Spectroscopy Immunoassay or Other Specific-Binding Assay; Eur. Pat. Appl. Ep587,008, Mar., 1994; US Appl. 944,138, Sept., 1992.

(140) I. Nabiev, I. Chourpa and M. Manfait; J. Raman Spectrosc., 1994, 25(1), 13

(141) S. L. Wright, K. J. Latas, A. N. Mortensen, E. A. Orr, J. V. Paukstelis, R. M. Hammaker and W. G. Fateley; Proc. SPIE-Int. Soc. Opt. Eng., 1993, 1857

(142) L. M. Cabalin, A. Ruperez and J. J. Laserna; Talanta, 1993, 40(11), 1741

(143) Dynamical Phenomena in Surfaces, Interfaces and Super Lattices: Springer Series in Surface Sciences, Vol. 3; F. Nizzoli, K. H. Rieder and R. F. Willis, Eds., Springer-Verlag, Berlin, New York, 1985

(144) E. L. Altman, R. J. Gorte; J. Phys. Chem., 1989, 93, 1993

(145) L. J. Richter, S. A. Buntin, R. R. Cavanagh, D. S. King; J. Chem. Phys., 1988, 89, 5344

(146) X. D. Zhu, Y. R. Shen, R. Carr; Surf. Sci., 1985, 163, 114

(147) X. D. Zhu, Th. Rasing, Y. R. Shen; Chem. Phys. Lett., 1989, 155, 459

(148) K. Domen, T. J. Chuang; J. Chem. Phys., 1989, 90, 3318

(149) K. Domen, T. J. Chuang; J. Chem. Phys., 1989, 90, 3332

(150) E. Tronconi, L. Lietti; Surf. Sci., 1988, 199, 43

(151) X. D. Zhu, Th. Rasing, Y. R. Shen; Phys. Rev. Lett., 1988, 61, 2883

(152) S. R. Meech, K. Yoshihara; Chem. Phys. Lett., 1989, 154, 20

(153) M. G. Tenner, E. W. Kuipers, A. W. Kleyn; J. Chem. Phys., 1988, 89, 6552

(154) E. W. Kuipers, M. G. Tenner, A. W. Kleyn; Phys. Rev. Lett., 1989, 62, 2152

(155) S. Sugai, H. Yoshikawa, H. Miki, T. Kioda, K. Kawasaki; Appl. Surf. Sci., 1988, 33/34, 301

(156) A. W. Kleyn, A. C. Luntz, D. J. Auerbach; Surf. Sci., 1982, 117, 33

(157) F. M. Hoffmann; J. Chem. Phys., 1989, 90, 2816

(158) J. E. Reutt-Robey, D. J. Doren, Y. J. Chabal, S. B. Christman; Phys. Rev. Lett., 1988, 61, 2778

(159) L. S. Brown, S. J. Sibener; J. Chem. Phys., 1988, 89, 1163

(160) W. C. Natzle, D. Padowitz, S. J. Sibener; J. Chem. Phys., 1988, 88, 7975

(161) Reactions at the Liquid-Solid Interface: Comprehensive Chemical Kinetics Series, Vol.28; R. G. Compton Ed., Elsevier, Amsterdam, 1989

(162) Electrode Kinetics: Comprehensive Chemical Kinetics Series, Vol.27; R. G. Compton, Ed., Elsevier, Amsterdam, 1987

(163) Electrode Kinetics: Comprehensive Chemical Kinetics Series, Vol.26; C. H. Bamford, R. G. Compton, Eds., Elsevier, Amsterdam, 1986

(164) W. Schmickler, J. W. Schultze; in Modern Aspects of Electrochemistry, Vol. 17, Chapter 5; J. O' M. Bockris, B. E. Conway, R. E. White, Eds., Plenum Press, New York, 1986

(165) B. E. Conway; in Modern Aspects of Electrochemistry, Vol.16, Chapter 2; J. O' M. Bockris, B. E. Conway, R. E. White, Eds., Plenum Press, New York, 1985

(166) C. E. D. Chidsey, R. W. Murray; J. Phys. Chem., 1986, 90, 1749

(167) C. E. D. Chidsey, R. W. Murray; Science, 1986, 231, 25

(168) R. W. Murray; Acc. Chem. Res., 1980, 13, 135

(169) R. W. Murray; in Electroanalytical Chemistry, Vol.13, pp191; A. J. Bard, Ed., M. Dekker, New York, 1984

(170) R. W. Murray; Ann. Rev. Mater. Sci., 1984, 14, 145

(171) D. J. Jeamaire, and R. P. VanDuyne; J. Electroanal. Chem., 1977, 84, 1

(172) M. Takahashi and M. Ito; Time Dependent SERS Study: An Implication of SERS Mechanism, in Time Resolved Vibrational Spectroscopy, Vol.5; H. Takahashi Ed., Springer-Verlag Berlin Heidelberg, 1992, pp177-178

(173) C. K. Chen, T. F. Heinz, D. Rcard and Y. R. Shen; Chem. Phys. Lett., 1981, 83(3), 455

(174) A. M. Stacy and R. P. VanDuyne; in "Time Resolved Vibrational Spectroscopy"; Eds. G. H. Atkinson; Academic Press, Inc., 1983, pp377-385

(175) J. E. Pemberton and R. P. Buck; J. Electroanal. Chem., 1982, 136, 201

(176) K. Kneipp and H. Kneipp; Spectrochim. Acta, 1993, 49A(2), 167

(177) K. Kneipp; J. Molec. Struct., 1990, 218, 357

(178) K. Kneipp, W. Jahr and G. Roewer; Chem. Phys. Lett., 1989, 163, 105

(179) H. G. Zhang, F. Z. Liu, T. J. He and H. W. Xin; Chemical Journal of Chinese University, 1993, 14(2), 261

(180) H. G. Zhang, H. W. Xin, T. J. He and F. C. Liu; Spectrochim. Acta, 1991, 47A(7), 927

(181) C. Shi, W. Zhang, R. L. Birke, D. K. Gosser, Jr., and J. R. Lombardi; J. Phys. Chem., 1991, 95, 6276

(182) C. Shi, W. Zhang, R. L. Birke and J. R. Lombardi; J. Phys. Chem., 1990, 94, 4766

(183) C. Shi, W. Zhang, R. L. Birke and J. R. Lombardi; "SERS Study of 4-Cyanopyridine Adsorption and Electro-reduction Process on a Ag Electrode", manuscripts

(184) C. Shi, W. Zhang, R. L. Birke and J. R. Lombardi; "Study of Adsorption and Electrochemical Reduction of 4-Pyridine carboxyaldehyde by Time-Resolved Surface Enhanced Raman Spectroscopy", manuscripts.

(185) C. Shi, W. zhang, R. L. Birke and J. R. lombardi; "SERS Study of the Protonation and Electrochemical Reduction of 4-(hydroxymethyl)pyridine", manuscripts.

(186) P. Gao, D. Gosztola and M. J. Weaver; Anal. Chim. Acta, 1988, 212, 201

(187) P. Gao, D. Gosztola and M. J. Weaver; J. Phys. Chem., 1988, 92, 7122

(188) M. R. Philpott, F. Barz, J. G. Gordon II and M. J. Weaver; J. Electroanal. Chem., 1983, 150, 399

(189) R. Dornhaus, M. B. Long, R. E. Benner and R. K. Chang; Surf. Sci., 1980, 93,240

(190) W. H. Li, Z. Q. Tian, J. S. Gao and Q. Xue; Chinese Chemical Letters, 1993, 4(9), 829

(191) S. Sun, R. L. Birke and J. R. Lombardi; J. Phys. Chem., 1988, 92, 5965

(192) N. S. Lee, Y. Z. Hsieh, M. D. Morris and L. M. Schopfer; J. Am. Chem. Soc., 1987, 109(5), 1358

(193) A. Henglein; Ber. Bunsenges. Phys. Chem., 1990, 94, 600

(194) W. Zhang, A. Vivoni, R. L. Birke and J. R. Lombardi; "SERS Studies of Adsorption of Flavin Mononucleotide and Its Hydroqinine and Cation on a Ag Electrode", to be published, 1995.

(195) W. Zhang, A. Vivoni, R. L. Birke and J. R. Lombardi; J. Phys. Chem., 1995, 99, 12846

(196) C. Shi, W. Zhang, J. R. Lombardi and R. L. Birke; J. Phys. Chem., 1992, 96, 10093

(197) R. L. McCreery and R. T. Packard; Anal. Chem., 1989, 61(13), 775A

(198) R. R. Cavanagh, D. S. King, J. C. Stephenson and T. F. Heinz; J. Phys. Chem., 1993, 97, 786

Chapter 3

(1) P. F. Heelis, Chem. Soc. Rec., **1982**, 11, 15

(2) K. Yagi and T. Yamano (Eds.), Flavins and Flavoproteins. Japan Scientific Press, Tokyo, **1980**

(3) K. Shiga, K. Horiike, Y. Nishina, A. Isomoto and T. Yamano, J. Biochem. Tokyo; **1977,** 81, 1465, and references cited therein.

(4) K. Yagi, N. Ohishi, A. Takai, K. Kawano and Y. Kyogoku, Biochemistry, **1976,** 15, 2877, and references cited therein

(5) G. Dryhurst, " Electrochemistry of Biological Molecules ", New York, 1977, Chapter 7 , 365

(6) M. F. J. M. Vehagen and Wilfred R. Hagen, J. Electroanal. chem., **1992** , 334, 339, and references cited therein.

(7) M. Abe, Y. kyogoku, T. Kitagawa, K. Kawano, N. Ohishi, A. Takai Suzuki and K. Yagi, Spectrochimica Acta, **1986,** 42A, No.9, 1059.

(8) M. Abe, In Spectroscopy of Biological Systems; Edited by R. J. H. Clark and R. E. Hester, John Wiley &Sons Ltd, **1986,** Chapter 7, and references cited therein.

(9) M. D. Morris and R. J. Bienstock, In Spectroscopy of Biological Systems, Edited by R. J. H. Clark and R. E. Hester, John Wiley &Sons Ltd, **1986,** Chapter 8, and references cited therein.

(10) C. Shi, W. Zhang, J. R. Lombardi and R. L. Birke, J. Phys. Chem., **1992,** 96, 10093.

(11) J. Xu, R. L. Birke and J. R. Lombardi, J. Am. Chem. Soc., **1987,** 109, 5645.

(12) V. Brabec, K. Niki , Chem. Lett., **1988,** 1445-1448.

(13) T. M. Cotton, In Surface and Interfacial Aspects of Biomedical Polymers; Edited by J. B. Anderade, Plenum: New York, **1985**, Vol. II, pp 161.

(14) R. L. Birke, T. Lu and J. R. Lombardi; In Techniques for Characterization of Electrodes and Electrochemical Processes; Edited by R. Varma and J. R. Selman; John Wiley & Sons, **1991**, Chapter 5.

(15) A. M. Stacy and R. P. Van Duyne, Time resolved vibrational Spectroscopy, Academic Press, Inc., **1983,** pp.377-385.

(16) R. Dornhaus, M. B. Long, R. E. Benner and R. K. Chang, Surface Science; North-Holland Publishing Company, **1980,** 93, pp240-262.

(17) P. Gao, D. Gasztola, M. J. Weaver, J. Phys. Chem., **1988,** 92, 7122.

(18) P. Gao, D. Gasztola, M. J. Weaver, J Anal. Chim. Acta, **1988,** 212.

(19) C. Shi, W. Zhang, R. L. Birke, D. K. Gosser, Jr., J. R. Lombardi, J. Phys. Chem., **1991,** 95(16), 6276.

(20) C. Shi, W. Zhang, R. L. Birke, J. R. Lombardi, J. Phys. Chem., **1990,** 94(12), 4766.

(21) S. Sun, R. L. Birke, J. R. Lombardi, K. Leung and A. Z. Genack, J. Phys. Chem., **1988,** 92, 5965.

(22) R. L. Birke, J. R. Lombardi, L. A. Sanchez, Surface Enhanced Raman Spectroscopy, Edited by K. M. Kadish, American Chemical Society, Washington DC, **1982,** adv. Chem. Ser., No.201, Chapter 4.

(23) W. Zhang, A. Vivoni, J. R. Lombardi and R. L. Birke, "SERS studies of adsorption of Flavin Mononucleotide and its Hydroquinone and Cation on a Ag Electrode", to be published, **1995**.

(24) J. C. Evans, Spectrochimica Acta, **1960,** 16, 1382.

(25) M. Sharp, M. Petersson and K. Edstrom, J. Electroanal. Chem., **1979,** 95, 123.

(26) S. Ueyama, S. Isoda and M. Maeda, J. Electroanal. Chem., **1989,** 264, 149.

(27) L. Gorton and G. Johansson, J. Electroanal. Chem., **1980,** 113, 151.

(28) H. Shinohara, M. Gratzel, N. Vlachopoulos and M. Aizawa, Bioelectrochemistry and Bioenergitics, **1991,** 26, 307.

(29) J. Yamase, Photochem. Photobiol. , **1981** , 34,11

Chapter 4

(1) C. Walsh; Enzymatic Reaction Mechanisms; W. H. Freeman; SanFrancisco, CA; 1979, pp 358-448.

(2) C. Walsh; Acc. Chem. Res.; 1980, 13, 148

(3) T. C. Bruice; ibid.; 1980, 13, 256

(4) J. T. McFarland; in Biological Applications of Raman Spectroscopy, Vol. 2; T. G. Spiro Ed.; 1987, John Wiley and Sons, p.1

(5) N. S. Lee, R. S. Sheng, M. D. Morris, and L. M. Schopfer; J. Am. Chem. Soc.; 1986, 108, 6179

(6) N. S. Lee, Y. Z. Hsieh, M. D. Morris, and L. M. Schopfer; J. Am. Chem. Soc.; 1987, 109, 1358

(7) R. E. Holt and T. M. Cotton; J. Am. Chem. Soc.; 1989, 111, 2815

(8) R. E. Holt and T. M. Cotton; J. Am. Chem. Soc.; 1987, 109, 1841

(9) R. A. Copeland, S. P. A. Fodor, and T. G. Spiro; J. Am. Chem. Soc.; 1984, 106, 3872

(10) I. Taniguchi, K. Yagi, H. Eguchi, and S. Tomimura; Denki Kagaku; 1989, 57(11), 1094

(11) M. J. Benecky, M. G. Dowling, M. J. Clarke, and T. G. Spiro; Inorg. Chem.; 1984, 23, 865

(12) M. J. Benecky, T. J. Yu, K. L. Watters, and J. T. McFarland; Biochem. Biophys. Acta; 1980, 626, 197

(13) R. K. Chang; in Spectroscopic and Diffraction Techniques in Interfacial Electrochemistry; C. Gutierrez and C. Melendres, Ed.; Kluwer Academic Publishers, Netherlands; 1990, pp.155-180

(14) B. L. Garrell; J. Bioact. Compat. Polym.; 1991, 6(3), 296-307

(15) M. J. Weaver, Ber. Bunsen-Ges. Phys. Chem.; 1987, 91(4), 450

(16) J. H. Choi and H. Kim; Bull. Korean Chem. Soc.; 1993, 14(3), 388

(17) R. L. Birke, J. R. Lombardi, L. A. Sanchez; Surface Enhanced Raman Spectroscopy; K. M. Kadish, Ed.; American Chemical Society, Washington, DC, 1982; Adv. Chem. Ser. No. 201, Chapter 4.

(18) R. A. Copeland, and T. G. Spiro; J. Phys. Chem.; 1986, 90, 6648

(19) N. S. Lee; Bull. Korean Chem. Soc.; 1994, 15(1), 91

(20) H. S. Yoo, N. S. Lee, I. Hanazaki; J. Raman Spectrosc.; 1992, 23, 239

(21) E. Liang, P. Zhang; Wuli Xuebo; 1991, 40(2), 198

(22) N. S. Lee; Bull. Korean Chem. Soc., 1991, 12(5), 465

(23) C. J. Fritchie, Jr.; J. Biol. Chem.; 1972, 247(23), 7459

(24) M. J. Clarke, M. G. Dowling, A. R. Garafalo, and T. F. Brennan; J. Am. Chem. Soc.; 1979, 101, 223

(25) R. E. Holt and T. M. Cotton; J. Am. Chem. Soc.; 1989, 111, 2815

(26) S. Nakamura, Y. Ogura; In Flavins and Flavoproteins; K. Yagi, Ed.; University of Tokyo Press; Tokyo, 1968, pp 164-176

(27) M. Abe, and Y. Kyogoku; Spectrochimica Acta; 1987, 43A(8), 1027

(28) W. D. Bowman, and T. G. Spiro; Biochemistry; 1981, 20, 3313

(29) W. Zhang, A. Vivoni, J. R. Lombardi and R. L. Birke; J. Phys. Chem.,

1995, 99, 12846

(30) T. Kitagawa, Y. Nishina, Y. Kyogoku, T. Yamano, N. Ohishi, A. T. Suzuki and K. Yagi; Biochemistry; 1979, 18, 1804

(31) A. Vivoni, J. R. Lombardi and R. L. Birke; Development of a Restricted Simpler Optimization for Normal Coordination Calculations, manuscripts, 1995

(32) I. Taniguchi, K. Yagi, H. Eguchi, S. Tomimura, and K. Yasukochi; Denki Kagaku; 1989, 57(11), 1094

(33) V. Brabec, and K. Niki; Chemistry Letters; 1988, 1445

(34) K. Takamura, A. Mori, and F. Kusu; Chem. Pharmaceut. Bull.; 1981, 29, 3083

(35) M. F. J. M. Verhagen, and W. R. Hagen; J. Electroanal. Chem.; 1992, 334, 339

(36) S. Ueyama, S. Isoda, and M. Maeda; J. Electroanal. Chem.; 1989, 264, 149

(37) L. Gorton, and G. Johansson; J. Electroanal. Chem.; 1980, 113, 151

(38) L. Muller, and W. Friedrich; Z. Chem.; 1977, 17, 70

(39) A. Vivoni, J. R. Lombardi and R. L Birke; Normal Mode Calculations of Ammonia and Pyridine Adsorbed on a Silver Electrode, Manuscripts, 1995

(40) E. Koglin, H. H. Lewinsky and J. M. Sequaris; Surf. Sci., 1985, 158, 370

(41) T. Lu, T. M. Cotton, R. L. Birke and J. R. Lombardi; Langmuir, 1989, 5(2), 406

(42) P. F. Heelis; Chem. Soc. Rec., 1982, 11, 15

(43) E. J. Land and A. J. Swallow; Biochemistry; 1969, 8(5), 2117

(44) P. K. Dutta and T. G. Spiro; Biochemistry; 1980, 19(8), 1590

(45) M. Ishikawa, Y. Matsuda, K. Yamamoto, and S. Fukuzumi; Chem. Lett; 1992, pp 2269-2272

(46) B. F. Lei, and J. E. Becvar; Photochem. and Photobiol.; 1991, 54(3), 473

(47) Y. Nishina, K. Shiga, H. Watari, R. Miura, Y. Miyake, H. Tojo, and T. Yamano; Biochem. Biophys. Research Communications; 1982, 106(3), 818

(48) C. Shi, W. Zhang, J. R. Lombardi, and R. L. Birke; J. Phys. Chem.; 1992, 96, 10093

Chapter 5

(1) R. K. Chang and B. L. Laube; CRC Crit. Rev. Solid State Mater. Sci., 1984, 12, 1

(2) R. L. Birke and J. R. Lombardi; in Spectroelectrochemistry: Theory and Practice, R. J. Gale, Ed., Plenum Press, New York, 1988

(3) D. L. Jeanmaire and R. P. Van Duyne; J. Electroanal. Chem., 1977, 84, 1

(4) A. M. Stacey and R. P. Van Duyne; Time Resolved Vib. Spectrosc. Proc. First Int. Conf. Time Resolved Spectrosc., 1983, 4, 377

(5) R. T. Packard and R. L. McCreery; Anal. Chem., 1987, 59, 2631

(6) R. T. Packard and R. L. McCreery; J. Phys. Chem., 1988, 92, 6345

(7) M. A. El-Sayed; ACS Symp. Ser., 1979, No. 102, Chapter 10, 215-227

(8) G. H. Atkinson; Time Resolved Raman Spectroscopy, R. J. H. Clark and R. E. Hester Eds., Hayden, London, 1982, Vol.9, pp1-62

(9) R. L. McCreery and R. T. Packard; Anal. Chem., 1989, 61, 775A

(10) S. Sun, R. L. Birke, J. R. Lombardi, K. P. Leung and A. Z. Genack; J. Phys. Chem., 1988, 92, 5965

(11) H. Bauer and S. M. Rosenthal; J. Am. Chem. Soc., 1944, 66, 611

(12) R. L. Shriner and R. C. Fuson; The Systematic Identification of Organic Compounds, Wiley, New York, 1940, pp61

(13) G. L. McIntire, D. M. Chiappardi, R. L. Casselberry and H. N. Blount; J. Chem. Phys., 1982, 86, 2632

(14) I. A. Titova, I. M. Levenson, V. G. Mairanovskii and A. B. Ershler; Elecktronimiya, 1973, 9, 424

(15) A. J. Fry; in The Chemistry of Amino, Nitroso, Nitro Compounds and Their Derivatives, Part I; S. Patai Ed., Wiley, New York, 1982, pp320

(16) I. Rubinstein; J. Electroanal. Chem. Interfacial Electrochem., 1985, 183,

379

(17) W. J. Albery, B. A. Coles and A. M. Couper; J. Electroanal. Chem. Interfacial Electrochem., 1975, 65, 901

(18) A. P. Tomilov, S. G. Mairanovskii, M. Ya. Fioshin and V. A. Smirnov; in Electrochemistry of Organic Compounds, Halsted Press, New York, 1972, pp233

(19) C. Nishihara and M. Kaise; J. Electroanal. Chem. Interfacial Electrochem., 1983, 149, 287

(20) L. Chuang, I. Fried and P. Elving; Anal. Chem., 1964, 36, 2426

(21) P. Gao, D. Gosztola and M. J. Weaver; J. Phys. Chem., 1988, 92, 7122

(22) P. Gao, D. Gosztola and M. J. Weaver; Anal. Chim. Acta, 1988, 212, 201

(23) C. Shi, W. Zhang, R. L. Birke, D. K. Gosser, Jr., and J. R. Lombardi; J. Phys. Chem., 1991, 95, 6276